
**Bicomponent Porous Fibrous Membranes with Special Fiber
Morphologies and Properties**

Dissertation

Zur

Erlangung des akademischen Grades eines Doktors

des Doktorgrades der Naturwissenschaften

(Dr. rer. nat)

in der

Bayreuther Graduiertenschule für Mathematik und Naturwissenschaften (BayNAT)

der Universität Bayreuth

vorgelegt von

Master of Science Ling Peng

aus Henan (V. R. China)

Bayreuth, im September 2017

Die vorliegende Arbeit wurde in der Zeit von 10. 2013 bis 09. 2017 in Bayreuth am Lehrstuhl Makromolekulare Chemie II unter der Betreuung von Frau Prof. Dr. Seema Agarwal angefertigt.

Vollständiger Abdruck der von der Bayreuth Graduiertenschule für Mathematik und Naturwissenschaften (BayNAT) der Universität Bayreuth genehmigten Dissertation zur Erlangung des akademischen Grades einer Doktorin/ eines Doktors der Naturwissenschaften (Dr. rer. nat.).

Dissertation eingereicht am: 27.10.2017

Zulassung durch das Leitungsgremium: 07.12.2017

Wissenschaftliches Kolloquium: 19.04.2018

Amtierender Direktor: Prof. Dr. Dirk Schüler

Prüfungsausschuss:

Prof. Dr. Seema Agarwal (Erstgutachterin)

Prof. Dr. Volker Altstädt (Zweitgutachter)

Prof. Dr. Peter Strohmriegl (Vorsitz)

Prof. Dr. Georg Papastavrou

For my parents

Outline

List of symbols and abbreviations	1
1. Introduction and aim of this work.....	4
2. Theoretical background	7
2.1 Biomaterials.....	7
2.1.1 Silk fibrion (SF).....	7
2.1.2 Polylactide (PLA).....	10
2.1.3 Polycaprolactone (PCL)	13
2.2 Smart Polymers	14
2.2.1 Poly(N-isopropylacrylamide) (PNIPAM)	15
2.3 Background of electrospinning.....	16
2.3.1 History of electrospinning development.....	17
2.3.2 Electrospinning theory and process.....	19
2.3.3 Bicomponent electrospinning.....	20
2.3.3.1 Side-by-side electrospinning.....	22
2.3.3.2 Coaxial electrospinning.....	23
3. Results and discussion	26
3.1 Side-by-side composite fibers of Silk fibroin (SF) and Poly(<i>L</i> -lactide) (PLLA): from single fibers to fiber mats	26
3.1.1 Side-by-side composite single fiber of SF and PLLA.....	29
3.1.2 Side-by-side composite fiber mat of SF and PLLA.....	39
3.1.3 Conclusion.....	58
3.2 A self-coiled bicomponent nanofiber of Poly(N-isopropylacryl amide) (PNIPAM) and thermoplastic polyurethane (TPU)	59
3.2.1 Bicomponent single fiber of PNIPAM and TPU.....	61
3.2.2 Conclusions	76
3.3 Self-rolled porous hollow tubes made up of biodegradable polymers with bicomponent layer-by-layer morphology	77
3.3.1 Bilayer self-rolled porous hollow tubes of PLA and PCL.....	79
3.3.2 Conclusions	95
4. Experimental part.....	97

4.1 Chemicals	97
4.2 Characterization methods	98
4.2.1 Tensile testing of single fiber	98
4.2.2 Tensile testing of fiber mat	100
4.2.3 Scanning electronic microscopy (SEM)	100
4.2.4 Conductivity measurements	101
4.2.5 Fourier transform infrared spectroscopy (FTIR)	101
4.2.6 Differential scanning calorimetry (DSC)	101
4.2.7 Confocal laser scanning microscopy (CLSM).....	102
4.2.8 Fourier self-deconvolution (FSD)	102
4.2.9 Transmission electron microscopy (TEM)	103
4.2.10 Digital Microscopy	103
4.2.11 Gel-Permeation Chromatography (GPC)	103
4.2.12 Porosity.....	103
4.3 General procedures for preparation of polymer solutions	104
4.3.1 Preparation of silk fibroin solution.....	104
4.3.2 Preparation of PLLA solution.....	104
4.3.3 Preparation of TPU solution.....	104
4.3.4 Preparation of PNIPAM solution	105
4.3.5 Preparation of PLA, PCL and PMMA solutions	106
5. Summary	107
6. Zusammenfassung.....	109
7. Outlook	111
8. Acknowledgments.....	113
9. References.....	115

List of symbols and abbreviations

A	cross-section area
$A_{//}$	parallel-polarized infrared absorbance intensity
A_{\perp}	perpendicular-polarized infrared absorbance intensity
ABP	4-acryloyl-benzophenone
AIBN	Azobisisobutyronitrile
Ala	Alanine
Amide I	C=O stretching
Amide II	C-N stretching and C-N-H bending
Butyl methacrylate	BMA
B. mori	Bombyx mori
CLSM	Confocal laser scanning microscopy
cm / mm / μm / nm	centimeter / millimeter / micrometer / nanometer
D / d	Diameter / inner diameter of tube
Da / kDa	Unified atomic mass unit
DMF	N, N'-dimethylformamide
DSC	Differential scanning calorimetry
ECM	Extracellular matrix
ESB	European society for biomaterials
etc	et cetera
F	applied load
FDA	Food and drug administration
FSD	Fourier self-deconvolution
FTIC I	Fluorescein isothiocyanate isomer I
FTIR	Fourier-transform infrared spectroscopy
Gly	Glycine
GPC	Gel permeation chromatography

g / mg	gram / milligram
h	hour
HFIP	1,1,1,3,3,3-hexafluoro-2-propanol
kV	kilovolt
L	Length
LCST	Lower critical solution temperature
L / mL	Liter / milliliter
MeOH	methanol
M_n	number average molar mass
M_w	weight average molar mass
Min	minute
MPa / GPa	Megapascal / Gigapascal
MWD	Molecular weight distribution
NaHCO ₃	Sodium hydrogen carbonate
n	number
N ₂	Nitrogen
OD	Offset-degree
PAN	Polyacrylonitrile
PCL	Polycaprolactone
PDO	Polydioxanone
PEI	Poly(ethyleneimine)
PEO	Poly(ethylene oxide)
PLA	Poly(lactide)
PLLA	Poly(L-lactide)
PMMA	Poly(methyl methacrylate)
PNIPAM	Poly(N-isopropylacrylamide)
PSI	Polysuccinimide
R	Dichroic ratio
r	radius
ROP	Ring-opening polymerization

rpm	revolutions per minute
RT	Room temperature
s	second
sd	standard deviation
Ser	Serine
SEM	Scanning electronic microscopy
SF	Silk fibroin
Silk I	Water-soluble state of silk
Silk II	The crystalline silk
Silk III	Interface orientation of silk
T / t	Thickness of fiber mat / thickness of layer
TEM	Transmission electron microscopy
T _g	Glass obtained
TPU	Thermoplastic polyurethane
UV	Ultraviolet
W	Width
1D / 2D / 3D	one- / two- / three- dimensional
ε	porosity
μS	micro-siemens
σ	tensile strength
ρ / ρ'	average density / standard density
°	Degree of contact angle
°C	Degree of temperature

1. Introduction and aim of this work

The application of electrospun nanofiber mats in various domains such as tissue engineering^[1-7], drug delivery^[6-8], gene delivery^[9-11], wound dressings^[7, 12-15], sensors^[16-18] and filtration membranes^[19-21], energy storage/conversion^[22] and electronic devices^[23,24] has increased enormously in the recent past and leads to an increased interests of scientists and engineers to invent novel structures involving nanofibers and efficient processes for producing them.

In recent years, a lot of works were carried out in order to improve the quality and functionality of the electrospun nanofibers. As one typical mode, bicomponent fiber has gained much attention and holds great promise in a variety of applications because of many excellent advantages^[25-29]: 1) It can utilize the properties of different polymers in one system; 2) It can improve the material performance suitable for specific needs by tailoring one or more properties with minimal sacrifice of other properties; 3) It can bring about multifunctional properties without the loss of mechanical properties; 4) It can exploit capabilities not existing in each of the individual polymers.

Such structures are of increasing interest for making nanofiber mats with special properties, such as biocompatible, biodegradable and stimuli-responsive.

Therefore, the broad aim of this thesis is to explore combination of polymer properties in form of bicomponent fibers and porous fibrous membranes with special morphologies, such as side-by-side, layer-by-layer and coaxial for potential

applications in medical field, textiles, sensors and actuators. To achieve the aim, bicomponent fibers and fibers membranes were made by bicomponent electrospinning techniques using special nozzles. In-depth studies were carried out for the formation, characterization and properties of the fibers and corresponding fibrous membranes with special morphologies. Biomaterials and responsive polymers are chosen for this work.

The results of this thesis are presented in three parts, in each part the systems are investigated in order to extend the understanding and possible application of these bicomponent fibers and fibers membranes.

In the first part, new two-in-one bio-based ductile composite fibers and fiber mats of poly(*L*-lactide) (PLLA) and silk fibroin (SF) with side-by-side morphology were produced by side-by-side electrospinning. Besides establishing the method of making fibers with side-by-side morphology, the effect of fiber diameter, orientation of fibers and molecular orientation on the resulting mechanical properties on the scale of single fiber and fiber mat is studied.

Further, the bicomponent morphology was studied using different combination of polymers to generate a responsive system. Thermoresponsive poly(*N*-isopropylacrylamide) (PNIPAM) was combined with a nonresponsive polymer such as thermoplastic polyurethane (TPU) in the form of a side-by-side or off-centered morphology. Due to the asymmetry in swelling of the fiber on putting in water at different temperature, compressive stress at the interface led to a reversible crimping of fibers. The results described in part 2 of the thesis.

The compressive stress at the interface can also be generated by creating asymmetry in swelling by making bicomponent layer-by-layer structure using responsive/nonresponsive polymers as two layers. This effect was studied and utilized in making a tubular scaffold by self-folding of 2D bilayer sheets in the last part of the work. For the bilayer system, two conventional biodegradable polymers polylactide (PLA) and polycaprolactone (PCL) were used. None of the two polymers (PLA and PCL) are responsive. Still the bilayer sheets rolled to tubular scaffold at 40 °C in wet/dry conditions. The phenomenon was studied in details and found to be due to the asymmetrical shrinkage. The inner diameter of the tube and the number of layers in the wall were dependent upon the temperature, thickness ratio of the two polymer fiber layers.

2. Theoretical background

2.1 Biomaterials

A biomaterial is defined as “a nonviable material used in a medical device, intended to interact with biological systems” in the first consensus conference of the European Society for Biomaterials (ESB) in 1976.^[30] However, with the evolution of the field of biomaterials, a biomaterial refers to “any material intended to interface with biological systems to evaluate, treat, augment or replace any tissue, organ or function of the body”.^[30,31] Biomaterials evolved from interacting to influencing with the body and toward to the goal of tissue regeneration.

From the sources, biomaterials can be divided into two fields: natural biomaterials and artificial biomaterials. The natural biomaterials group includes naturally occurring biomaterials and chemical modifications of these materials, such as silk, gelatin, collagen, cellulose, amylose, chitin, etc. All synthesized biomaterials like polymers, ceramics, composite or metallic components belong to artificial biomaterials. Each of these individual biomaterial groups has specific advantages. Usually, natural biomaterials have better biocompatibility, biodegradability and remodeling ability. But artificial biomaterials are easy to manufacture and modify.

2.1.1 Silk fibroin (SF)

Silk is a natural protein fiber, which produced by lepidoptera larvae like silkworms and by members of class Arachnida (spiders), etc.^[32, 33] Silk from the silkworm *Bombyx*

mori (*B. mori*) has been used in the traditional textile industry for more than 5000 years due to the good mechanical properties and pearly luster.^[34,35] Recently, it has gained interest as a biomaterial because of its biocompatibility, chemical modification capability, tunable degradation, processing into multiple formats and sufficient supply.^[32,33,35-37]

Mainly, the silk consists two different proteins: fibroin (70-75%) and sericin (25-30%)(figure 1).^[36,38] Sericin is a kind of adhesive protein, which coats the fibroin molecules to keep the structural integrity of the fibers.^[35, 38] Silk fibroin (SF) is the core protein, which provides the biocompatibility, biodegradability for using as a biomaterial. To get the fibroin, sericin must be removed by a degumming thermochemical process.^[36]

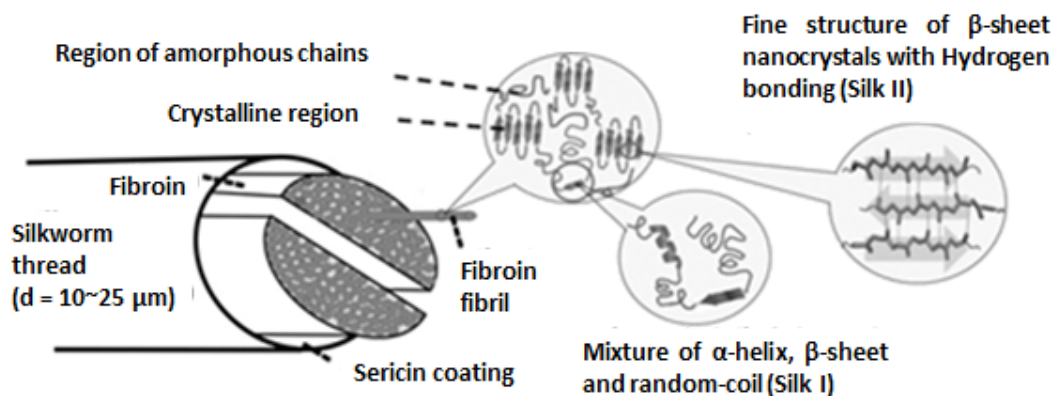


Figure 1: Schematic representation of the deduced silk fiber structure. (Reprinted with permission from Ref 38, Copyright 2015 John Wiley & Sons)

The silk fibroin consists of two proteins: a light chain ($M_w \sim 26$ kDa) and a heavy chain ($M_w \sim 390$ kDa). These two proteins are linked by a single disulfide bond at the

C-terminus of the two subunits with a 1:1 ratio.^[35,36,39] The amino acid composition of SF from *B. Mori* consists primarily of glycine (Gly, 43%), alanine (Ala, 30%) and serine (Ser, 12%).^[33,35,40] The hydrophobic domain of heavy chain contain a repetitive amino acid sequence of Gly-Ala-Gly-Ala-Gly-Ser (figure 2).^[35,40,41] The light chain is more hydrophilic and elastic, because of the non-repetitiveness of the amino acid sequence.^[33,35]

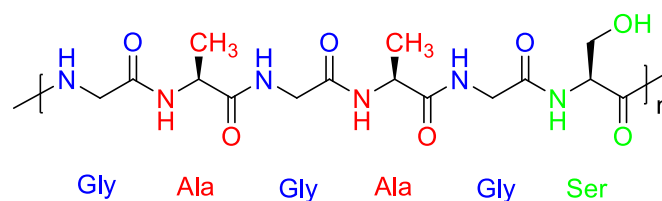


Figure 2: Amino acid sequence of hydrophobic domain of heavy chain.

SF has three structures: the water-soluble state (Silk I), the crystalline silk (Silk II) and an interface orientation (Silk III).^[33,38] The Silk I structure is a metastable structure, belonging to the orthorhombic system. The Silk II structure is an anti-parallel β -sheet structure, belonging to the monoclinic system.^[35] With a heating or methanol treatment, Silk I structure converts to Silk II structure very easily.^[33,35]

The US Food and Drug Administration (FDA) recognized SF as a biomaterial in 1993.^[35] Many studies about SF were carried out in recent years. With the versatile process ability, SF solution can be fabricated into different formats like fibers, mats, films, microspheres, tubes, sponges, hydrogels, etc.^[36,42] With these morphologies, SF has a range of potential applications such as drug delivery, scaffolds for tissue engineering, surgical suture, optics, sensing, etc.^[42]

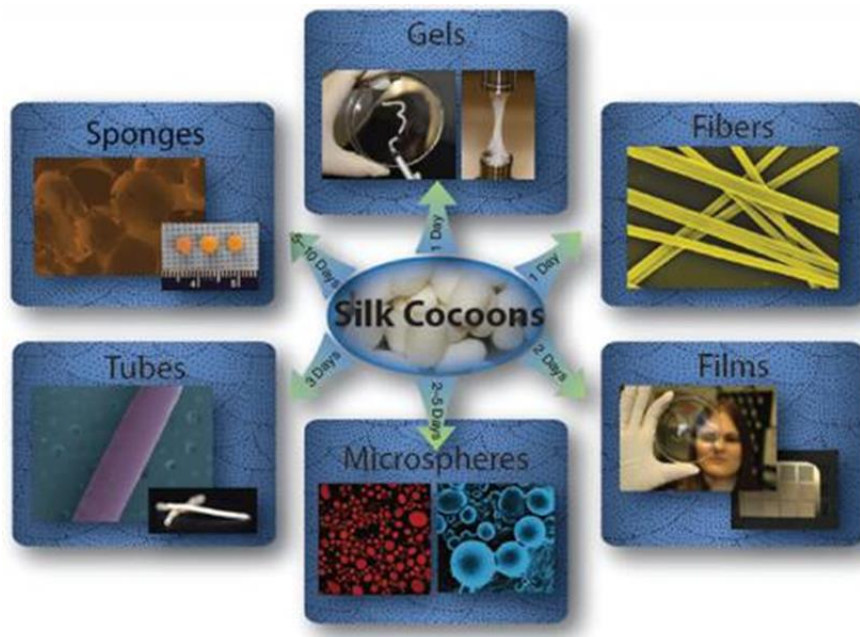


Figure 3: Various morphologies of SF, fabricated from SF solution (organic and aqueous). (Reprinted with permission from Ref 36, Copyright 2011 Nature Publishing Group)

2.1.2 Polylactide (PLA)

Polylactide (PLA, figure 4) is one of the well-known biodegradable and bioactive thermoplastic aliphatic polyester, which pioneered by Carothers in 1932. ^[43] The molecular weight of Carothers' PLA was low. The production of PLA with high molecular weight was patented by DuPont in 1954. ^[43]

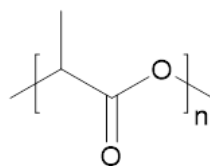


Figure 4: Chemical structure of PLA.

Two methods were used to produce the monomer of PLA, lactic acid (2-hydroxy propionic acid): fermentation and petrochemical. Lactic acid is chiral, consisting of two optical isomers: L-(+)-lactic acid and D-(-)-lactic acid. A mixture of the two isomers in equal amounts is called DL-lactic acid or racemic lactic acid.

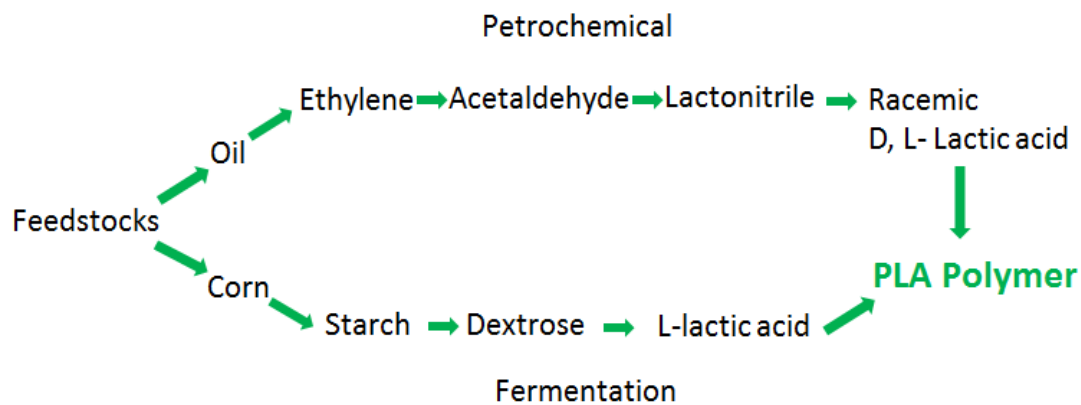


Figure 5: Two preparation methods of lactic acid. (Reprinted with permission from Ref 44, Copyright 2015 Budapest University of Technology and Economics Faculty of Mechanical Engineering Department of Polymer Engineering)

Compared to the petrochemical process, industry prefers to use fermentation process to produce lactic acid because the synthetic routes have many major limitations: limited capacity because of occurrence of side products, inability to make the desirable L-lactic acid stereoisomer only and high manufacturing costs. ^[45,46]

In comparison to other biopolymers, the advantages of PLA are numerous: 1) renewable agricultural source such as corn; 2) fixation of significant quantities of carbon dioxide; 3) significant energy saving; 4) the ability to recycle back to lactic

acid by hydrolysis or alcoholysis; 5) the capability of producing hybrid paper-plastic packaging that is compostable; 6) reduction of landfill volumes; 7) improvement of the agricultural economy and 8) the all-important ability to tailor physical properties through material modifications.^[45,47]

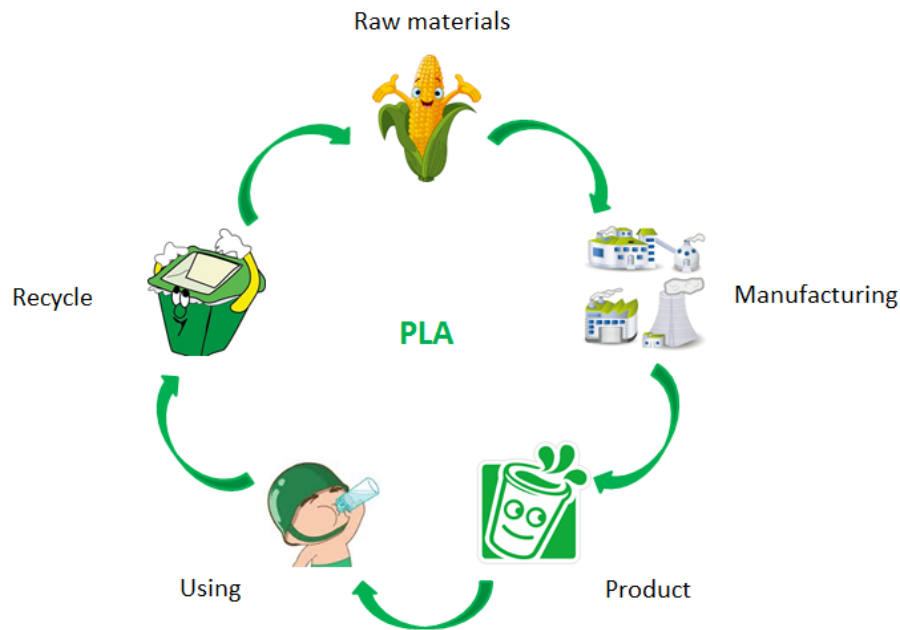


Figure 6: Life cycle of PLA, from raw material to final disposal.

PLA is widely used in biomedical fields due to its ability to degrade into innocuous lactic acid. From medical implants, including anchors, screws, plates, pins and rods, to membrane applications, such as wound covers, and also for surgical sutures, drug delivery systems, PLA shows a great potential. ^[45,48,49] PLA can also be used as a decomposable packing material. Cups and bags such as food packing, loose-fill packing, compost bags, have been made from this material. (Figure 6)^[45]

2.1.3 Polycaprolactone (PCL)

Polycaprolactone (PCL, figure 7) is another well-known biodegradable aliphatic polyester. It is a hydrophobic, semi-crystalline polymer with a glass transition temperature (T_g) of $-60\text{ }^\circ\text{C}$ and a melting point ranging between 59 and $64\text{ }^\circ\text{C}$, which firstly synthesized by the Carothers group in the early 1930s. ^[50]

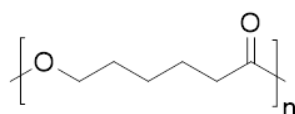


Figure 7: Chemical structure of PCL.

Two main pathways are used to produce polycaprolactone: polycondensation of 6-hydroxyhexanoic acid and ring-opening polymerization (ROP) of ϵ -caprolactone. ^[51] Several papers describe the preparation of PCL by polycondensation with and without catalysts. ^[51-54] Limitation of polycondensed PCL is the low molecular weight and high polydispersity. Unlike polycondensation, ROP occurs under milder reaction conditions and can give polymers with higher molecular weight and lower polydispersity. ^[55] Therefore, industry prefers to use ROP process to produce PCL.

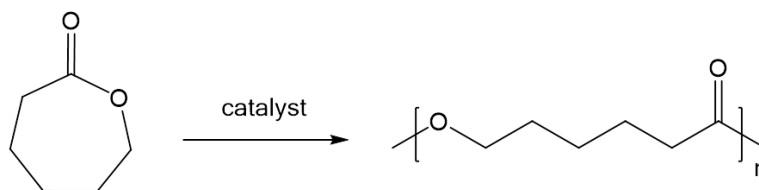


Figure 8: Ring-opening polymerization of ϵ -caprolactone.

There are four main mechanisms which affect the ROP of PCL. According to catalyst, they can be divided into anionic, cationic, monomer-activated^[56] and coordination-insertion ROP.^[51] Each method affects the molecular weight, molecular weight distribution of PCL.^[50]

With the excellent biocompatibility, flexibility, thermoplasticity, miscibility with a large range of other polymers and biodegradability, PCL has been proposed for use in biomedical and biomaterial application, such as drug delivery, sutures, wound dressings, contraceptive devices, fixation devices, dentistry, etc.^[50, 57]

Dictated by the crystalline nature, superior rheological and viscoelastic properties, PCL can be easily manufactured and manipulated into scaffolds, and shows a great potential application in tissue engineering. Many studies about PCL in bone, cartilage, tendon and ligament, cardiovascular, blood vessel, skin and nerve engineering have been carried out.^[50] Otherwise, PCL has also uses in microelectronics^[58], adhesives^[59] and packaging^[60] fields.

2.2 Smart Polymers

Smart polymers or stimuli-responsive polymers are high performance polymers which have ability to respond to external stimuli in different environment. The stimuli include temperature, humidity, pH, ionic strength, electric or magnetic field, light, etc. Consequently, the smart polymers have a wide range of applications in drug delivery, gene delivery, tissue engineering, textile engineering, sensors, actuators, molecular gates and switches, stimuli-responsive surfaces, etc.^[61, 62]

2.2.1 Poly(*N*-isopropylacrylamide) (PNIPAM)

Several polymer systems respond to temperature, undergoing a lower critical solution temperature (LCST) phase transition: above the LCST, these polymers become insoluble in water. (Figure 9)

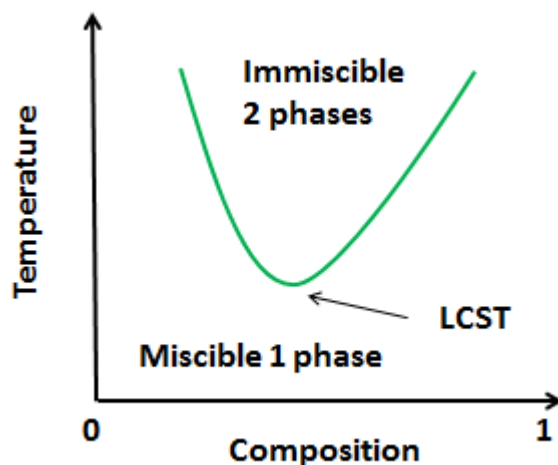


Figure 9: Phase diagram for a polymer solution exhibiting an LCST.

A well known polymer with the LCST behavior is PNIPAM, which first described by Heskins and Guillet.^[63,64] It is synthesized via a free-radical polymerization (figure 10) and exhibits a coil-to-globule phase transition at 32 °C^[65] which is close to normal physiological body temperature.

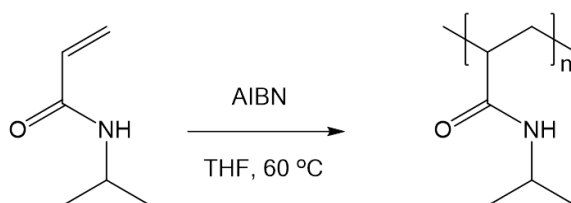


Figure 10: Free-radical polymerization of *N*-isopropylacrylamide with radical initiator azobisisobutyronitrile (AIBN).

Several architecture based on PNIPAM such as macroscopic gel, microgel, nanogel, membranes, films and surfaces were produced and they have a wide range of applications for drug delivery, biosensing, tissue engineering, micro-actuators, artificial muscles and cartilages, matrices for biseparation, flexible bioelectronics, stimuli-responsive electronic devices, self-adaptive electronics, etc.^[66-73]

2.3 Background of electrospinning

Electrospinning is a fascinating process of fabricating of continuous polymeric fibers with diameter ranging from several nanometers to several micrometers.^[74-77] So far, this method is used for synthetic and natural polymers, including conventional polymers, functional polymers, proteins, peptides, to produce fibers with micro- or nano-scale.^[74, 77,78] Polymers loaded with carbon nanotubes^[79-83], electronic^[84], biological^[85, 86], magnetic^[87, 88], optical materials^[89, 90], also some microorganisms such as bacteria^[91-93] and virus^[91, 94], and cells ^[95-98] were spun with this method to obtain multifunctional nanofibers for some amazing applications. Various modified electrospinning techniques and further treatments for producing special fibers with complex architectures like side-by-side, core-shell or hollow fibers have been reported in the literature ^[74, 113], such as silk ^[26,99], ceramic ^[100-102], metal ^[103,104], metal-oxide ^[105, 106] nanofibers and polymeric ^[107, 108], ceramic^[109,110], metal^[111], metal-oxide ^[112] hollow nanofibers. Diverse structures of nanofibers ranging from single fibers to ordered arrangements of fibers can also be fabricated by electrospinning. ^[114-117] Electrospun fibers have a very broad scope of applications in

medicine, filtration, sensor, electronics fields, which already mentioned at the beginning of the introduction.

2.3.1 History of electrospinning development

Electrospinning is an old technique. Bose found that, when high electric potentials are applied to drops of fluids, aerosols will be formed, in 1745. This process was named as electrostatic atomization or electrospray. After over 100 years, Lord Rayleigh studied the unstable equilibrium of a charged drop of liquid in 1882.^[118] He mentioned that, when the charge repulsion is over the surface tension of the charged drop, electrostatic atomization will occur. 20 years later, Cooley and Morton patented the first devices for electrically dispersing of fluids in 1902.^[74] Later, Zeleny studied the instability of surfaces of liquid drops under a high electric field.^[119, 120] In 1929, a manufacturing method of artificial silk by applying electric current was patented by Hagiwara.^[74] Anton Formhals patented firstly the process and apparatus about electrospinning of polymers in the year 1934, and this patent was considered as the beginning of preparation of fibers by electrospinning technique.^[74] From 1930s to 1980s, the process of development of electrospinning technique was relatively slow. In 1971, Baumgarten obtained fibers with diameter less than 1 μ m by electrospinning from dimethyl formamide (DMF) solution of acrylic resin.^[121] In 1987, Hayati *et al.* studied the effects of electric field, experimental conditions and the factors affecting the fiber stability and atomization.^[122] But there was still little interest in the technique of electrospinning technique till the nineties.

In the 1990s, the research work about electrospinning by Reneker's group ^[123] gained substantial academic attention. ^[74] The reason for the captivation of electrospinning is the increased knowledge on the application potential of nanofibers in different areas, such as filtration, textile, catalyst and adsorbent materials. ^[75] The rapid development of electrospinning technique is reflected by the sky rocketing numbers of scientific publications and patents as shown in figure 11. Although the number of scientific publications and patents in 2016 is a little less than in 2015, with development of new electrospinning technique and applications, the number increased again (in only half year of 2017, over 3000 scientific publications and patents about electrospinning have been already reported).

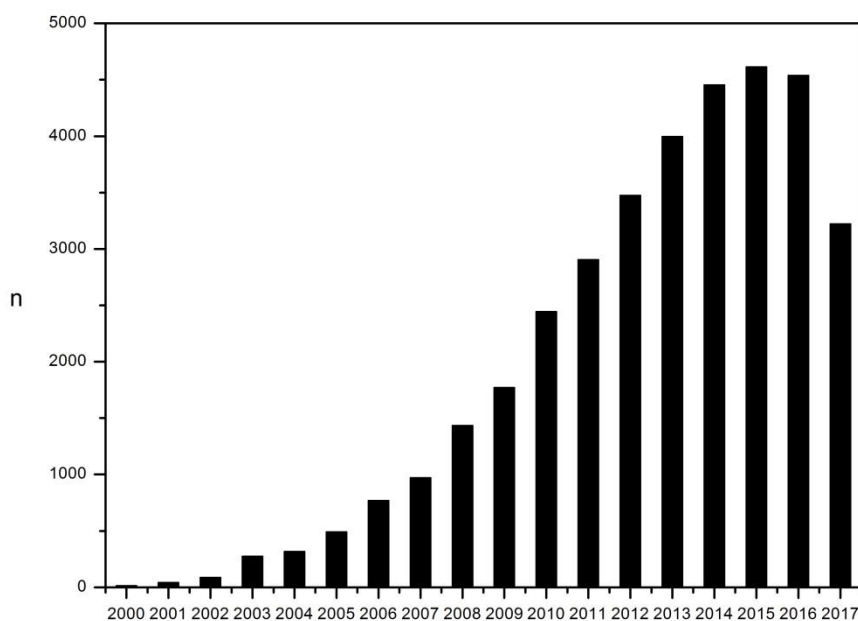


Figure 11: Number (n) of scientific publications and patents per year (01. 2000–07. 2017) with the keyword “electrospinning” (source: SciFinder Scholar).

2.3.2 Electrospinning theory and process

Electrospinning is a unique technique of producing continuous ultra-thin fibers by using electrostatic forces. The setup for electrospinning is shown in figure 12. In this technique, a polymer solution or the melt is passed through a spinneret by using of syringe pump to form a drop at the capillary tip and a collector is placed opposite to the spinneret. High voltage potential is applied between the spinneret and the collector. Both spinneret and collector have electrical conductivity and separated by an optimum distance. The polymer solution obtained free charges after pressing through the charged spinneret. The interaction of the charges in the polymer solution in response to the applied external electric field and the charged ions move towards the opposite polarity charged collector. At the capillary tip, the pendant droplet deformed into a cone like projection called the “Taylor cone” in the presence of the electric field. When the applied potential reaches a critical value at which repulsive electrostatic forces overcome the surface tension of the liquid, a fine charged jet of liquid is ejected from the tip of the Taylor cone. After the initiation from the Taylor cone, the charged jets undergo a whipping motion and elongate continuously until they are deposited onto the collector as the fine fibers.^[124] The jets travel through the atmosphere, the solvent evaporates, leaving behind a dry fiber on the collecting device. In this process, the solutions properties (molecular weight of polymers^[125], concentration^[121,126], viscosity^[121], surface tension^[127], conductivity^[121], solvents^[128] and temperature of polymer solution^[129]), operating parameters (applied voltage^[126], solution feeding rate^[121], distance between spinneret and collector^[130] and diameter of spinneret^[131])

and surroundings parameters (temperature^[132] and humidity^[133]) will influence the formation of nanofibers.^[75] Therefore, electrospun fibers with various morphologies and diameters can be produced by changing of the electrospinning parameters.

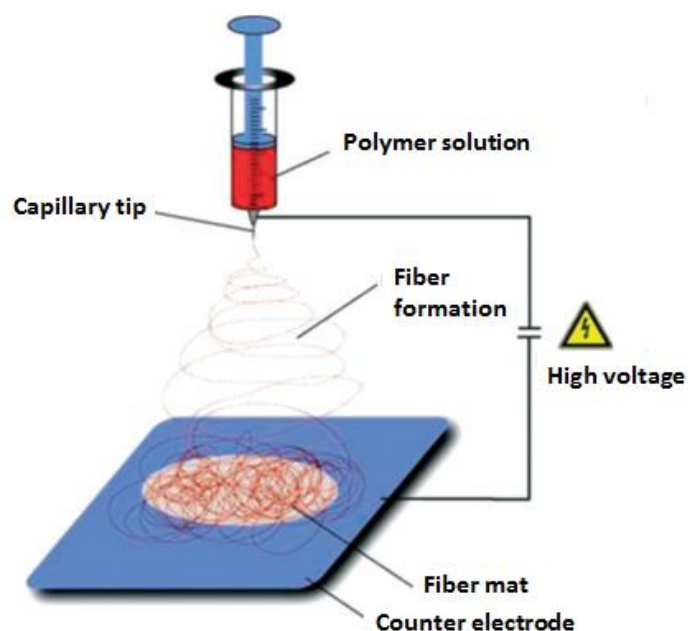


Figure 12: Schematic diagram of setup for electrospinning. (Reprinted with permission from Ref 74, Copyright 2007 John Wiley & Sons)

2.3.3 Bicomponent electrospinning

It is mentioned already at the beginning of introduction that bicomponent fibers have gained much attention and holds great promise in a variety of applications. To get multicomponent fibers via electrospinning technique, single spinneret must be modified with number of channels/capillaries for bi-, tri- or multi-component electrospinning. For bicomponent electrospinning, core-shell and side-by-side electrospun fibers can be produced by controlling the location of two channels/capillaries with core-shell and side-by-side way. (Figure 13) Moreover,

coaxial electrospinning becomes gas-jacketed/assisted electrospinning after replacing one polymer solution by gas in the outer tube.

With various modified electrospinning technique, bicomponent fibers with novel morphologies such as side-by-side ^[135, 136], core-shell ^[137, 139], “islands-in-the-sea” ^[138], segmented-pie ^[139] types, were produced. (Figure 14)

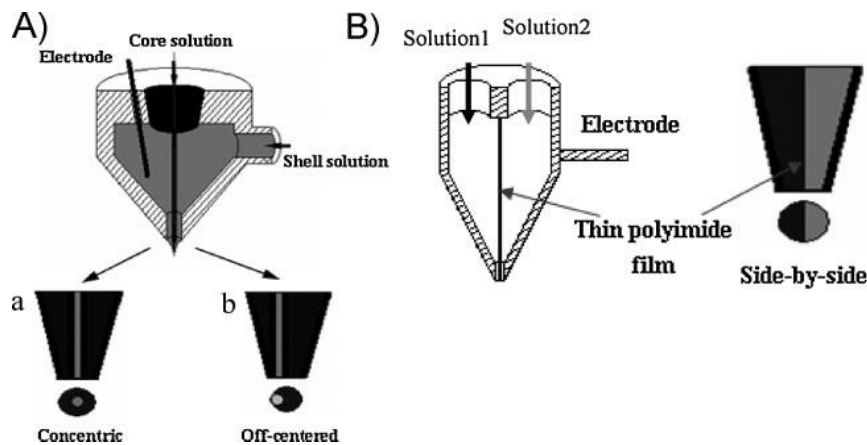


Figure 13: Schematic diagram of bicomponent electrospinning spinnerets, A) a) coaxial, b) off-centered and B) side-by-side electrospinning spinnerets. (Reprinted with permission from Ref 134, Copyright 2009 John Wiley & Sons)

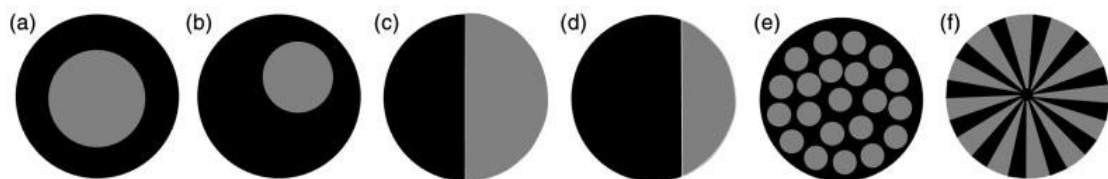


Figure 14: Schematic diagrams showing the typical cross sections of various bicomponent polymers in a single filament: (a) concentric core/shell; (b) eccentric core/shell; (c) 50/50 side-by-side; (d) unequal side-by-side; (e) islands-in-the-sea; and (f) segmented-pie fibers. (Reprinted with permission from Ref 139, Copyright 2016 SAGE Publications)

2.3.3.1 Side-by-side electrospinning

The side-by-side electrospinning is a common and popular bicomponent electrospinning technique. In side-by-side electrospinning, two polymer solutions are delivered through a spinneret which is separated by a thin polymer or metal film into two cavities. (Figure 13 B) At the capillary tip, a pendant droplet contains two kinds of solutions. Only one jet is generated on the tip of the deformed droplet after applying voltage. (Figure 15) In an ideal case, a side-by-side nanofiber is created.

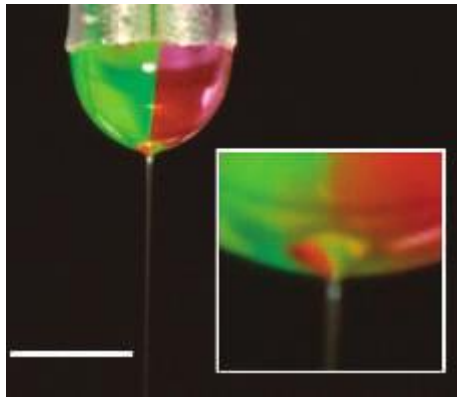


Figure 15: Digital image of a typical biphasic side-by-side Taylor cone with jet. Two phases were labelled with fluorescein isothiocyanate-conjugated dextran (green) and rhodamine-B- conjugated dextran (red) respectively. (Scale bar: 1 mm) (Reprinted with permission from Ref 140, Copyright 2005 Nature Publishing Group)

In side-by-side electrospinning, controlling the electric field strength is more important than in normal electrospinning. Gupta *et al.* who demonstrated firstly the potential of bicomponent electrospinning found that: when the distance between the nozzle tip and the collector is too far, the electric field strength is insufficient to

initiate electrospinning; however, when the distance is too near, the field strength is relatively too strong and induces a strong electrostatic repulsion force, therefore, two separate Taylor cones were formed. ^[141]

Side-by-side nanofiber is an anisotropic system. Polymers with different physical characteristics are combined in one fiber by an anisotropic but regular way, this leads to some interesting mechanical behavior, such as bending, crimping etc.^[134, 135] This behavior has been attributed to differential shrinkage within the fibers which causes one of the components to compress. An advantage of the side-by-side fibers is that each component can show its own properties in one single fiber.

2.3.3.2 Coaxial electrospinning

The coaxial electrospinning is another common and popular bicomponent electrospinning technique. In coaxial electrospinning, two polymer solutions are delivered through a spinneret which contains two concentrically aligned channels/capillaries. (Figure 13 A) Under a high voltage, the electrospinning liquid is drawn out from spinneret and forms a compound Taylor cone with a core-shell structure. (Figure 16) After coaxial jet, the core-shell structure will be built and kept in the fibers on collecting on a collector.

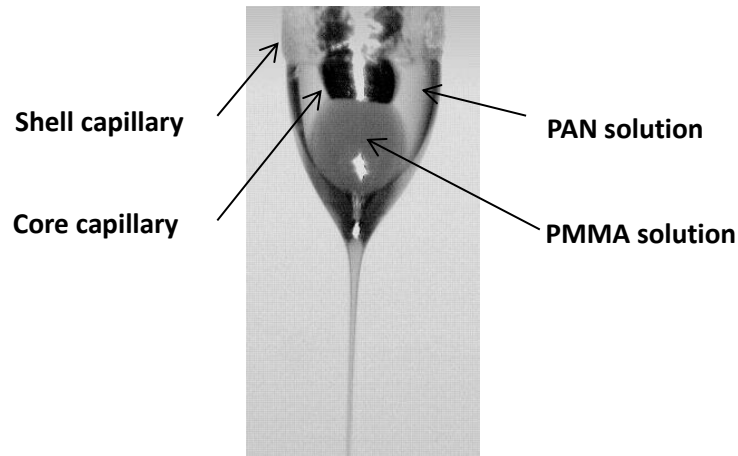


Figure 16: Digital image of a typical biphasic core-shell Taylor cone with jet. PAN: Polyacrylonitrile; PMMA: Poly(methyl methacrylate) (Reprinted with permission from Ref 142, Copyright 2006 John Wiley & Sons)

In this process, one common problem is that the outer droplet can be transformed into a jet, while the inner droplet cannot because there are no surface charges on inner droplet. The deformation of the inner droplet into the core fiber is left to viscous forces alone. It also has been illustrated by a mathematical model that the formation of core/shell jets and nanofibers via coaxial electrospinning in the considered range of parameters is greatly facilitated when the core tube protrudes outside the shell tube by around 0.5 of its radius. ^[143]

Not only polymer solutions but also non-polymeric liquid or powder (as core) can be used for coaxial electrospinning. Systems with discontinuous drop-shaped inclusions inside a continuous shell can also be generated. This drop-shape core morphology is of interest for inclusion of biological objects, such as bacteria, virus, cells or drugs as mentioned before. The interest in encapsulation may be motivated by many reasons: to isolate an unstable component from an aggressive environment, to avoid

decomposition of a labile compound under a certain atmosphere, to deliver a given substance to a particular receptor, and so forth. ^[146]

Another excellent function of coaxial electrospinning is production of hollow and non-spinnable material nanofibers by selective of the removed core or shell of nanofibers. ^[113, 142-145] When the inner component in the core-shell fibers is removed by selective solvents or heat treatment, hollow nanofibers are obtained. The non-spinnable solutions can be extruded through the inner capillary while the spinnable solution is extruded through the outer capillary. The outer solution would carry the inner solution during electrospinning. When the outer polymer is removed, the desired inner nanofiber is retained.

3. Results and discussion

3.1 Side-by-side composite fibers of Silk fibroin (SF) and Poly(L-lactide) (PLLA): from single fibers to fiber mats

(This work has been published in *Macromol. Mater. Eng.* 2016, 301, 48-55, with the title: “ Two-in-one composite fibers with side-by-side arrangement of silk fibroin and poly(L-lactide) by electrospinning” by Ling Peng, Shaohua Jiang, Maximilian Seuß, Andreas Fery, Gregor Lang, Thomas Scheibel and Seema Agarwal)

Silk proteins can be processed into different forms such as hydrogels, sponges, composites, microspheres, thin films and fibers.^[33, 36] Silk fibers are used in textile industry and for biomedical applications like sutures, wound dressing, tissue engineering scaffolds etc..^[147, 148] Electrospinning is one of the fiber forming techniques which is highly used in the recent times for making nanofibers.^[74, 76, 77] Electrospinning of silk proteins from different sources in solvents such as formic acid, hexafluoroisopropanol (HFIP) and hexafluoroacetone is also documented.^[149-152] The protein secondary structure in electrospun fibers is dependent upon the type of solvent used for spinning. Formic acid as solvent for electrospinning provides immediately β -sheet structures in the silk fibers which is in contrast to fiber mats produced by spinning from HFIP, which mainly show random coil and helical structure.^[153] In most of the studies the silk fibrous mats were electrospun with an aim to get artificial scaffolds for tissue engineering.^[154] The nanofibrous network structure produced by electrospinning and material properties of silk proteins provide one of the best

combinations for mimicking the extracellular matrix (ECM). Electrospun silk fibrous mats were already shown to support growth and proliferation of various cell lines like normal human keratinocytes, fibroblasts and osteoblasts. [155]

Recently hybrid fibers were produced using blends of silk with other synthetic and natural biodegradable and biocompatible polymers like chitosan^[156], polyethylene oxide^[157], cellulose acetate^[158], gelatin^[159], polycaprolactone (PCL)^[160, 161] and polydioxanone (PDO)^[160], poly(lactide)^[162] either to make electrospinning of silk more feasible or tune its properties.

Another way of combining properties of two polymers in one material is the sequential spinning leading to layered structures. One of such examples is the sequential electrospinning of silk fibroin (SF)-gelatin solutions followed by poly(*L*-lactide) (PLLA) spinning forming randomly oriented layered fibrous structure as studied by Wang *et al.*^[163]

Other possibilities of combining silk with synthetic polymers are in the form of bicomponent fibers with core-shell and side-by-side morphology. The combination of SF with another biopolymer in side-by-side parallel arrangement in one fiber (two-in-one bio-composite fibers) with retained secondary structure of silk would open up many new application possibilities. Unlike blends, layer-by-layer and core-shell structures, the side-by-side morphology offer many potential advantages. The side-by-side fibers will make both sides available for post-spinning modifications. Moreover, they have potential as compatibilizers in fiber reinforced biodegradable composites, co-culture of different cells, tuning degradability profile and drug-release

from scaffolds utilizing different surface chemistry of the two sides. Electrospinning can be used as a tool for making side-by-side biofibers. The first ever side-by-side electrospun fibers were produced by Wilkes et al. using poly(vinyl chloride)/segmented polyurethane and poly(vinyl chloride)–poly(vinylidene fluoride) as two sides.^[27] Polymeric nanosprings were made by Agarwal et al. previously by combining polymers of different modulus in a side-by-side morphology.^[28, 164] Getting homogenous side-by-side fibers for any new combination of polymers is still not trivial.

In this work bio-based PLLA and *Bombyx mori* silk fibroin are combined in a single fiber with side-by-side morphology i.e. the two polymers making different sides of the same fiber. The fibers will be designated as SF-s-PLLA in the subsequent text. The process of making two-in-one fibers with uniform morphologies using side-by-side electrospinning nozzles is presented in this chapter. The two-in-one fibers were characterized for morphology using SEM and confocal laser scanning microscope and showed presence of side-by-side structure with an asymmetric wrapping-up morphology with SF wrapping PLLA fibers from one side. The secondary structure of polymers in SF-s-PLLA fibers was studied using Fourier transformed infrared spectroscopy. The effect of fiber alignment on morphology, molecular orientation and mechanical properties was also studied in comparison to the randomly oriented fibers and fibers made from blends of PLLA and SF.

3.1.1 Side-by-side composite single fiber of SF and PLLA

Two-in-one bio-composite fibers of silk fibroin and synthetic biodegradable polymer poly (*L*-lactide) (PLLA) (denoted as SF-s-PLLA; SF: PLLA 5:2 wt:wt) were made by electrospinning using special side-by-side nozzle in which two sides were separated by a thin copper foil. The nozzle used for side-by-side spinning is similar as described in publication 28. [28] Both silk fibroin and PLLA were dissolved in HFIP at 100 mg/mL and 40 mg/mL, respectively. Two injector jet pumps were used to control the flow rates of the two solutions (0.33 ml/h each) (Figure 17). The distance between the nozzle and the collector was 15 cm and the applied voltage was 12.5 kV. A stainless steel frame with an inner rectangular size 17.5 x 3.0 cm was used as the collector to collect the side-by-side single fibers. A rotating disk (diameter 20 cm) was used with a rotation speed of 1800 rpm to collect the aligned fiber mats.

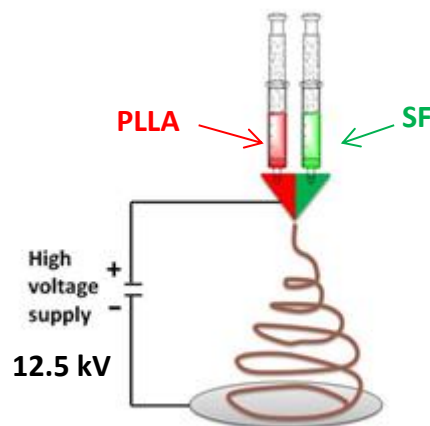


Figure 17: Sketch for side-by-side electrospinning

Scanning electron micrographs showed randomly oriented uniform cylindrical asymmetric side-by-side structure in the form of a wrapped-up morphology i.e. thin

fibers (around 150 nm diameter) wrapped-up on one side with thicker fibers (Figure 18). The overall average fiber diameter was $698 \text{ nm} \pm 136 \text{ nm}$. The electrospinning of pure SF from HFIP using single nozzle provided belt shaped fibers whereas PLLA fibers were cylindrical with average diameters around $322 \text{ nm} \pm 66 \text{ nm}$ (Figure 18). Many researchers ^[165-167] considered that the elongation of the jet and evaporation rate of the solvent changed the shape and the charge of the jet, which determined the final morphology. Under our experimental conditions, the side-by-side spinning of SF (tendency to flatten) and PLLA (tendency to make cylindrical fibers) using side-by-side nozzle provided bicomponent fibers with asymmetric morphology. The PLLA fibers were wrapped by belt shaped SF fibers from one side as shown in Figure 18b and sketched in Figure 19. The conductivity of SF-HFIP solution ($20.3 \text{ } \mu\text{S/cm}$) is much higher than the conductivity of PLLA-HFIP solution ($0.4 \text{ } \mu\text{S/cm}$). Fast evaporation of the spinning solvent from PLLA side leads to collapse of SF side giving wrap-up morphology.

Confocal laser scanning microscopy (CLSM) was further used for confirming the bicomponent nature and the asymmetric sides of the fibers. The spinning solutions were dyed with different fluorescent dyes (Fluorescein sodium and Rhodamine B were added in SF and PLLA solutions, respectively) and the resulting fibers were observed using a confocal microscope. The fluorescence of both dyes within one fiber can be shown by superimposition while three dimensional images confirm asymmetric side-by-side morphology (Figure 20). CLSM studies were carried out in collaboration with Prof. Fery's group.

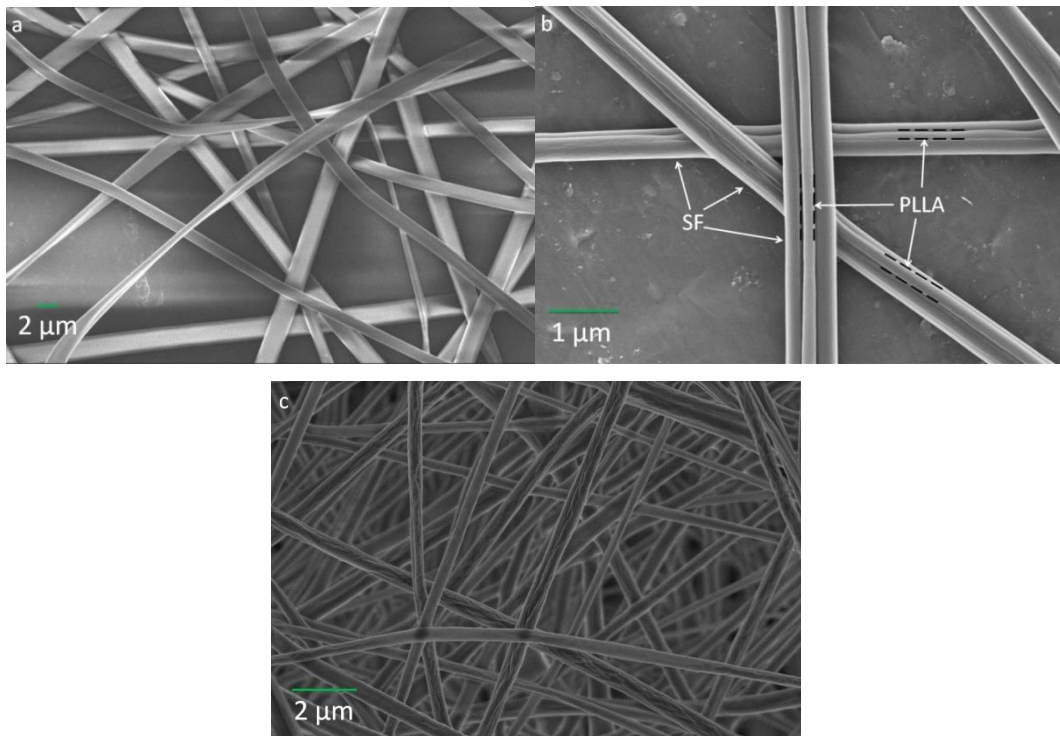


Figure 18: SEM images showing surface morphology of randomly oriented electrospun fibers: (a) silk fibroin fibers (SF) (b) two-in-one (SF-s-PLLA) fibers (c) poly(*L*-lactide) fibers (PLL).

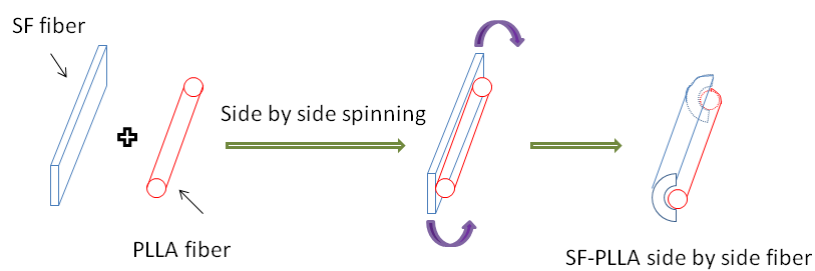


Figure 19: Schematic of formation of asymmetric wrap-up morphology by side-by-side spinning.

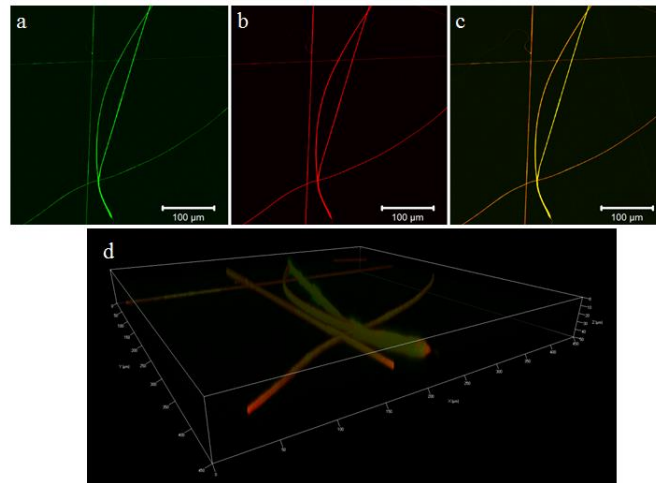


Figure 20: CLSM images of fluorescence labeled two-in-one SF-s-PLLA fibers showing the bicomponent nature. (a) Fluorescence image of Fluorescein sodium labeled SF; (b) fluorescence image of Rhodamine B labeled PLLA; (c) superimposition of (a) and (b); (d) three dimensional image.

The cross-section area is needed to measure the mechanical properties of single fibers. SF single fibers have a belt-like form. (Figure 18a) To get the cross-section area of SF single fiber, both the width and thickness of the SF nanofibers should be measured. The cross sectional area of SF nanofiber should be equated with diameter. For example, in figure 21, the thickness (T) and the width (W) of SF nanofiber are 270.8 nm and 914.0 nm respectively. The cross sectional area is: $A = T \times W = 270.8 \text{ nm} \times 914 \text{ nm} = 2.475 \times 10^{-5} \text{ nm}^2$, $A = \pi D^2/4$. So the equated diameter of SF nanofiber in figure 34 is about 561 nm.

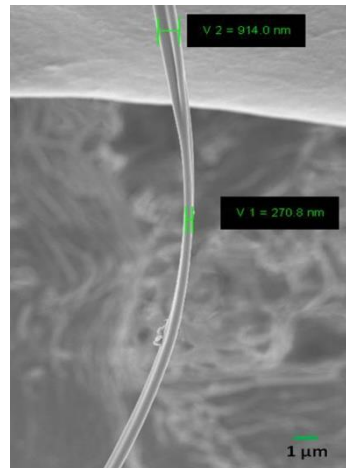


Figure 21: SEM image of SF single nanofiber after tensile test.

The E-modulus, true stress and strain at break were used to describe the mechanical properties of nanofibers. The values about the mechanical properties were extracted from individual tensile test results of single nanofibers. The variations of mechanical properties of single as-spun SF nanofibers are showed in figure 22. The analysis shows that, the mechanical properties of SF nanofibers are not as good as that of PLLA nanofibers. The average strain at break of SF nanofibers is only about 4 %. Maybe that is the major reason, which limits the study about mechanical properties and application of single SF nanofibers. After the methanol treatment, the SF nanofibers were too brittle for the tensile test and no measurements could be performed. To improve the mechanical properties and at the same time not decrease the biocompatibility of SF nanofibers, combination of SF with some other biomaterials which have good mechanical properties is a good strategy.

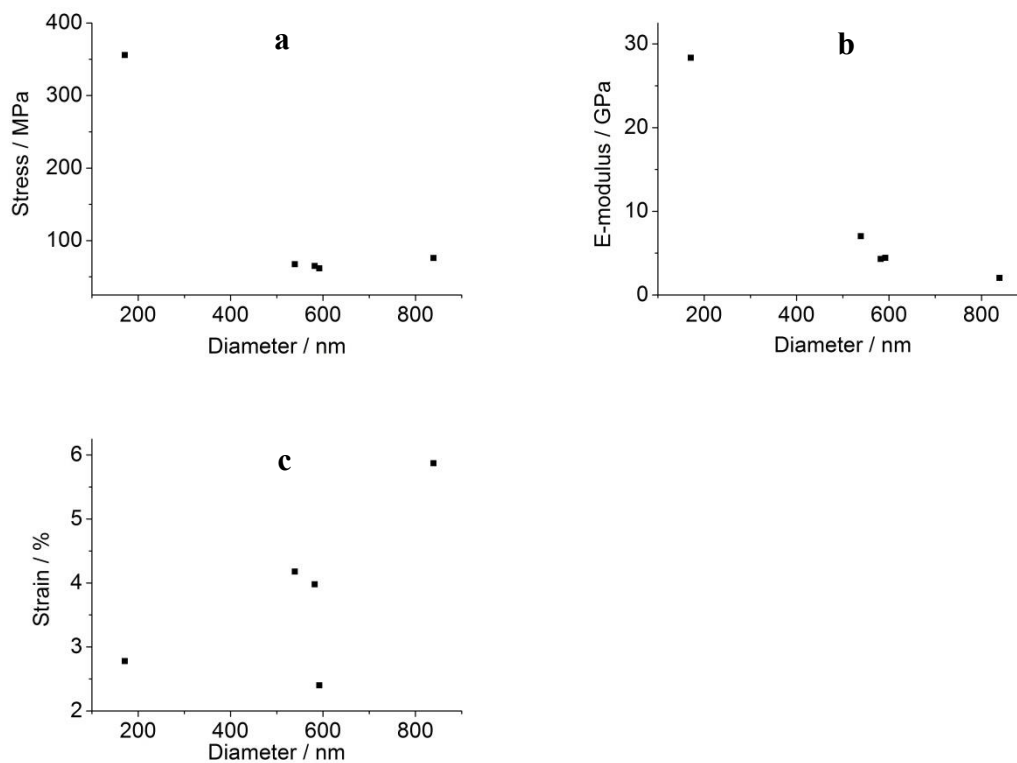


Figure 22: Mechanical properties of as-spun SF single nanofibers: (a) true stress, (b) E-modulus and (c) true strain at break.

In some previous studies, the crystallinity was discussed as the most important factor for the mechanical properties of single nanofibers. Papkov *et al.* reported that with higher crystallinity, the strength and E-modulus of PAN nanofibers will increase, but the strain will be lower [168]. The crystallinity of PLLA fibers will increase by annealing at 80 °C. [169] It is very interesting to study the mechanical properties of as-spun and annealed PLLA single nanofibers.

The variations of mechanical properties of single as-spun and annealed PLLA nanofibers are shown in figure 23. The analysis shows that, after annealing the mechanical properties of single PLLA nanofibers are similar to that of as-spun PLLA

single nanofibers. Both stress and E-modulus have a size effect: with decreased diameter (especially under 400 nm), the mechanical properties had an intensive increasing. The average strain at break of PLLA nanofibers is about 150 %. With the analysis results of PLLA single nanofibers, it would be hypothesized that not crystallinity but chain orientation in ultrafine nanofibers is the major cause of change of mechanical properties.

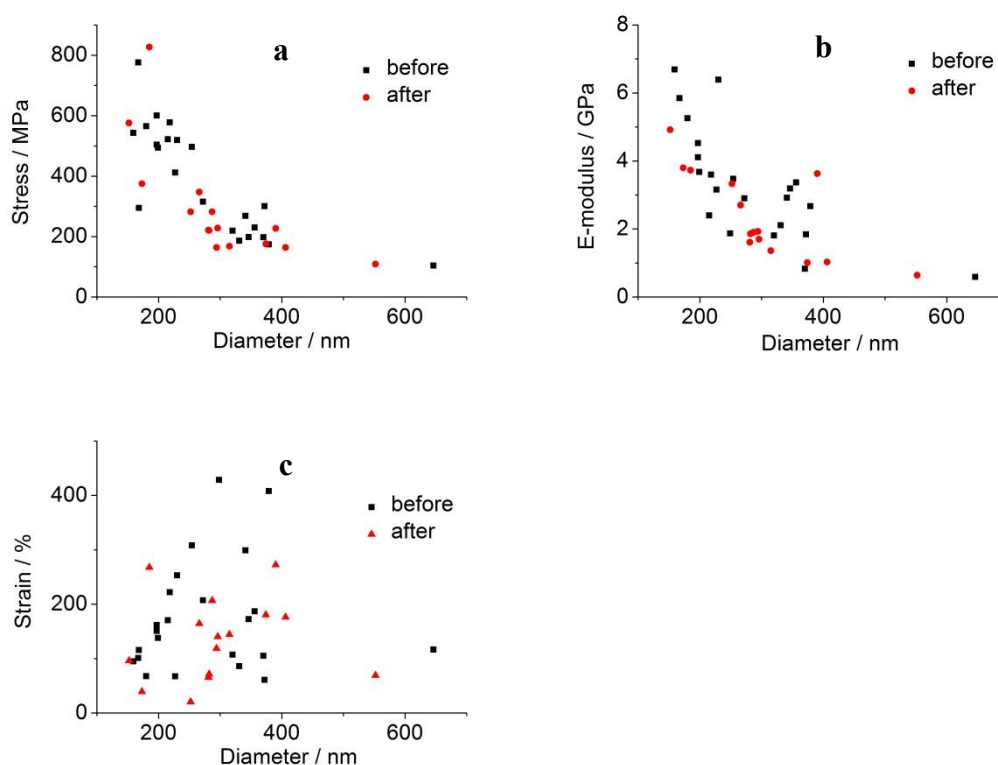


Figure 23: Mechanical properties of PLLA single nanofibers (before and after annealing): (a) true stress, (b) E-modulus and (c) true strain at break.

From the results, the true stress and E-modulus showed a size effect very clearly (figure 23 a, b). When the diameter of nanofibers decreased, especially below 400 nm,

they increased rapidly. This effect was not obvious for strain at break. The average strain at break of PLLA nanofibers is about 190 %, the average strain at break of SF-s-PLLA nanofibers is about 50% and the average strain at break of SF nanofibers is about 4%. The true strain at break of SF single nanofibers has a detectable improvement after combination with PLLA in other side.

Because of the size effect, the fibers with similar diameters were chosen to compare the mechanical properties of SF-, PLLA-and SF-s-PLLA single nanofibers. As shown in figure 24, both the strain and stress of SF fibers are weaker than the of SF-s-PLLA and PLLA fibers. Because of the high sensitivity, the curves were not smooth. The SF fibers were brittle, the strain of SF fiber is very low (<4 %). When the brittle SF fibers combined with PLLA through side-by-side electrospinning to form side-by-side SF-s-PLLA fibers, the strain of the nanofibers increased from about 4% to 50%. The mechanical properties of same nanofibers were also dependent on diameter. Thinner nanofibers have higher stress and lower strain, that's why E-modulus increased so rapidly.

The possible reason about the size effect of nanofibers is the polymer chain orientation. When the nanofiber diameter decreased, the inner space for the polymer chains is limited; as a result, the polymer chains will be oriented. High orientation caused the change in the mechanical properties.

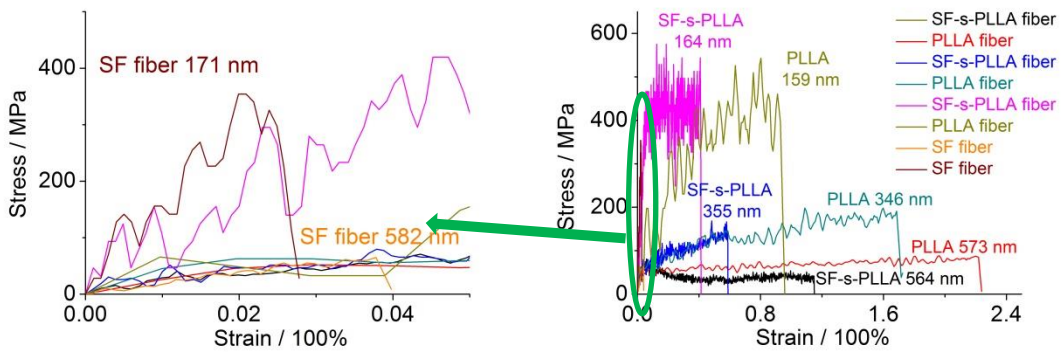


Figure 24: Typical stress-strain curves of single as-spun nanofibers with different diameter.

The strains at break of two sides in SF-s-PLLA fibers are very different. Whether the two sides during the tensile tests break at the same time or not was studied further in this work.

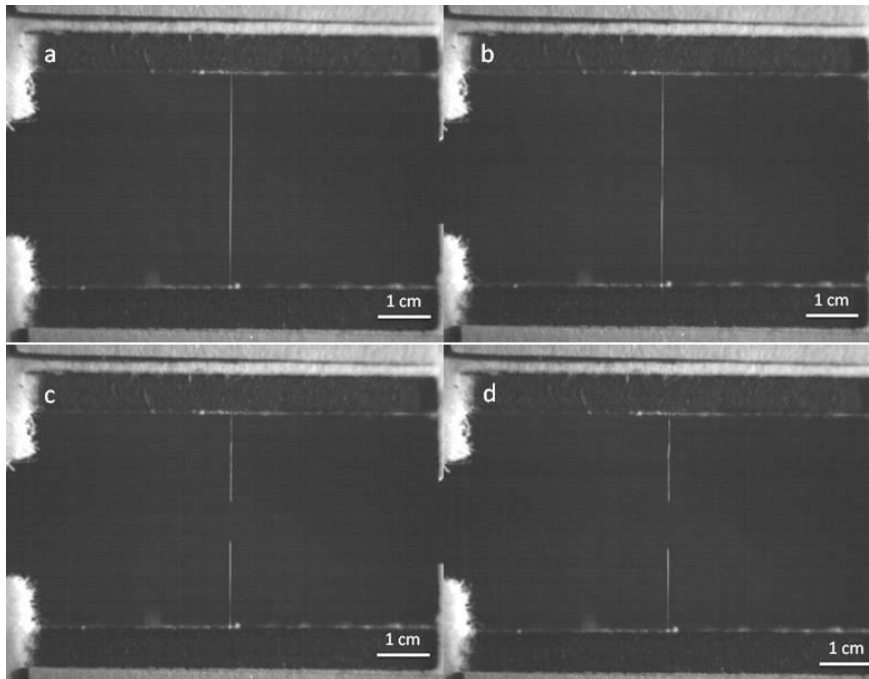


Figure 25: Photos of point at break of single as-spun SF-s-PLLA nanofiber (diameter of as-spun fiber: 429 nm)

The tensile process was monitored by high speed camera, which can take 4000 photos per second. Figure 25 shows the break moment of single SF-s-PLLA nanofiber. It broke at the middle of the nanofiber. Some tensile tests of SF-s-PLLA nanofibers were stopped before sample broke at different elongations to study the surface morphology of two sides. As show in figure 26, at 10% and 20% elongations, the surfaces of side-by-side fiber were still smooth, although the elongations were already higher than the elongation of strain at break of SF nanofiber. At about 30% elongation some cracks were obvious on one side of the SF-s-PLLA nanofiber.

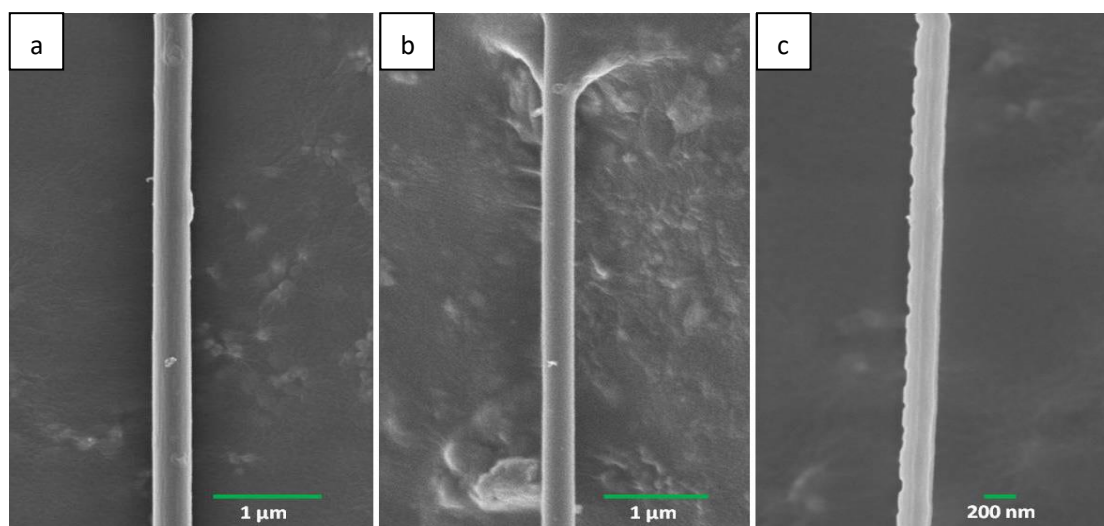


Figure 26: SEM images of the surface morphology of electrospun SF-s-PLLA fibers at different elongations: (a) 10%, (b) 20% and (c) 30%.

Significant improvement in the mechanical properties of SF fibers could be achieved by PLLA in combination with a side-by-side fibrous morphology. The strain at break of nanofiber was increased from <4% (SF) to about 50% (side-by-side), there was no cracks till elongation 20% of SF-s-PLLA fiber. Because of better mechanical

properties, the SF-PLLA nanofiber may expand the application area of SF nanofiber.

3.1.2 Side-by-side composite fiber mat of SF and PLLA

The preparation processing and results of morphological studies of SF and PLLA fibers were already shown in part 3.1.1. The use of a disk (diameter 20 cm) rotating with a speed of 1800 rpm as collector provided macroscopic alignment of (SF-s-PLLA) composite fibers (Figure 27). Better alignment by increasing the rotation speed of the collector was tried. The large amounts of samples for further characterization at high rotation speeds beyond 1800 rpm could not be made due to the fast evaporation of the solvent (HFIP) used for electrospinning leading to an unstable spinning process with frequent clogging of the needle.

The molecular orientation of polymer chains within the fibers were studied using polarized FTIR. The fibers collected at 1800 rpm showed a significant difference in characteristic absorption peak intensities of various bonds (carbonyl and amide) in the

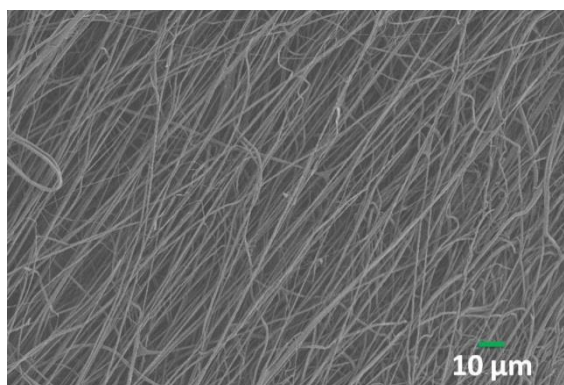


Figure 27: SEM image of two-in-one (SF-s-PLLA) fibers collected on a rotating disk with 1800 rpm.

polarized IR spectra obtained in perpendicular and parallel directions to the fiber axes (Figure 28a). Dichroic ratio (R), which is calculated by the ratio of $A_{//} / A_{\perp}$ ($A_{//}$ and A_{\perp} are the parallel-polarized and the perpendicular-polarized infrared absorbance intensity, respectively) for a particular vibration band was used to define the molecular orientation.^[170] The carbonyl stretching vibrations of PLLA centered at 1755 cm^{-1} , and amide I at 1650 cm^{-1} of SF showed R values of 0.43 and 0.36, respectively due to the perpendicular polarization to the fiber axis. For the vibration band of Amide II of SF observed between 1480 to 1580 cm^{-1} , the R value is 0.53 (Table 1). This is due to the two mutually perpendicular vibrations in Amide II: C-N stretching is parallel and at the same time C-N-H bending is perpendicular to the polypeptide backbone. On the other hand, the absorption peaks from PLLA and SF in two-in-one SF-s-PLLA fiber mats having randomly oriented fibers in any two perpendicular directions are similar and showed R values of 0.97-0.98 with almost no macroscopic molecular orientation (Figure 28b). A similar behavior was observed for pristine PLLA and SF fibers as shown in the Figures 29 and 30.

Table 1: Dichroic ratio of different absorption peaks of PLLA and SF in two-in-one (SF-s-PLLA) random and aligned fibers for studying molecular orientation.

Vibration band (cm^{-1})	Dichroic ratio (R)	
	Aligned fibers	Random fibers
1720-1790 (C=O stretching PLLA)	0.43	0.98
1590-1710 (C=O stretching Amide I)	0.36	0.97
1480-1580 (C-N stretching and C-N-H bending Amide II)	0.53	0.98

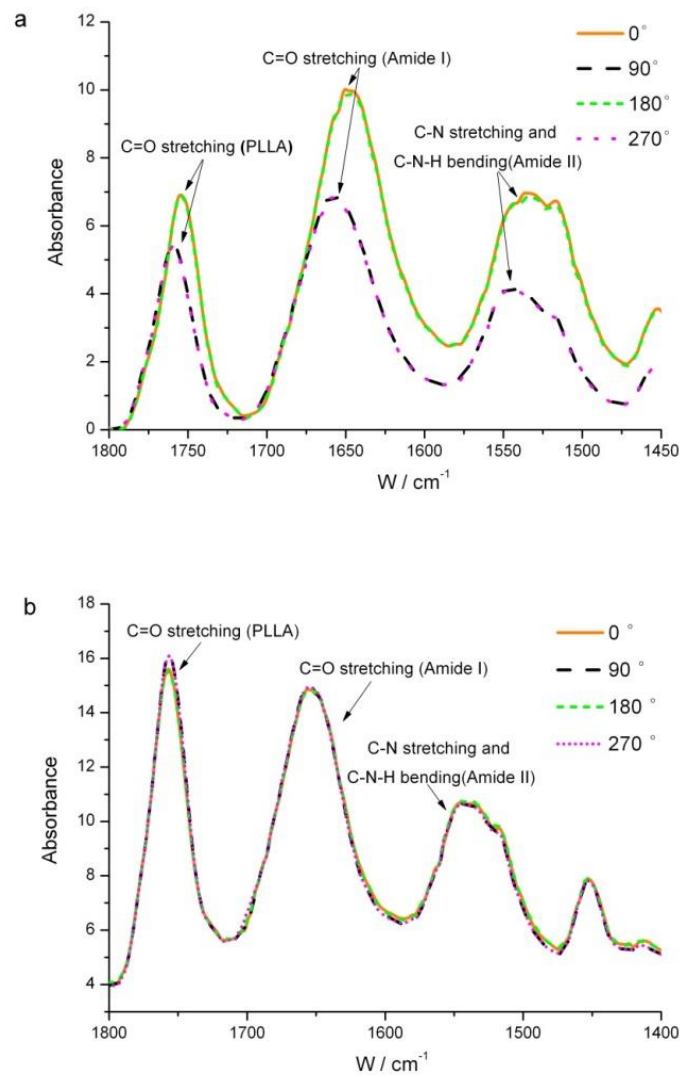


Figure 28: Polarized FTIR spectra of (a) aligned and (b) randomly oriented two-in-one (SF-s-PLLA) nanofibers: angle of the IR beam perpendicular to the fiber axis (0° and 180°) and parallel to the fiber axis (90° and 270°), respectively.

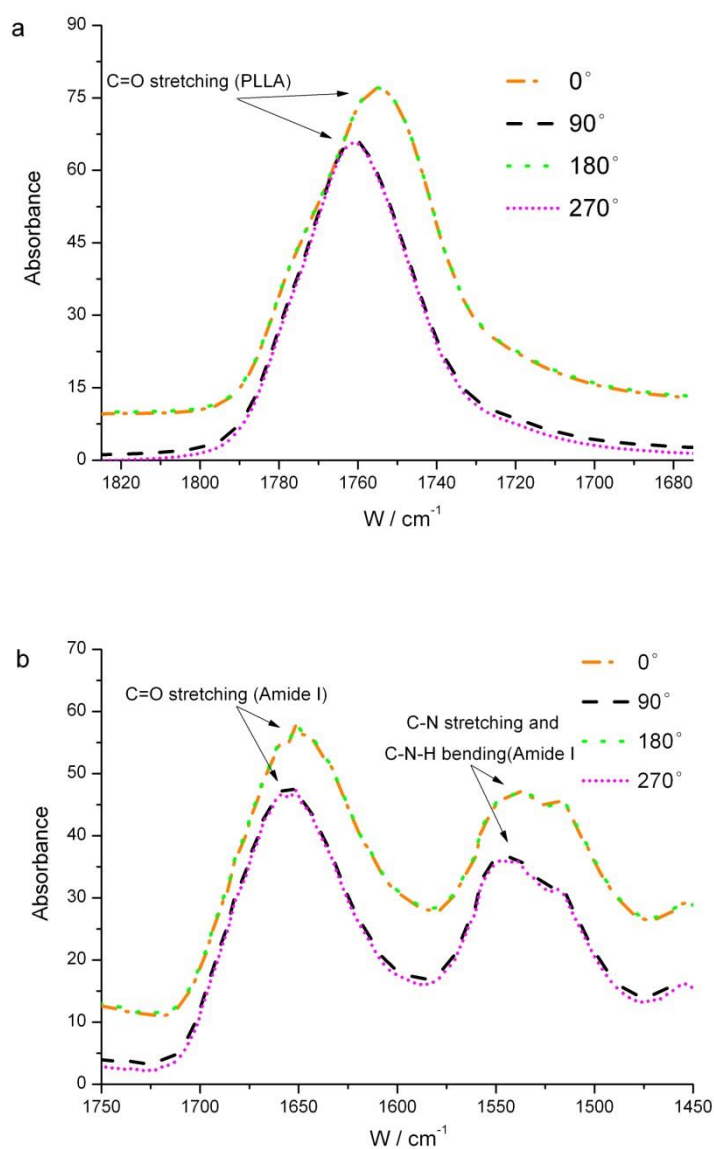


Figure 29: Polarized FTIR spectra of aligned PLLA (a) and SF (b) nanofibers: electric vector of IR beam perpendicular to the fiber axis (0° and 180°) and parallel to the fiber axis (90° and 270°), respectively.

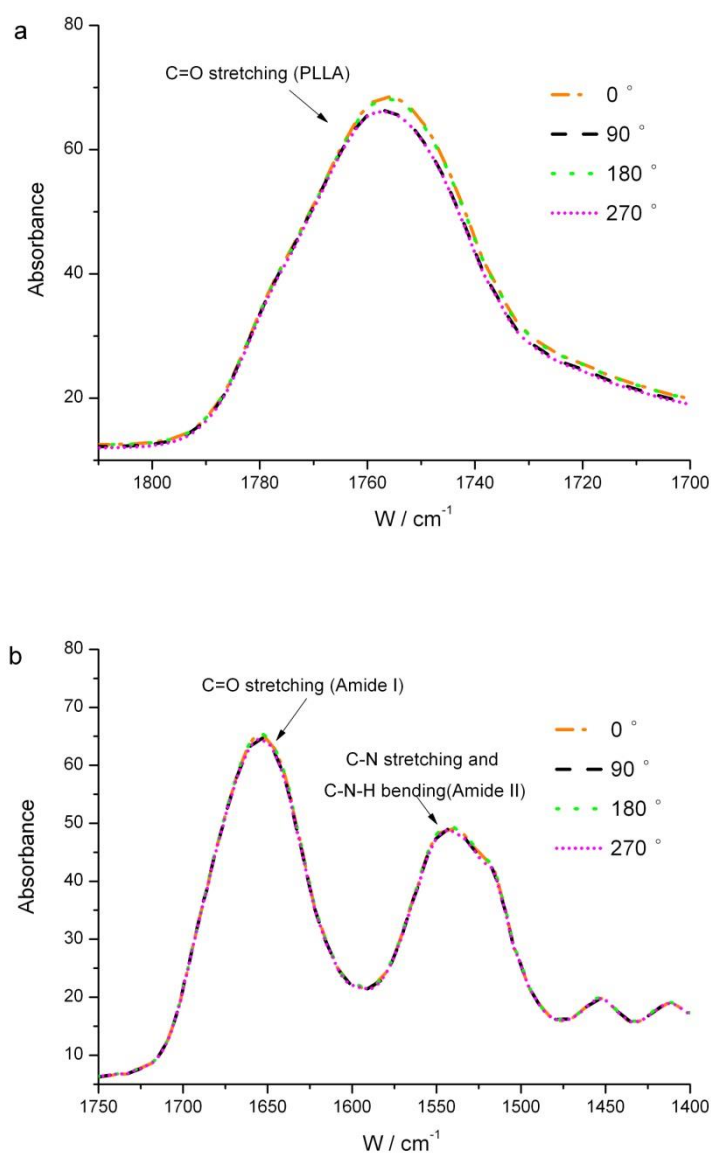


Figure 30: Polarized FTIR spectra of randomly PLLA (a) and SF (b) nanofibers: electric vector of IR beam perpendicular to the fiber axis (0° and 180°) and parallel to the fiber axis (90° and 270°), respectively.

Further, FTIR was used to monitor the crystallinity and secondary structure of two-in-one (SF-S-PLLA) fibers. The effect of post-spin treatment on secondary structure and crystallinity was also monitored. Infrared spectroscopy is a good

technique to monitor the crystallinity of PLA and secondary structure of SF. [171-173] In general, the SF protein in side-by-side fibers can have random coil, α -helix or β -sheet structure which might change with annealing (post-spin treatment) conditions. Similarly, PLLA side can be amorphous or semi-crystalline. For comparison purposes pure PLLA and SF fibers made by electrospinning were also analyzed. It was interesting to study if the interface between SF and PLLA in two-in-one SF-s-PLLA composite fibers could transmit/affect an intentional change in the supramolecular structure from one side to the other. Annealing of two-in-one fibers at 80 °C for 1 h led to change in position and shape of absorption band at 1751 cm^{-1} (C=O stretching band of PLLA) as shown in Figure 31. The peak shifted to higher frequency and became narrow signifying increased crystallinity as shown previously for PLLA fibers by Ribeiro *et al.* [169] The fiber morphology was retained after annealing (Figure 32). The time of thermal annealing was optimized by studying crystallisation of pure PLLA electrospun fibers by differential scanning calorimetry (DSC). A change in crystallinity of randomly oriented PLLA fibers from almost amorphous to around 47% on annealing at 80°C for 1h (Figure 33) was observed. The % crystallinity did not change further on increasing the annealing time to 10 h. The as-spun aligned PLLA fibers were semi-crystalline (crystallinity 22%) and showed enhanced crystallinity to around 59% after annealing. The molecular orientation as observed by polarized FTIR could be responsible for high crystallinity in aligned side-by-side fibers. Stress-induced crystallization is easier for oriented macromolecules.

A change in secondary structure of MeOH annealed SF fibers from random coil to a

β -sheet conformation was also observed by FTIR in two-in-one fibers. As shown in figure 31, the characteristic absorption peaks of SF in two-in-one nanofibers were observed at 1539 cm^{-1} (amide II), 1651 cm^{-1} (amide I) together with a small shoulder at 1520 cm^{-1} in as-spun randomly oriented and aligned two-in-one fibers showing mainly random coil conformation with small amounts of β -sheet structure. The absorption peak at 1520 cm^{-1} is attributed to the β -sheet structure. [173]

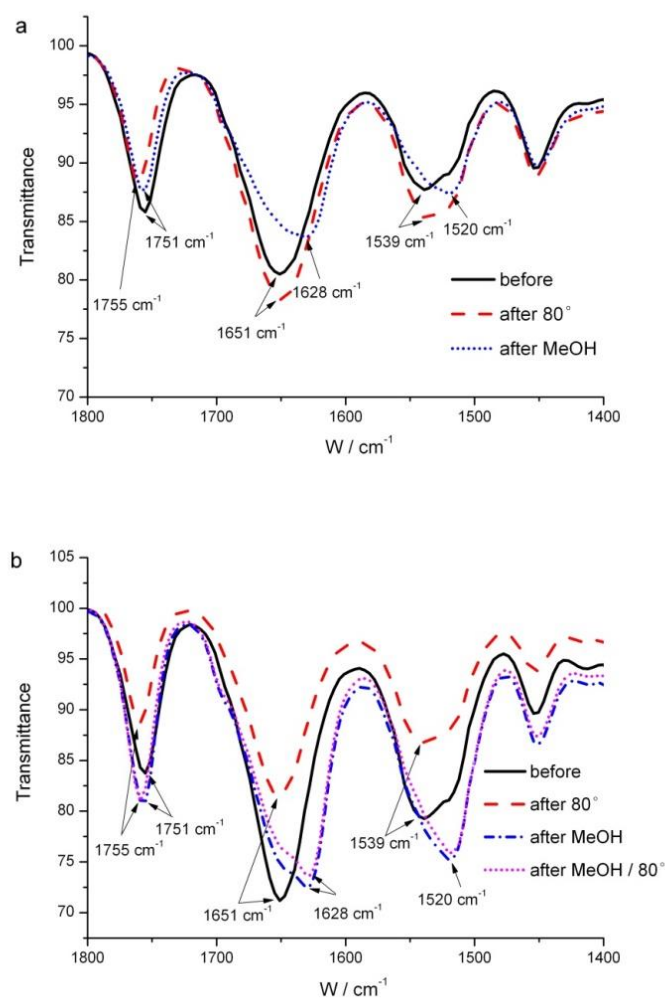


Figure 31: FTIR transmission spectra of two-in-one (SF-s-PLLA) electrospun nanofiber mats (a: randomly oriented and b: aligned fibers) with different post-spin treatments.

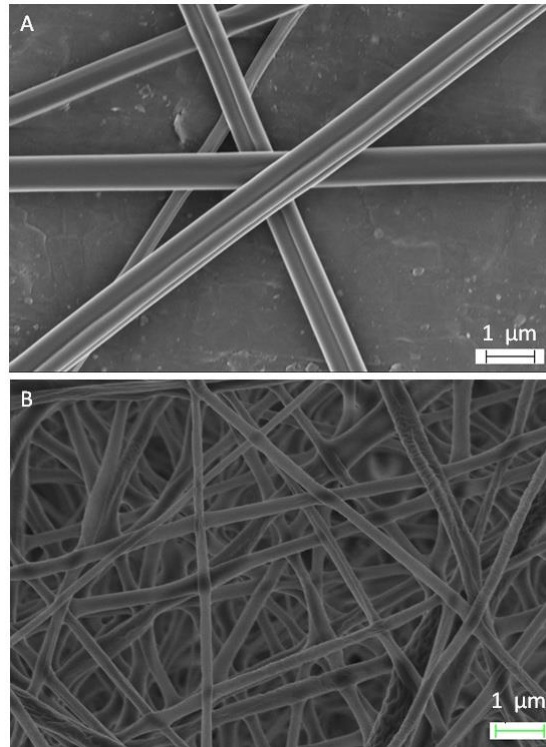
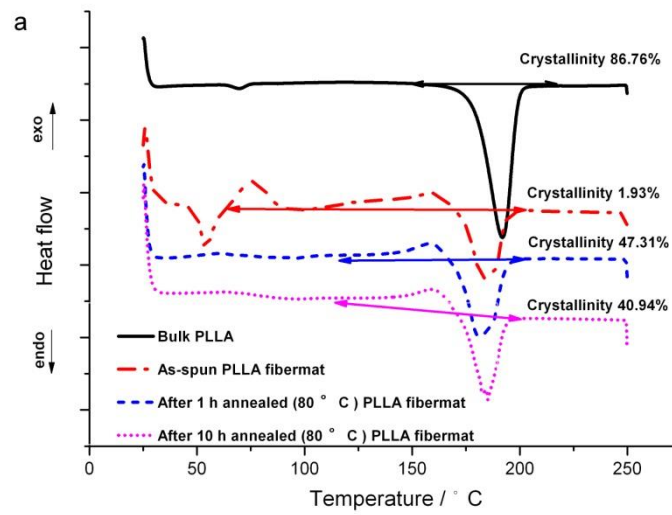


Figure 32: Side-by-side (A) and PLLA (B) fibers after annealing at 80 °C for 10 h.



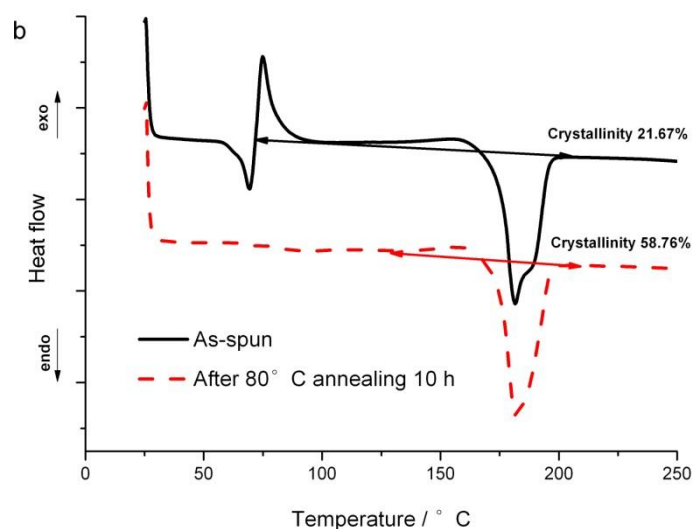


Figure 33: DSC thermograms of PLLA and PLLA electrospun fiber mats (a: random b: aligned fiber mats): before and after annealing at 80°C for different times (1 and 10 h). The DSC measurements were carried out under N₂ atmosphere from 25 to 250 °C with a heating rate of 10 K/min.

After methanol treatment the peaks were shifted to 1520 and 1628 cm⁻¹, which were attributed to the change in structure of SF fibers to mainly β -sheet structure. Fourier self-deconvolution (FSD) of the infrared spectra was carried out to quantify change in secondary structure of as-spun fibers after annealing.^[171] Figure 34 shows the FSD spectra in the amide I region of two-in-one (SF-S-PLLA) aligned fibers before and after MeOH annealing. The fraction of β -sheet structure in MeOH annealed two-in-one aligned fibers was 35% which was significantly increased from 7-9 % β -sheets structure in as-spun fibers (Table 2). At the same time, the fractions of other structures like random coils and turns decreased from 40-45% and 30-34% to 30-33 % and 21-23%, respectively on MeOH treatment. The similar behavior was also

observed for two-in-one randomly oriented fibers (Figure 35 and Table 3). There was no influence of MeOH treatment on the structure of PLLA. The thermal annealing conditions (80 °C for 1h) used for PLLA also did not bring any structural change in SF side. The two sides of two-in-one composite fibers reacted to different annealing conditions individually. FSD studies were carried out in collaboration with Prof. Scheibel's group.

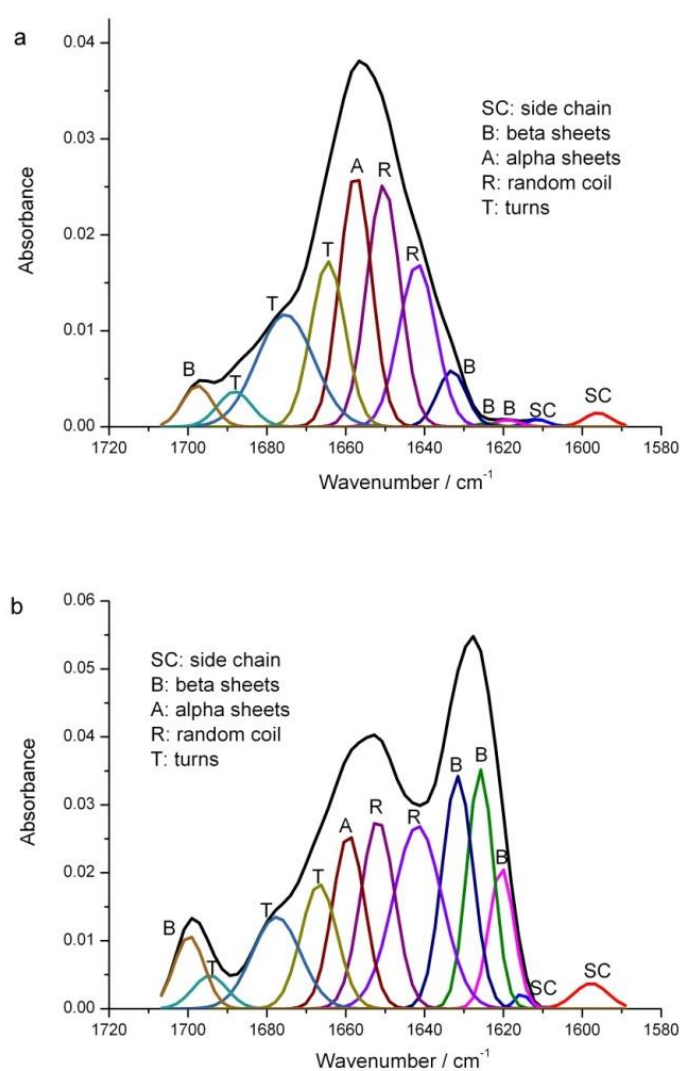
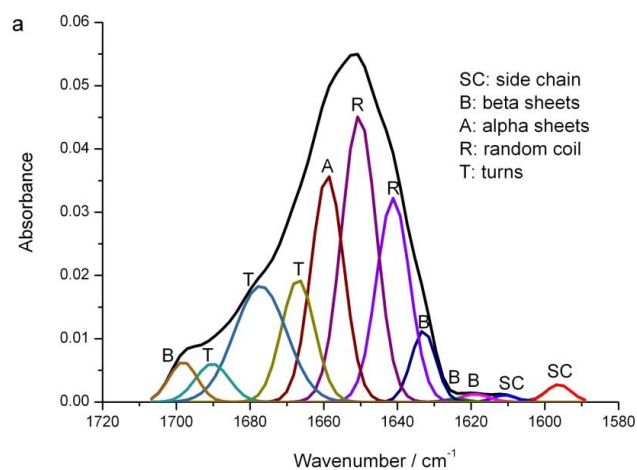


Figure 34: Fourier self-deconvoluted absorbance spectra of two-in-one SF-s-PLLA aligned fibers in amide I region (a) as-spun fiber mat; (b) after MeOH and 80 °C

post-spin treatment.

Table 2: Secondary structure of two-in-one (SF-S-PLLA) aligned fibers before and after post-spin treatments as determined by fourier self-deconvolution in amide I region

	Wavenumber [cm ⁻¹]	1605-1615	1616-1637, 1697-1703	1656-1662	1638-1655	1663-1696
	Assignment	Side chain	β -sheets	α -helices	random coils	turns
As-spun	fraction [%]	0.44	6.77	17.16	44.78	30.85
	sd [%]	0.18	0.91	1.29	2.19	3.38
80 °C	fraction [%]	0.67	9.10	16.76	39.62	33.85
	sd [%]	0.38	2.14	1.13	2.18	2.50
MeOH	fraction [%]	0.34	34.52	11.50	32.62	21.02
	sd [%]	0.72	2.33	0.47	1.48	2.03
80°C	fraction [%]	0.58	34.94	10.73	30.48	23.27
MeOH	sd [%]	0.61	1.39	0.70	1.65	0.42



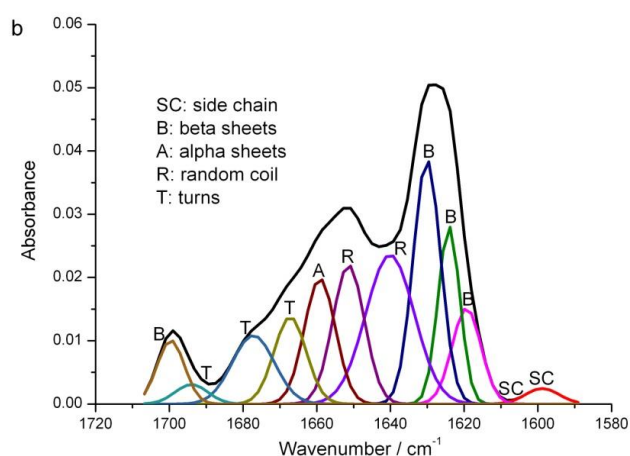


Figure 35: Fourier self-deconvoluted absorbance spectra of two-in-one SF-s-PLLA randomly fibers in amide I region (a) as-spun fiber mat; (b) after MeOH and 80 °C post-spin treatment.

Table 3: Secondary structure of two-in-one (SF-S-PLLA) randomly oriented fibers before and after post-spin treatments as determined by fourier self-deconvolution in amide I region.

	Wavenumber [cm ⁻¹]	1605-1615	1616-1637, 1697-1703	1656-1662	1638-1655	1663-1696
	Assignment	Side chain	β -sheets	α -helices	random coils	turns
Before	fraction [%]	0.48	7.71	18.12	43.19	30.50
	sd [%]	0.28	0.72	2.26	2.74	1.72
80 °C	fraction [%]	0.40	6.31	20.65	41.71	30.93
	sd [%]	0.03	2.90	1.75	2.24	1.58
MeOH	fraction [%]	0	44.23	10.04	28.80	16.93
	sd [%]	0	1.73	0.64	0.62	1.15
80°C MeOH	fraction [%]	0	40.52	10.51	31.08	17.89
	sd [%]	0	0.44	0.64	0.86	0.82

It is interesting to study mechanical properties of side-by-side biocomposite fibers. In general, the electrospun silk fibers have low mechanical properties and brittle in nature. The *Bombyx mori* silk fiber mat with randomly oriented fibers made by solution electrospinning in formic acid showed ultimate tensile strength of 7.25 MPa, elongation at break 3.2% and initial modulus of 515 MPa, respectively. ^[153] It is worth mentioning that use of formic acid for electrospinning provides β -sheet structure which is expected to provide better mechanical properties than the fiber mats with random coil structure as produced by spinning from HFIP. The SF fiber mat spun from HFIP in the present work showed tensile strength 2.66 ± 0.23 MPa, modulus 61.8 ± 8.98 MPa (the modulus was calculated from the ratio of stress and strain for 1-2% elongation, Figure 36 and Table 4) and elongation at break 12.9 ± 1.3 %. The side-by-side SF-s-PLLA fibers were ductile with improved mechanical properties. This could be due to the strong interface between PLLA, SF sides and PLLA bearing applied load. Randomly oriented bio-based synthetic PLLA fibers showed higher tensile strength (4.9 ± 0.72 MPa), modulus 39.9 ± 10.4 MPa and significantly higher elongation at break (136.9 ± 34.7 %) (Figure 37 and table 5). The randomly oriented SF-s-PLLA fibers with side-by-side morphology showed tensile strength of 3.83 ± 0.9 MPa, modulus 73.8 ± 18.7 MPa with elongation at break of 39%. The tensile strength and elongation at break for two-in-one fibers lie between the corresponding values for PLLA and SF randomly oriented fibers.

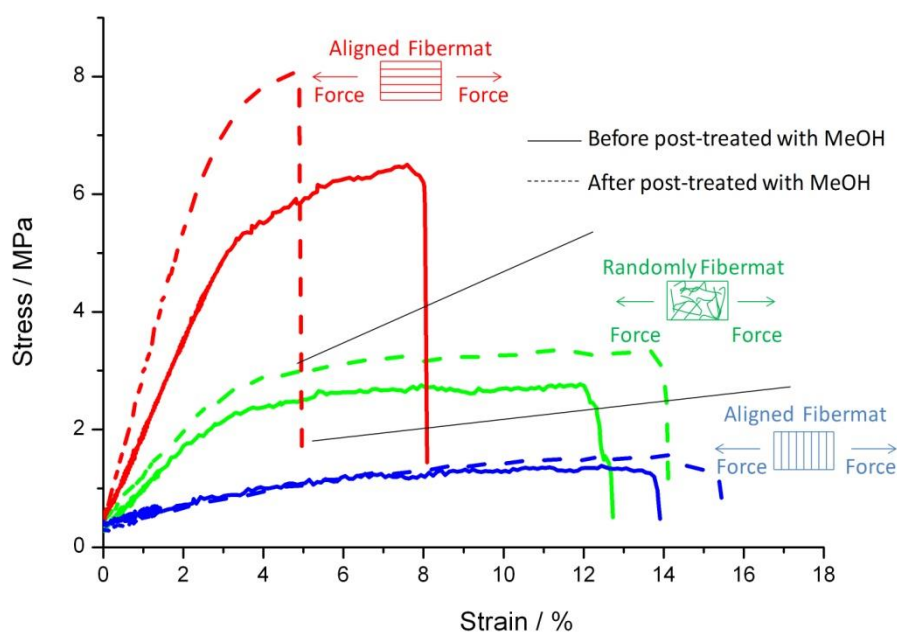


Figure 36: Stress-Strain curves of SF nanofiber mats (randomly and aligned, before and after MeOH treatment).

Table 4: Mechanical properties of SF nanofiber mats

	E-moduls (GPa)	Stress (MPa)	Strain %
As-spun random	0.0618 ± 0.00898	2.66 ± 0.23	12.9 ± 1.3
Treatment* random	0.0731 ± 0.0165	3.52 ± 0.63	14.0 ± 4.9
As-spun parallel	0.17 ± 0.021	7.19 ± 0.98	8.4 ± 1.2
Treatment* parallel	0.194 ± 0.0484	7.05 ± 1.54	6.1 ± 2.0
As-spun orthogonal	0.0166 ± 0.00332	1.40 ± 0.09	11.2 ± 1.5
Treatment* orthogonal	0.0209 ± 0.00353	1.49 ± 0.18	13.4 ± 3.9

* Treatment: The SF nanofiber mats were treated in MeOH atmosphere for 24 h.

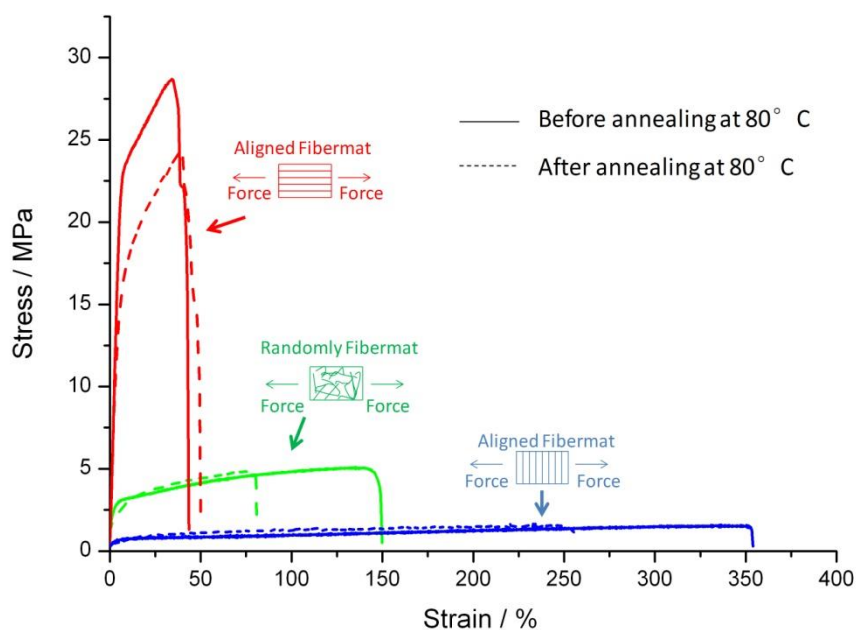


Figure 37: Stress-Strain curves of PLLA nanofiber mats (random and aligned, before and after annealing).

Table 5: Mechanical properties of PLLA nanofiber mats

	E-moduls(GPa)	Stress (MPa)	Strain %
As-spun random	0.0399 ± 0.0104	4.90 ± 0.70	136.9 ± 34.7
Annealed* random	0.0219 ± 0.00476	5.06 ± 1.40	95.9 ± 28.0
As-spun parallel	0.358 ± 0.109	25.72 ± 3.97	38.6 ± 6.5
Annealed* parallel	0.319 ± 0.0364	24.80 ± 2.20	51.8 ± 5.0
As-spun orthogonal	0.0073 ± 0.00329	1.70 ± 0.20	349.1 ± 28.1
Annealed* orthogonal	0.00660 ± 0.00105	1.90 ± 0.40	253.8 ± 5.3

*Annealed: The PLLA nanofiber mats were annealed at 80 °C for 10 h.

Additionally, the aligned fiber morphology for scaffold applications could be highly desirable to guide cellular behavior including cell attachment and proliferation for future applications. Therefore, macroscopically aligned fibers were also tested for mechanical properties. Anisotropy in the mechanical properties i.e. directional dependent mechanical properties were observed in aligned fiber mats. Mechanical properties were much higher in the direction of fiber alignment in comparison to randomly oriented fibers or in the direction perpendicular to fiber alignment. Tensile strength and modulus were 13.97 ± 1.67 MPa and 299 ± 48.7 MPa, respectively, in the direction of fiber alignment with 20% elongation at break and showed strain hardening. The elongation was less than in the randomly oriented fibers due to more entanglements in random fibers and therefore alignment during tensile testing.^[174] The tensile strength and modulus were low in the direction perpendicular to the fiber alignment (1.67 ± 0.11 and 32.8 ± 3.79 MPa) with higher elongation at break (52%) (Figure 38). The anisotropy in mechanical properties is a common behavior in oriented fibers^[175] due to the fact that applied forces act on strong covalent bonds in parallel direction in which unfolded molecules are aligned in the direction of the fiber axis whereas in the perpendicular direction it acts on weak *van der Waals* forces between the macromolecules leading to higher elongation and lower strength and modulus. Similar behavior was also observed for pure PLLA and SF fibers (Figure 36 and 37). PLLA fibers showed much higher tensile strength and modulus in the direction of fiber alignment (25.72 ± 3.97 MPa, 358 ± 109 MPa) in comparison to SF fibers (7.19 ± 0.98 MPa and 170 ± 21 MPa) which could be due to the stress-induced

crystallinity in PLLA fibers during alignment described in the previous section bringing more strength in parallel direction besides load being carried out by covalent bonds. SF fibers had predominantly α -helix structure. Mechanical properties could be further improved by annealing of both sides of SF-s-PLLA fibers by MeOH and heat treatment at 80 °C (structural changes described in previous sections). SF-s-PLLA annealed fibers with predominantly β -sheet structures in SF-side with highly crystalline PLLA side provided tensile strength 16.46 ± 1.38 MPa, modulus 205 ± 20.6 MPa and elongation at break $53.1 \pm 8.1\%$. The values are comparable to the fibers made from a blend of SF and PLA (5:2 wt:wt) by conventional electrospinning and annealed under similar conditions which shows tensile strength 14.82 ± 0.34 MPa, modulus 239 ± 12 MPa and elongation at break $67.7 \pm 5.9\%$ (Figure 39, table 6). 1D biocomposite fibers with side-by-side morphology makes two sides available for further biofunctionalisation, co-culture of cells, drug carrier with dual release-profile etc. which is either limited or not possible with monolith blend fibers. Future research will be directed towards use of these fibers for various applications including cell-culture studies.

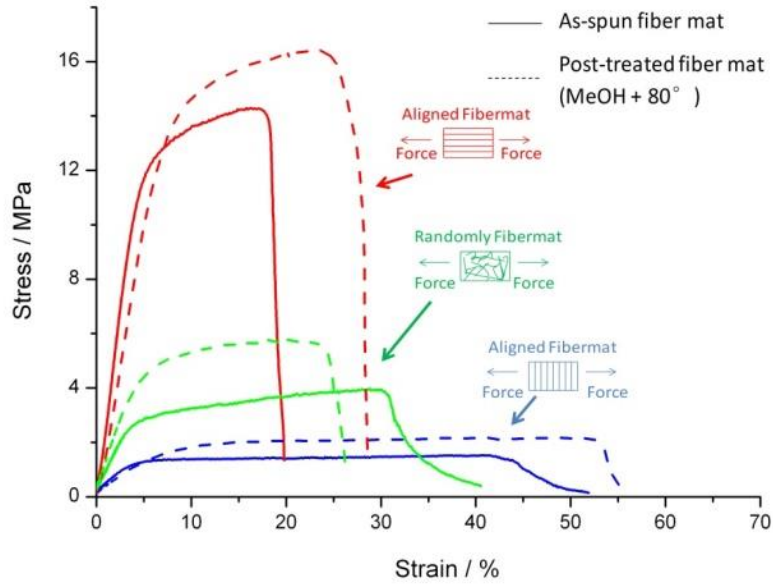


Figure 38: Stress-Strain curves of SF-s-PLLA fiber mats (randomly oriented and aligned, fibers before and after post-spin treatments).

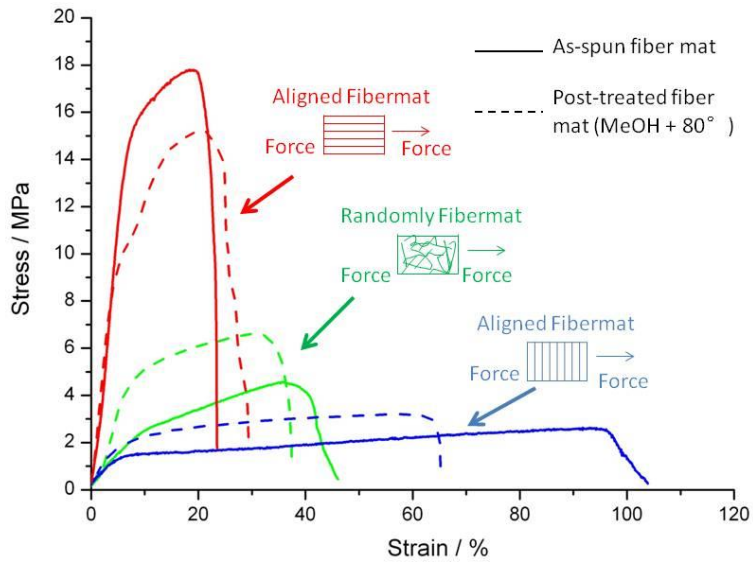


Figure 39: Stress-Strain curves of fiber mats made from a blend of SF and PLLA (SF:PLLA 5:2 wt:wt) (randomly oriented and aligned, fibers before and after post-spin treatments).

Table 6: Mechanical properties of fibers made from a blend of SF and PLLA

	E-moduls(GPa)	Stress (MPa)	Strain %
As-spun random	0.0652 ± 0.0349	6.54 ± 0.83	44.3 ± 11.3
Annealed* random	0.0905 ± 0.0307	6.64 ± 0.98	38.5 ± 11.9
As-spun parallel	0.2790 ± 0.0144	18.16 ± 1.09	24.8 ± 2.1
Annealed* parallel	0.2390 ± 0.0120	14.82 ± 0.34	30.4 ± 4.5
As-spun orthogonal	0.0281 ± 0.0045	2.72 ± 0.09	101.8 ± 4.0
Annealed* orthogonal	0.0360 ± 0.0064	3.14 ± 0.14	67.7 ± 5.9

*Annealed: The nanofiber mats were treated in MeOH atmosphere for 24 h then at 80 °C for 10 h.

The results about the mechanical properties of single nanofiber and nanofiber mats show that, the crystallinity is not the key point for the mechanical properties. From our results, the most important factor for mechanical properties is the orientation of polymer chains and nanofibers.

As show in figure 40, in thin nanofiber, the orientation of polymer chains is higher than in thick nanofiber. The stress of single fiber increased with the increase of orientation of polymer chains. Similar in nanofiber mats, both aligned and randomly nanofiber mat were spun at the same conditions, only difference is the aligned nanofiber mat has a higher orientation of nanofibers, as a result, the stress of aligned nanofiber mat (parallel) is also higher.

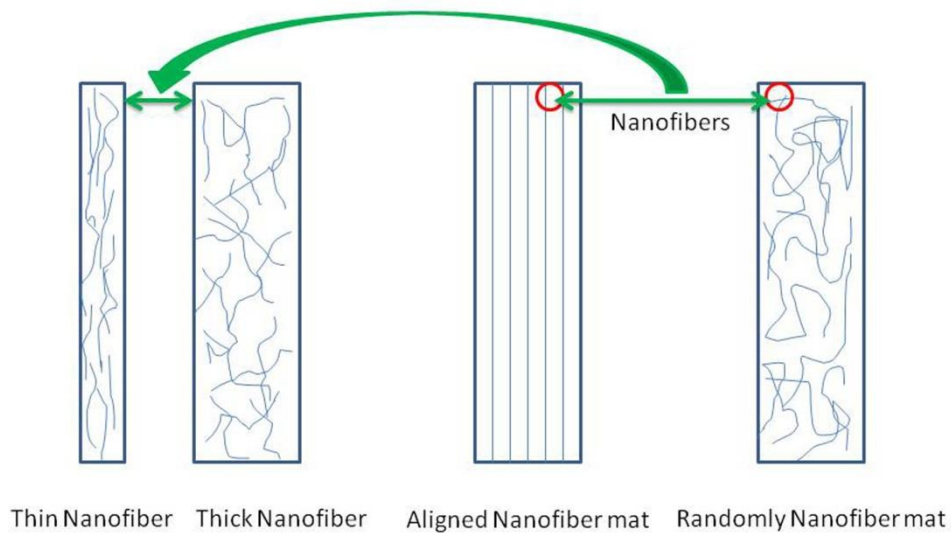


Figure 40: Polymer chains in single nanofiber and nanofiber mats.

3.1.3 Conclusion

A combination of appropriate reinforcing material and morphology is necessary for the properties improvement of a polymeric fibrous material. Two-in-one (SF-s-PLLA) (PLLA: SF = 2:5, wt: wt) bio-based ductile composite fibers with side-by-side morphology and good mechanical properties were generated using bicomponent electrospinning. Significant improvement in the mechanical properties of SF fibers could be achieved by PLLA in combination with a side-by-side fibrous morphology. The strain at break of nanofiber was increased from <4% (SF) to about 50% (side-by-side), there was no cracks till elongation 20% of SF-s-PLLA fiber. Because of better mechanical properties, the SF-PLLA nanofiber may expand the application area of SF nanofiber.

The size of nanofiber is the most important factor for the mechanical properties. In the ultrafine nanofibers, the polymer chains will be oriented. After annealing the crystallinity of PLLA nanofibers increased. But mechanical properties of annealed

PLLA nanofibers are almost same mechanical properties of as as-spun PLLA nanofibers. As a result, the most cause of size effect is high orientation of polymer chains. It is possible to make the nanofibers with the aimed mechanical properties through combination of different materials and control of diameter of nanofibers.

The two sides of two-in-one fibers retained their individual secondary structure before and after annealing without affecting each-other in a significant way. The annealed fibers on both sides by MeOH and heat treatment at 80 °C provided predominantly crystalline and β -sheet structures with tensile strength 16.5 ± 1.4 MPa, modulus 205 ± 20.6 MPa and elongation at break $53 \pm 8\%$ in silk based electrospun fibers. These values are very similar to the fibers made from a blend of SF and PLLA using similar ratio of the two components (SF: PLLA 5:2) as used for making side-by-side fibers. It would be interesting to use such fibers for biodegradation studies, cell culture, scaffold and drug-release applications in the future to exploit the utility of side-by-side morphology, and surface chemistry of two sides.

3.2 A self-coiled bicomponent nanofiber of Poly(N-isopropylacrylamide) (PNIPAM) and thermoplastic polyurethane (TPU)

(Part of this work has been published in *Macromol. Mater. Eng.* 2017, 1700248 with the title: “ Tailoring the Morphology of Responsive Bioinspired Bicomponent Fibers” by Marvin Gernhardt, Ling Peng, Matthias Burgard, Shaohua Jiang, Beate Förster, Holger Schmalz and Seema Agarwal)

After establishing conditions for the formation of side-by-side fibers combination of

SF and PLLA, it was of interest to use such fiber morphologies for different combination of polymers. One of the interesting combinations could be PNIPAM and TPU.

PNIPAM is one of the widely used thermoresponsive polymers for different applications including actuators. It possesses the lower critical solution temperature (LCST) around 32°C. The cross-linked PNIPAM reveals temperature dependent swelling / shrinkage below and above LCST. Thermoresponsive actuators are based on a bilayer structure with an active polymer undergoing swelling / shrinkage at different temperatures in water and a passive layer which is not affected by temperature and water.^[176-178] In bilayer structures with PNIPAM as an active layer, the differential swelling / shrinkage between the two layers leads to actuation. The actuation time varies from many seconds to minutes and hours depending on the layer size and materials used in bilayers.^[179-183] Recently, our group demonstrated ultra-fast thermoresponsive rectangular-shaped actuators with direction-controlled reversible rolling, coiling and bending motions at different temperatures in water based on bilayer fibrous nonwovens in 0.6-5 s.^[180, 181] PNIPAM and thermoplastic polyurethane (TPU) fibers oriented in different directions were used as active and passive layers, respectively.

The polymers of different polarity, functionality, physical properties, etc. can also be combined in one fiber in the form of side-by-side and coaxial structures and provide novel opportunities of getting special morphologies, dual functionality, extreme dipole moments, multiple drug release profiles, etc.^[26, 28, 184-188] One of the

interesting aspect of the bicomponent morphology in textile fibers is to make self-crimping synthetic fibers by using difference in modulus or differential shrinkage of the two components in the fiber.^[189-191] Very thin (250-400 nm) self-crimping / coiling synthetic fibers with two components were discussed in literature using various combinations of polymers such as polyacrylonitrile-polyurethane^[135], poly(m-phenylene isophthalamide)-polyurethane^[28, 164] formed by electrospinning^[76]. Not only side-by-side but off-centered coaxial morphology of fibers also provide coiled fibers.^[28] Forming self-crimping fibers is inspired by the structurally asymmetrical self-crimping wool fibers in which ortho-cortical and para-cortical cells adhere to each other as two sides of a fiber in a side-by-side morphology.^[192, 193] The differential swelling on two sides of the fibers with moisture leads to the fiber crimp. Side-by-side bilayer micro-fibers with poly(vinyl cinnamate) (swellable in organic solvent) and chemically cross-linked 1 : 1 mixture of poly(ethyleneimine) (PEI)/(PEO) (hydrogel; swellable in water) revealed a reversible change between coils and straight fibers when put in dioxane and water respectively.^[184]

In this work experimental results of temperature-triggered reversible coiling and decoiling of bicomponent fibers of PNIPAM and TPU are presented. The effect of temperature and the ratio of two polymers on coiling behavior were also studied.

3.2.1 Bicomponent single fiber of PNIPAM and TPU

Bicomponent fibers were combined a copolymer of NIPAM and 4-acryloyl-benzophenone (ABP) as responsive polymer and TPU as a nonresponsive polymer.

The bicomponent fibers of PNIPAM-ABP and TPU were prepared using special off-centered and side-by-side nozzle^[28] using 32 and 18 wt.% solutions of PNIPAM-ABP and TPU, respectively, in DMF (Figure 41). Fluorescein isothiocyanate isomer I (FTIC I, 0.8 wt% with respect to the weight of PNIPAM) was added to the PNIPAM solution. ABP (4 wt% with respect to the weight of TPU) was added to TPU solution. Two injector jet pumps were used to control the flow rates of the two solutions to form bicomponent fibers with different polymer ratios. The distance between the nozzle and the collector was 15 cm and the applied voltage was 12.5 kV. An aluminum frame was used for collecting single fibers.

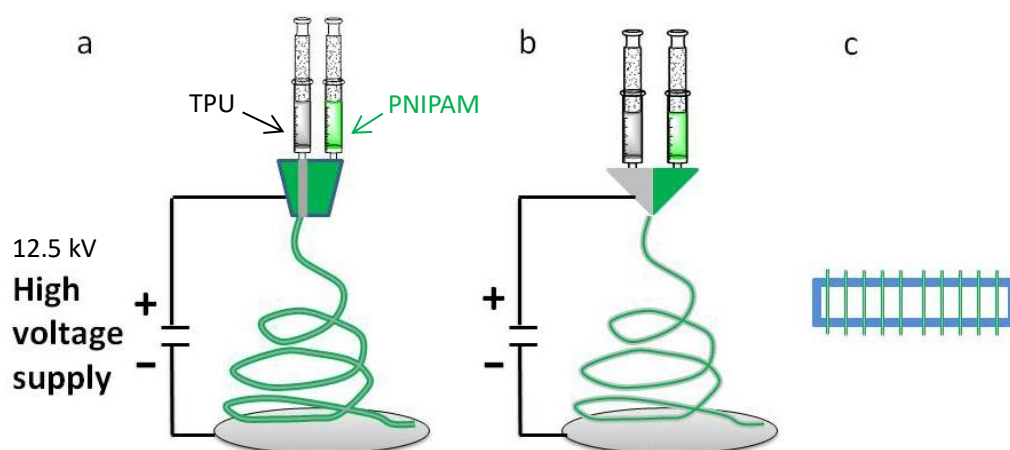


Figure 41: a) Sketch of off-centered electrospinning; b) Sketch of side-by-side electrospinning; c) aluminium frame for collecting single fibers.

PNIPAM shows thermal dependent water solubility, to provide a water stable bicomponent fiber with PNIPAM as one of the components, it was necessary to cross-linked PNIPAM. Therefore a copolymer of NIPAM with 4 wt% photo cross

linkable ABP monomer was used as active responsive component. This cross linked PNIPAM-ABP fibers shows LCST at 27 °C. (Figure 42) This work was done by Li Liu, a PhD student of our group.

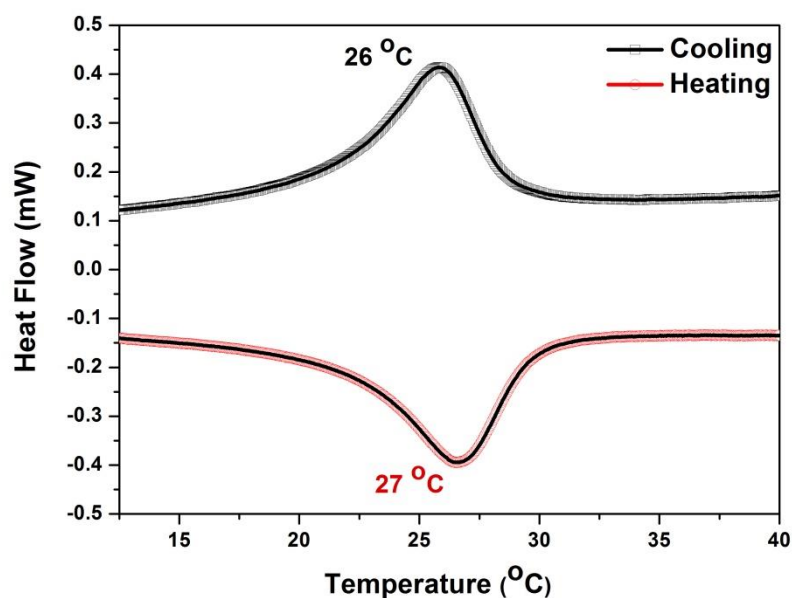


Figure 42: μ -DSC curve of PNIPAM-ABP.

After spinning the PNIPAM side was cross-linked by exposing to UV light of 320-400 nm wavelength for 30 min. The PNIPAM-ABP and TPU fibers using side-by-side spinneret with different ratios of polymers in two sides were prepared as shown in Figure 43. The morphology of fibers was revealed by scanning SEM and fluorescence microscopy. The PNIPAM side with FTIC showed green color under 450-490 nm light (Figure 44).

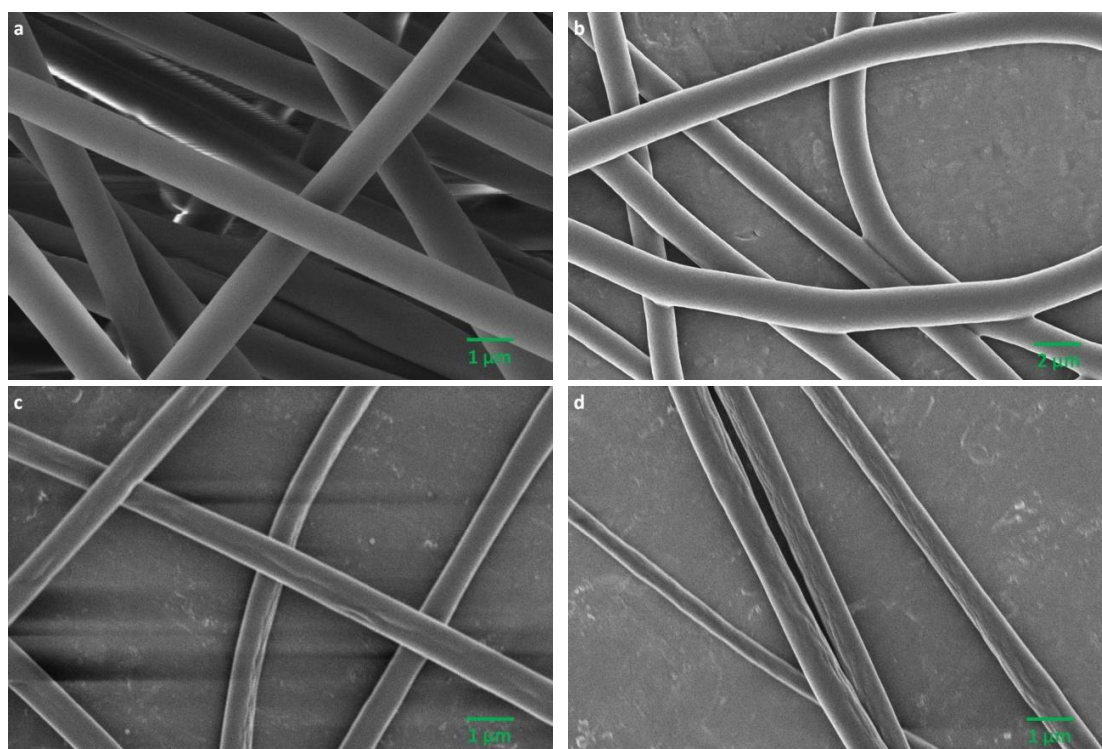


Figure 43: SEM images of side-by-side as-spun (a) PNIPAM, (b) TPU, (c) PNIPAM-ABP:TPU (7:3) and (d) PNIPAM-ABP:TPU (3:7) fibers.

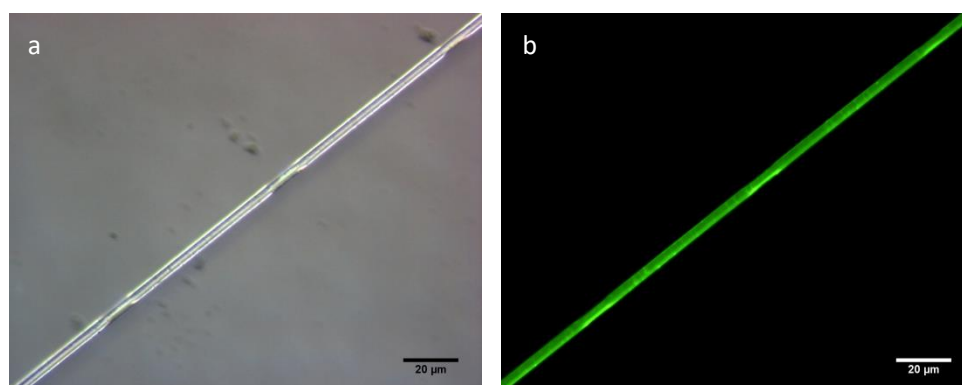


Figure 44: Images of side-by-side as-spun PNIPAM-TPU fibers under fluorescence microscopy: (a) normal light; (b) 450-490 nm light. Scale bar 20 μm.

For unambiguous characterization of fiber morphology, the fiber cross-sections were scanned by TEM. After cutting of fibers embedded in epoxy, the off-centered

morphology of fibers was revealed by scanning TEM. As show in figure 45, off-centered fibers were formed from both off-centered and side-by-side spinnerets.

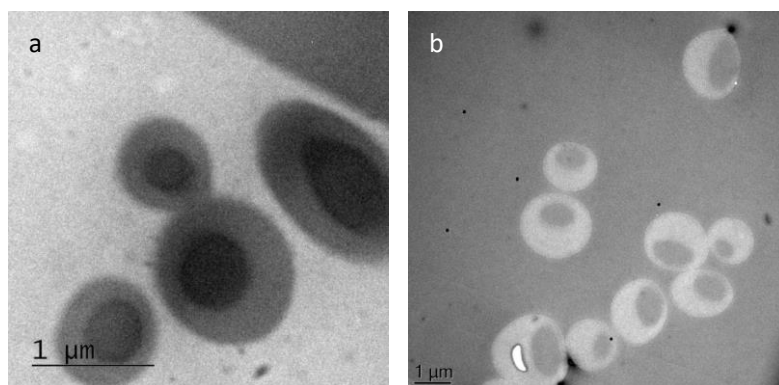


Figure 45: TEM images of cross section of as-spun PNIPAM-ABP: TPU (7:3) fibers: (a) off-centered spinning; (b) side-by-side spinning

Cross section of fibers with different polymer weight ratios on the two sides of the spinneret were also scanned with TEM. It shows clearly that, polymer areas are different in fibers (figure 46). The indirect experiment of changing the weight ratios of the two polymers clearly showed that the PNIPAM-ABP made the shell and TPU made the core of the fibers. The off-centered morphology was also proved by the results of fluorescence microscopy: the FTIC labelled PNIPAM part covered TPU part in fiber and the fiber showed only green color under fluorescence microscope (figure 44).

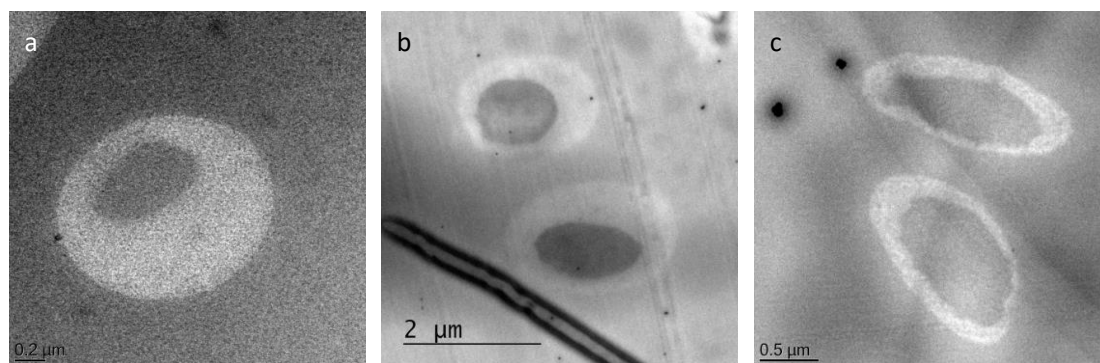


Figure 46: TEM images of cross section of side-by-side as-spun PNIPAM-ABP: TPU fibers: polymer ratio PNIPAM-ABP: TPU = (a) 7:3; (b) 1:1 and (c) 3:7.

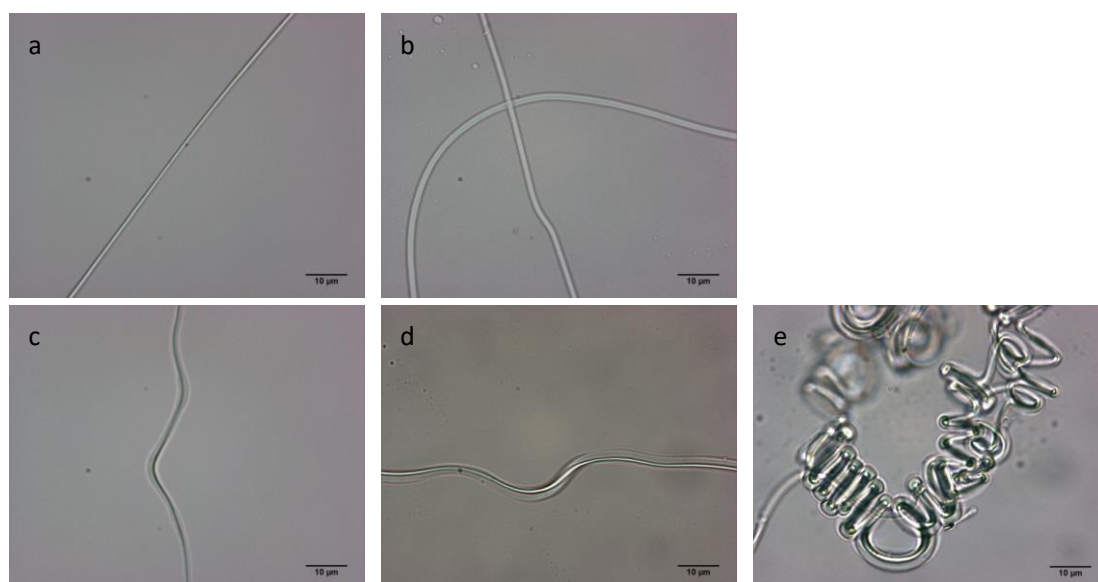


Figure 47: Images of side-by-side as-spun fibers under fluorescence microscope in aqueous environment: (a) pure TPU fiber in ice water; (b) pure PNIPAM-ABP fiber in ice water; (c) PNIPAM-ABP-TPU fiber in 40 °C water; (d) PNIPAM-ABP-TPU fiber in 18°C water and (e) PNIPAM-ABP-TPU fiber in ice water. Scale bar 10 μm.

PNIPAM-ABP swelled in water. Compared with pure TPU or PNIPAM-ABP fibers, the PNIPAM-ABP-TPU fibers show clearly two components in one fiber: the transparent component (outside) is PNIPAM-ABP, the other component (inside) is

TPU. (Figure 47)

Single fiber self-crimping test was carried out on a glass slide with off-centered spun single fibers. One end of the single fiber was fixed on the glass slide with glue. The other end of fiber was free. The fiber was free lying on the glass slide. Then a pipette was used to put on the fiber a drop cold or hot aqueous water.

Under different polymer ratios, 5 single fibers with different diameters (the diameter of fibers was determined by SEM, figure 48) were tested respectively. Results are show in table 7.

Table 7: Self-crimping test of off-centered spun fibers with dfferent polymer ratios:

Ratio: (PNIPAM:TPU)	The number of fiber coiled	The number of fiber did not coiled
7:3	1	4
1:1	0	5
3:7	0	5

As show in figure 49, most of off-centered spun fibers have no self-crimping ability. Only some bending/buckling behaviors were observed. Although the single fibers have different diameters, these fibers had similar behavior in self-crimping test. That means diameter should have no influence on crimping behavior of fibers.

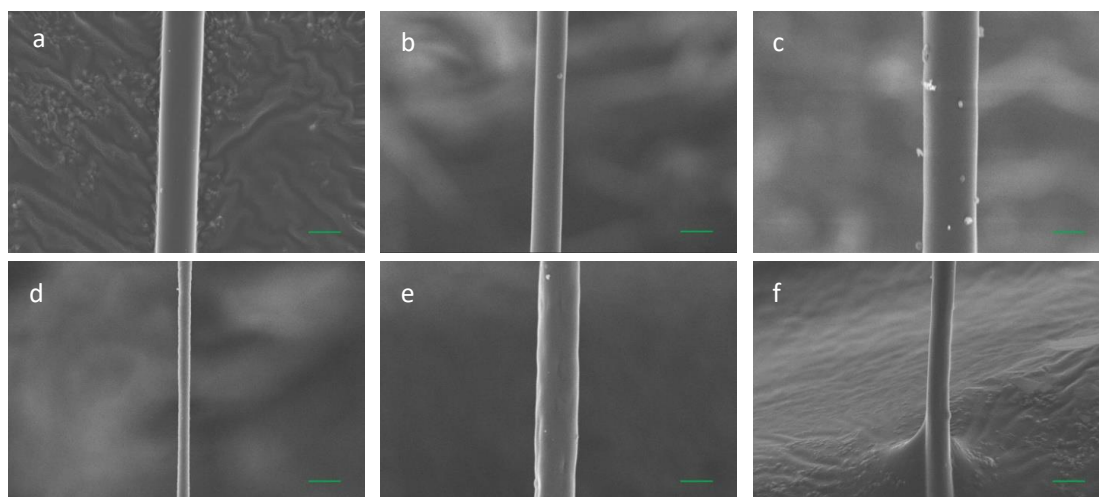
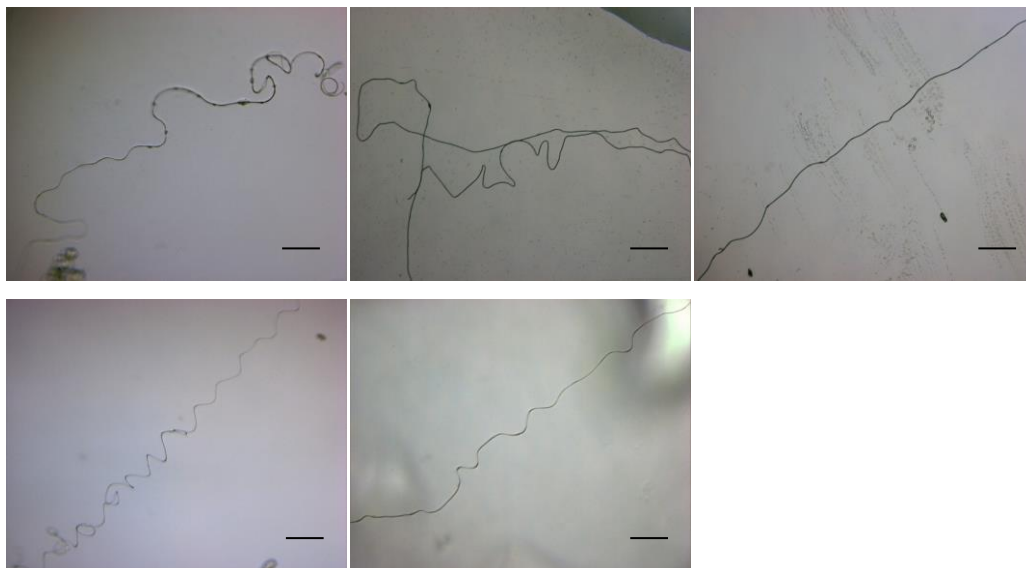


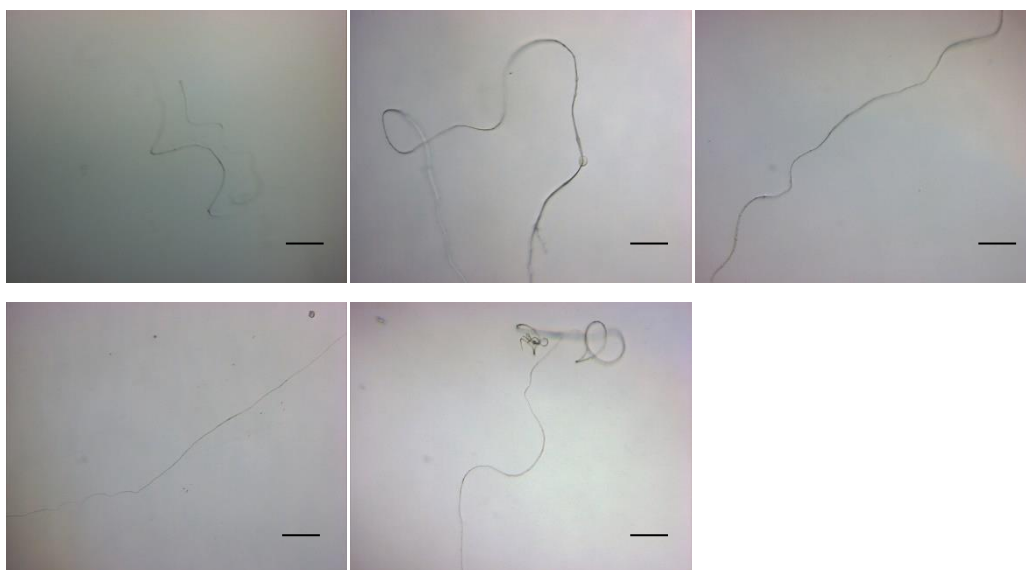
Figure 48: SEM images of off-centered spun fibers: PNIPAM-ABP:TPU (7:3) (a, b); PNIPAM-ABP:TPU (1:1) (c, d); PNIPAM-ABP:TPU (3:7) (e, f) fibers. Scale bar 1 μm .

As shown in Figure 45, because of difference of electrical conductivity of polymer solutions (TPU: 4.1 $\mu\text{S}/\text{cm}$; PNIPAM-ABP: 1.5 $\mu\text{S}/\text{cm}$), the side-by-side spun fibers have also an off-centered morphology. Same single fiber self-crimping tests were carried out with these fibers. The fiber coiled in ice-cold water (0 $^{\circ}\text{C}$, temperature below LCST) and the sizes of the coils were dependent upon the ratio of the two polymers. More PNIPAM-ABP in side-by-side spun fibers (7:3 PNIPAM-ABP: TPU) provided smaller coils (radius $\sim 9 \mu\text{m}$) in comparison to the fibers with more TPU (1:1 PNIPAM-ABP: TPU, radius $\sim 12.6 \mu\text{m}$; 3:7 PNIPAM-ABP: TPU, radius $\sim 21 \mu\text{m}$). The coils unraveled which resulted in straight fibers in water at temperature 40 $^{\circ}\text{C}$ (temperature above LCST) (Figure 50). The process was reversible. Results of self-crimping test of side-by-side spun fibers are show in table 8. Five samples were tested each time and the reproducibility is also documented in table 8.

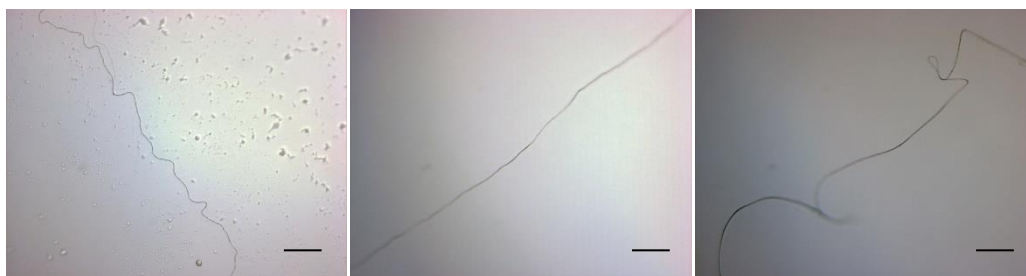
PNIPAM-ABP: TPU = 7:3



PNIPAM-ABP: TPU = 1:1



PNIPAM-ABP: TPU = 3:7



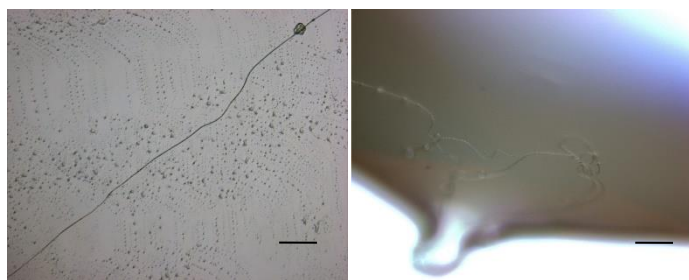


Figure 49: Self-crimping test of off-centered spun PNIPAM-ABP: TPU fibers with different polymer ratios. Scale bar 100 μm .

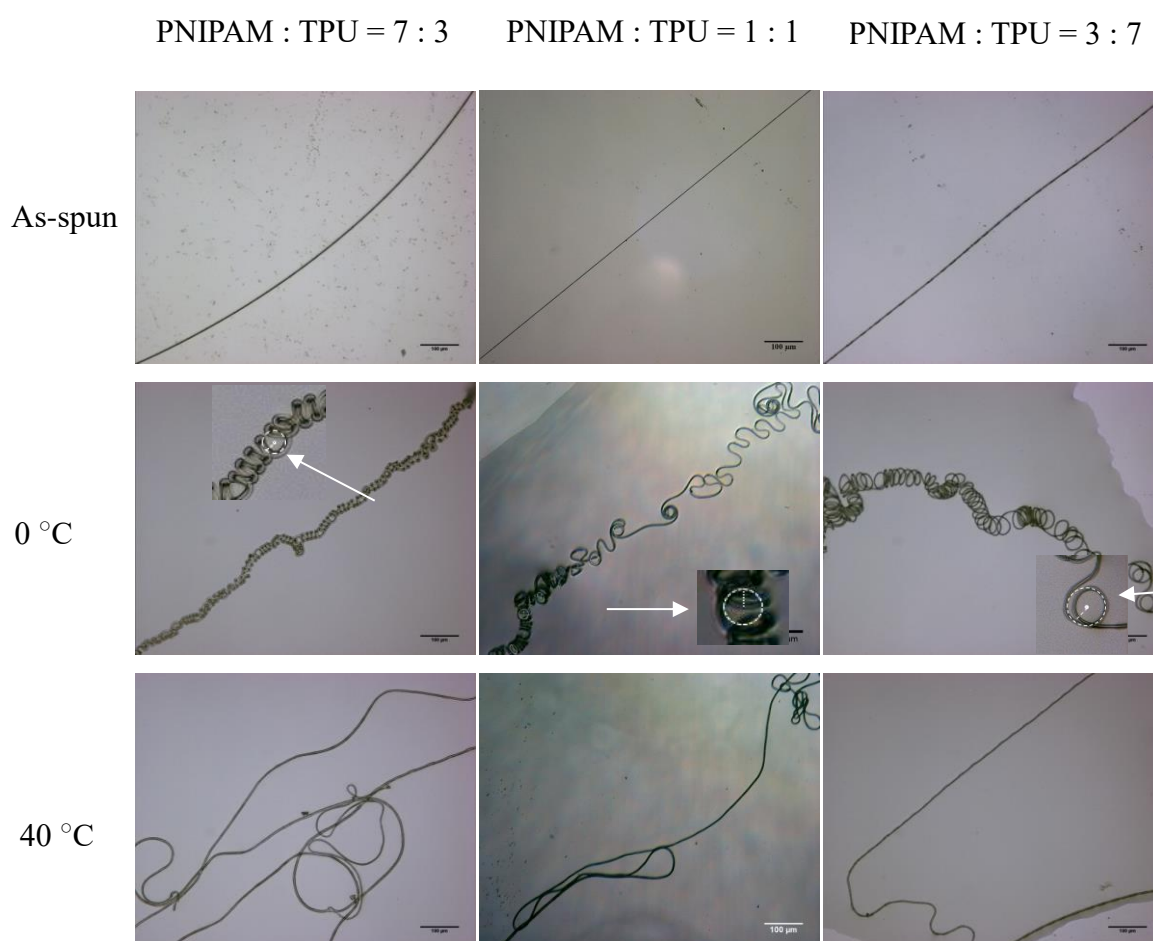


Figure 50: Images of PNIPAM-TPU fibers with different ratios of PNIPAM and TPU at different temperatures in water. Scale bar 100 μm .

The curvature = $1/r$ was used to describe the coiling degree of PNIPAM-ABP-TPU

single fiber in ice water. As shown in table 8 and figure 50, the curvature of single fiber was increased with higher PNIPAM-ABP ratio. The curvature is linearly increased against PNIPAM-ABP ratio. (Figure 51)

Table 8: Self-crimping test of PNIPAM-ABP-TPU fibers using side-by-side spinneret with different polymer ratios

Ratio (PNIPAM:TPU)	The number of fiber coiled	The number of fiber did not coiled	Curvature (μm^{-1})
7:3	5	0	0.11 ± 0.004
1:1	4	1	0.079 ± 0.003
3:7	4	1	0.047 ± 0.001

Although both off-centered and side-by-side spun fibers have off-centered morphology, but in side-by-side spun fibers, the position of two polymer layers is more asymmetrical (Figure 45), this caused the different behaviors of electrospun single fiber in ice water. Offset-degree (OD) was used to define the off center morphology of these fibers. As show in figure 52, in cross section of one fiber, the largest distance d_1 and the smallest distance d_2 between outside surface and inner interface were found out. d_1 and d_2 should be in one line, and this line should pass through the center point of this fiber. The offset-degree $OD = d_1/d_2$. $OD \geq 1$. When the fiber is core-shell fiber, $d_1=d_2$, $OD = 1$; When the fiber is side-by-side fiber, $d_2 = 0$, $OD \rightarrow \infty$.

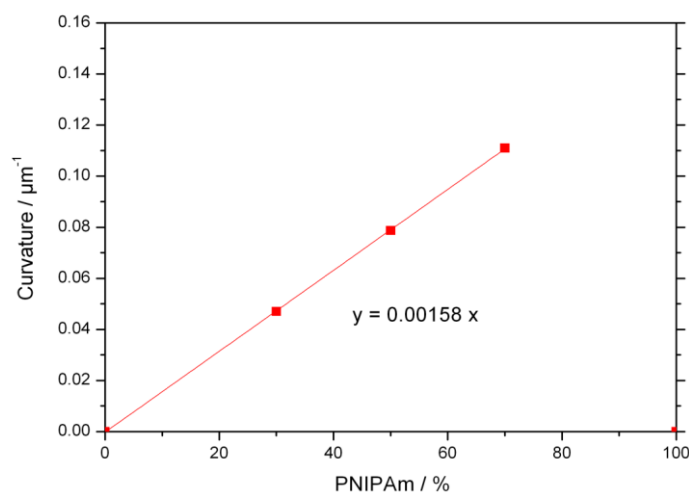


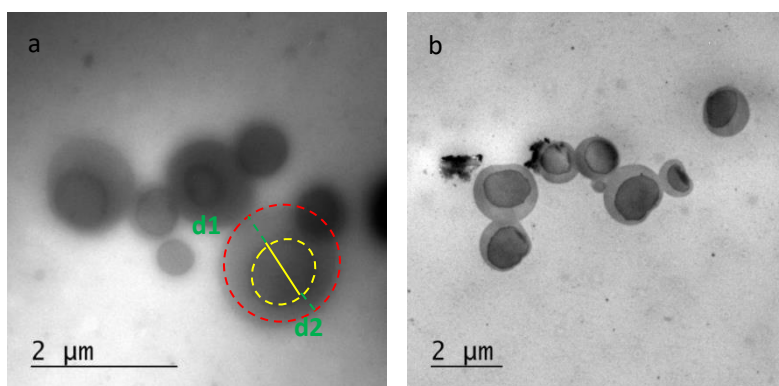
Figure 51: Plot of curvature against PNIPAM ratio in PNIPAM-TPU single fiber.

Table 9: Offset degree of different fibers:

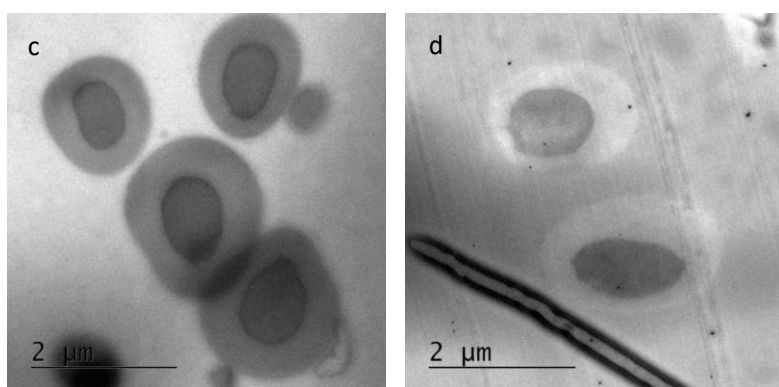
Ratio (PNIPAM:TPU)	3:7	1:1	7:3
Use of side-by-side spinneret	3.56 ± 1.23	3.71 ± 0.69	6.35 ± 0.93
Use of off-set coaxial spinneret	1.61 ± 0.54	1.66 ± 0.05	1.83 ± 0.19

As show in table 9, the “side-by-side” spun fibers have higher OD value. With higher PNIPAM-ABP ratio, the electrospun fibers have higher OD value. Compared with “off-set” spun fibers, the “side-by-side” spun fibers show more anisotropic morphology. That’s the reason, why the “side-by-side” spun fibers show more intensive coiling behavior than “off-set” spun fibers in ice water.

PNIPAM-ABP: TPU = 3:7



PNIPAM-ABP: TPU = 1:1



PNIPAM-ABP: TPU = 7:3

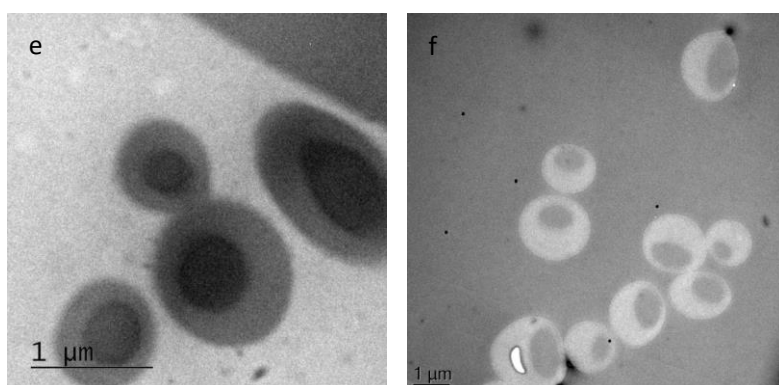


Figure 52: TEM images of cross section of off-center spun (a, c and e) and side-by-side spun (b, d and f) PNIPAM-ABP-TPU fibers with different polymer weight ratios.

PNIPAM-ABP-TPU (7:3) single fiber was used to study time temperature dependent coiling. At 18 °C (even kept for 30 min) the fiber showed buckling. The same fiber coiled on decreasing the temperature to 0 °C by putting ice. (Figure 53)

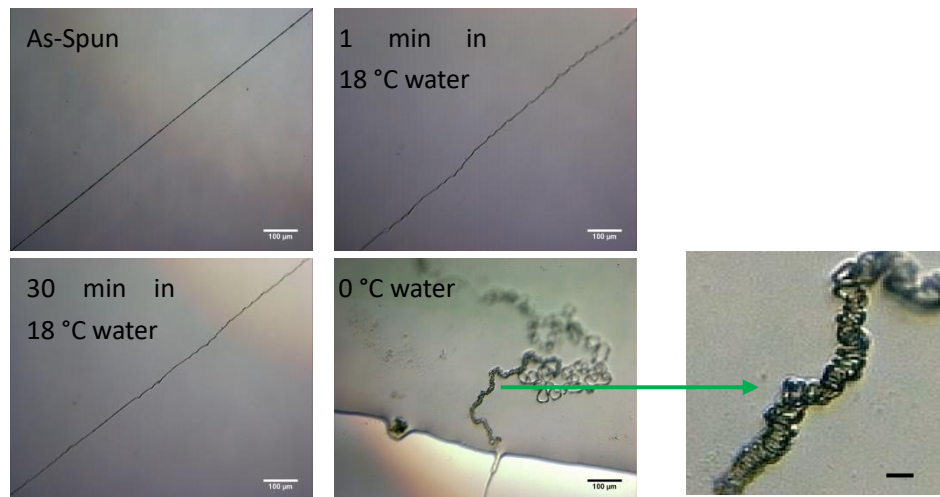


Figure 53: PNIPAM-TPU 7:3 side-by-side spun fiber in water at different temperatures. Scale bar 100 μm ; scale bar in magnified image 10 μm .

Further to test our hypothesis, we tried another combination of PNIPAM and a copolymer of methyl methacrylate and butyl methacrylate (P(MMA-co-BMA)) (1:1). The bicomponent fiber shows a clearly side-by-side morphology.^[240] The work was done by Marvin Gernhardt, a former master student of our group. This single fiber was used to study temperature dependent coiling. The coiled fiber decoiled itself when temperature increased. (Figure 54)



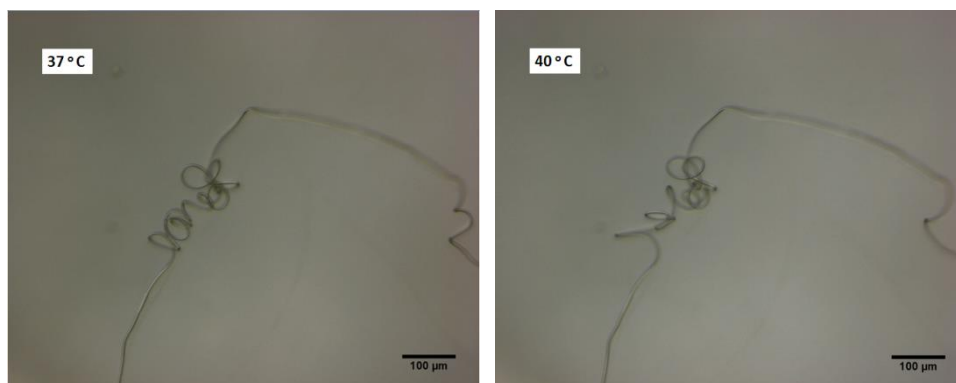


Figure 54: PNIPAM-P(MMA-co-BMA) 1:1 side-by-side spun fiber in water at different temperatures. Scale bar 100 μm .

3.2.2 Conclusions

A self-coiled bicomponent (PNIPAM-TPU) fiber with off-centered morphology was generated by using bicomponent electrospinning. The off-centered morphology was confirmed by TEM and SEM. PNIPAM was proved as shell where TPU was as core. Unlike off-centered spun PNIPAM-TPU fiber, due to higher asymmetry of two polymers in fiber, the side-by-side spun PNIPAM-TPU fiber shows a self-crimping ability. The single side-by-side spun fiber showed reversible self-coiling/decoiling in water when the temperature is changed. The sizes of the coils were dependent upon the ratio of the two polymers. The curvature of single fiber was increasing with higher PNIPAM-ABP ratio. Temperature is a very important factor for self-coiling behavior of single fiber. In water the coiled PNIPAM-P(MMA-BMA) bicomponent fiber showed a self-decoiling process with increasing of temperature.

3.3 Self-rolled porous hollow tubes made up of biodegradable polymers with bicomponent layer-by-layer morphology

(This work has been published in *Macromol. Rapid. Commun.* 2017, DOI: 10.1002/marc.201700034, with the title: “Self-Rolled Porous Hollow Tubes Made up of Biodegradable Polymers” by Ling Peng, Jian Zhu and Seema Agarwal)

Similar to reversible self-coiling/decoiling ability of PNIPAM-ABP-TPU bicomponent single fiber, reversible shape change in an aqueous solution in response to external triggers such as temperature and pH is a common phenomenon for polymeric bilayer architectures. In these bilayers, one layer is active (thermo-responsive) responding to the stimulus leading to change in volume and the other one is passive (not affected by the external stimulus).^[194-200] Not only simple bending but also curling, rolling, and complex motions are possible in a reversible way.^[201-204] Reversibility is seen as an advantage because the actuation can last for many cycles in a reproducible way. On the other hand, if actuation/shape change is stopped at the first stage, the irreversible actuation can provide designed 3D structured materials at small scale which otherwise is either not possible or requires sophisticated bottom-up approaches such as phase-separation and self-assembly procedures.^[205, 206] Making 3D structures at the macroscale is straightforward, but going to micro- and nanoscales requires special methods and optimizations.^[207-212] The 3D polymeric structures are of importance as scaffolds for tissue engineering, confined catalysis, etc. One of these desirable structures is the polymeric hollow tubes of diameters smaller than 6 mm, which are of interest for tissue engineering of

vascular grafts.^[213-225] Coating of polymers on glass rod of appropriate diameter and electrospinning on a rotating mandrel-type collector are some of the methods of making hollow polymeric tubes of small diameter.^[209, 212, 213] However, the detachment of hollow tube from the glass rod or collector is a tricky step and might lead to cracks.

Making 3D structures by the irreversible actuation of polymeric bilayers due to differential shrinkage/swelling is rare. In one of the examples, a cross-linked polysuccinimide (PSI)/polycaprolactone (PCL) bilayer was used. Hydrolysis of PSI in physiological buffer led to in situ formation of water-swelling biodegradable polyaspartic acid, which leads to formation of tubes. Since hydrolysis of PSI is a slow process, it took several hours (at least 9 h) for tube formation and provided uncontrolled rolling.^[226] In another study, a cross-linked gelatin-hydrophobic polymer bilayered film folded irreversibly at 37 °C, but the folding was nonuniform, leading to half-open tubes.^[227]

In our group recently showed the formation of highly stable hollow tubes made by very fast self-rolling of 2D bilayer porous membrane of poly(N-isopropylacrylamide) (poly(NIPAm)) in contact with water. The asymmetry in swelling/shrinkage required for irreversible rolling was created by fiber alignment along the membrane thickness.^[228] In this part of the work, I studied stimulus triggered formation of 3D hollow tubes with the following uniqueness: (1) the tubes are formed by actuation of a bilayer 2D porous membrane in water without use of any classical thermoresponsive polymer. The bilayer is composed of PLA and PCL; (2) formation of 3D hollow

porous tubes takes place within minutes in water at 40 °C due to the temperature-induced relaxation of intrinsic stress in as-prepared porous PLA side of the membrane; (3) the tube walls allow exchange of gases while the tubes retain water without leakage; (4) the diameter of the tube is controlled by the thickness of PLA and PCL, whereas the number of rolls are dependent upon the sample size; and (5) the tubes keep their form and size in water at all temperatures once they are formed. Notably, the nonpolymeric curled structures including nanotubes with diameter less than 1 μm made by self-folding of stressed thin films are known. [229-232]

3.3.1 Bilayer self-rolled porous hollow tubes of PLA and PCL

A bilayer fibrous mat of PLA and PCL was fabricated by sequential electrospinning of PLA and PCL on a rotating disk-type collector. PLA and PCL were dissolved in HFIP and 8 wt% solution of each was used for spinning. The flow rates of the polymer solutions (0.88 mL h^{-1}) were regulated by injector jet pumps. The distance between the electrodes (nozzle and collector) was 15 cm and the voltage applied was 12.5 kV. The rotating disk type collector of diameter 20 cm was used for collecting the aligned fibers. It was rotating with a rotation speed of 800 rpm.

The PLA and PCL fiber mats had fibers with average fiber diameters 1.4 ± 0.2 and $2.4 \pm 0.1 \mu\text{m}$, respectively (Figure 55 a, b). The porosity was more than 60%–70%, as calculated using Equation (7) (Table 10). The fibers were aligned along the long axis of the sample with degree of alignment $\approx 95\%$ and 92% in PLA and PCL fiber mats, respectively. A minimum of 100 fibers were considered for calculating the degree of

alignment values from SEM images using the literature procedure.^[233]

Interestingly, upon placing the PLA fiber mat in water at 40 °C for about 30 min, a significant asymmetric change in dimensions was observed. The length decreased by almost 35% whereas the decrease in width was less than 10%. The thickness of the mat increased from 46 to 61 μm . In contrast, there was no change in the dimensions of PCL mat under similar conditions (Figure 55 c, Table 11). The PLA fibers shrank in the direction of fiber alignment significantly. The thermal transitions and degree of crystallinity of PLA remained the same even after putting in water at 40 °C, as determined by DSC and FTIR (Figures 56 and 57, Table 12). Therefore, change in the crystallinity or melting of crystallites could not be the reason of causing shrinkage.^[234]

It is known from the literature that, in several cases, the electrospun fibers are collected in an energetically unstable stretched state just after spinning and try to acquire the low-energy unstretched conformation when heated near their glass transition temperature or come in contact with an appropriate solvent due to the chain movement.^[180,181,202,235] The glass transition of electrospun PLA fibers is around 50 °C, as noted from DSC (Figure 56). PLA fibers, when put in water at 40 °C, most probably led to easy chain movement due to the combined effect of temperature close to T_g and plasticization by water and hence the shrinkage. Heating at 40 °C under dry conditions showed only 3.4% shrinkage in length whereas heating at 20 °C (much below the glass transition temperature) even in water did not show any change in dimensions (Figure 58, Table 13).

PLA and PCL porous membranes with aligned fibers were combined in the form of a

bilayer (PLA-bi-PCL) by sequential spinning. The bilayer showed an intermingled interface with adhesion between the two layers (Figure 55d). The bilayer (PLA:PCL 2:1 thickness ratio, PLA = 25 μm ; PCL = 50 μm) rolls to a hollow tube with multilayered wall on putting in water at 40 °C for 5 min due to differential shrinkage in length (PLA side shrinks in length whereas PCL length remained the same) exerting compressive stress on PCL. The diameter of the tube was $419.7 \pm 7.4 \mu\text{m}$ (Figure 55e).

Table 10: Porosity of PLA, PCL and PLA-bi-PCL fiber mats (as-spun and 40 ° C water treated for 30 minutes).

Samples	Porosity / %
PLA as-spun	74 ± 1
PCL as-spun	67 ± 1
PLA:PCL=1: 3 as-spun	67 ± 3
PLA:PCL=1: 3 treated	69 ± 2
PLA:PCL=3: 1 as-spun	74 ± 1
PLA:PCL=3: 1 treated	73 ± 1

Table 11: Size of PLA and PCL aligned fiber mat (as-spun and 40 ° C water treated for 30 minutes)

	PCL as-spun	PCL treated	PLA as-spun	PLA treated
Length / cm	6.0	6.0	6.0	3.9
Width / cm	1.0	1.0	1.0	0.9
Thickness/ μm	48	47	46	61

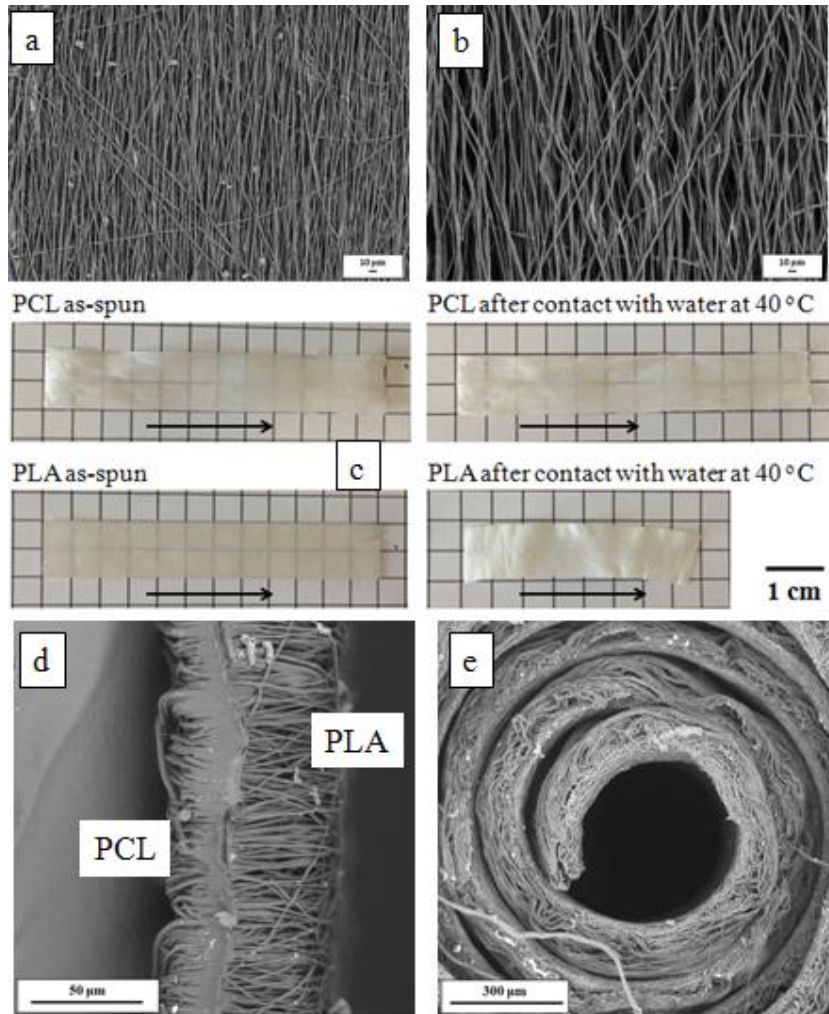


Figure 55: Images of PLA, PCL and PLA-bi-PCL electrospon fiber mats. (a) SEM image of PLA (scale bar 10 μm), (b) SEM image of PCL (scale bar 10 μm), (c) Photos of PCL and PLA fiber mats (fibers are aligned along arrow direction) before and after putting in water at 40 °C for 30 minutes, (d) Cross-sections of PLA-bi-PCL (PLA: PCL 2:1 thickness ratio, PLA= 25 μm; PCL = 50 μm) and (e) PLA-bi-PCL after putting in water at 40 °C for 30 minutes.

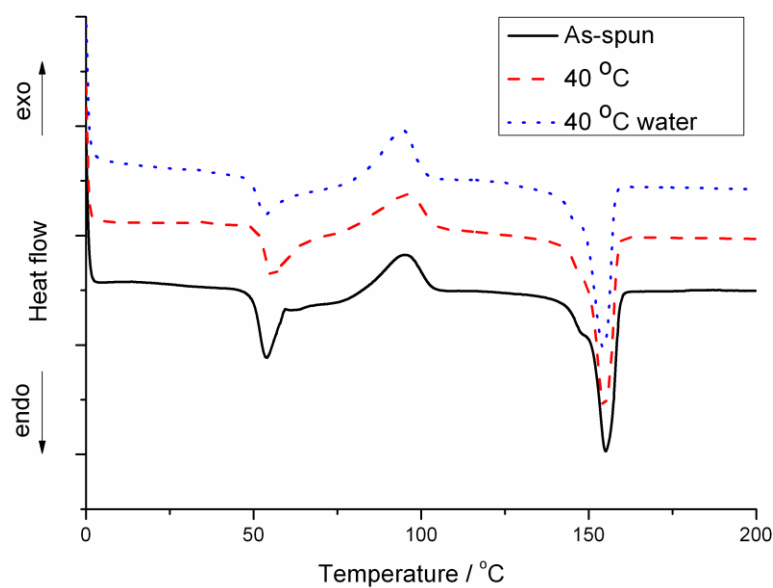


Figure 56: DSC normalized thermograms of PLA fiber mat samples (as-spun and heated at 40 °C for 30 minutes with and without water).

Table 12: T_g and Crystallinity of PLA fiber mat samples

	Glass transition temperature (T_g)	Crystallinity
As-spun	50 °C	5 %
40 °C	53 °C	5 %
40 °C water	50 °C	5 %

Table 13: Size of PLA aligned fiber mat (20 °C water and 40 °C oven treatment)

	PLA as-spun	20 °C water	PLA as-spun	40 °C oven
Length / cm	6.0	6.0	6.0	5.8
Width / cm	1.0	1.0	1.0	0.95
Thickness / μm	38	38	43	43

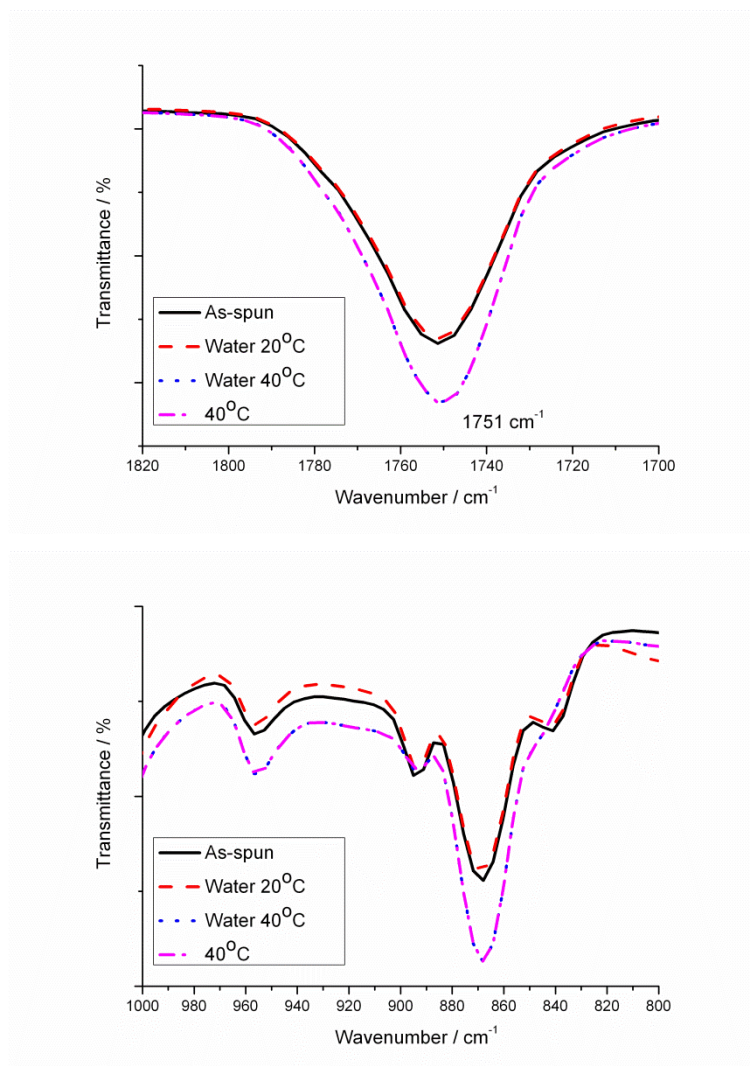


Figure 57: FTIR spectra of PLA fiber mats (as-spun and heated at 40 °C for 30 minutes with and without water).

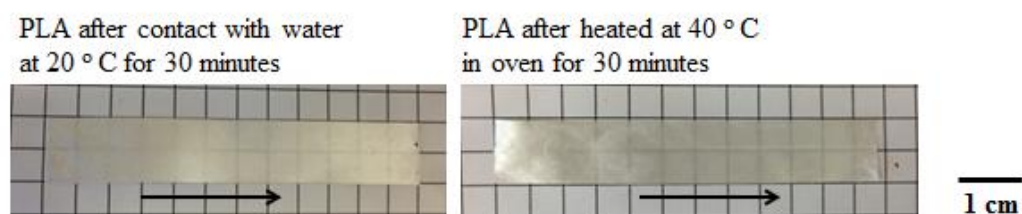


Figure 58: Photos of PLA aligned fiber mats (fibers are along arrow direction).

The folding of bilayer, inner diameter of the tube, and the number of layers comprising the wall of the tubes were dependent upon the temperature, thickness ratio of the two layers, that is, PLA and PCL, and the length of the fibrous mat. The rolling of PLA-bi-PCL bilayer fiber mat with a PLA: PCL thickness ratio of 2:1 was tested at different temperatures (from 20 to 40 °C) in water. The sample started bending and rolled to a hollow tube of diameter around 0.25 cm at 28 ° C in about 30 min with PLA, making an inside layer. On increasing the temperature, more compact hollow tubes were made in less time with a greater number of rolls. A hollow tube at 40 °C was made by self-rolling with diameter $419.7 \pm 7.4 \mu\text{m}$ in 5 min (Figure 59A). The tube kept its form and size on changing the temperature. The self-rolling was irreversible and the tube does not open again in cold water. Tubes were dried and kept their form and size even in air at room temperature.

Further, the PLA layer thickness had significant influence on the diameter of the tube formed after self-rolling (Figure 59B). On increasing the PLA thickness in bilayers the inner diameter of the tubes decreased. A hollow tube with inner diameter $321.5 \pm 1.4 \mu\text{m}$ was generated on using PLA: PCL thickness ratio 3:1.

In the next experiment, we kept the length and width of the samples the same ($L = 5$ cm length in the direction of fiber alignment; $W = 1$ cm) and studied the effect of PLA: PCL thickness ratio on the number of coils. The increase in the thickness of PLA in PLA-bi-PCL led to hollow tubes with lower diameter and greater number of coils. The sample with thickness ratio (PLA: PCL) 2:1 made a tube with nine layers whereas the one with PLA: PCL thickness ratio 1:3 had only six layers. (Figure 59C) Interestingly,

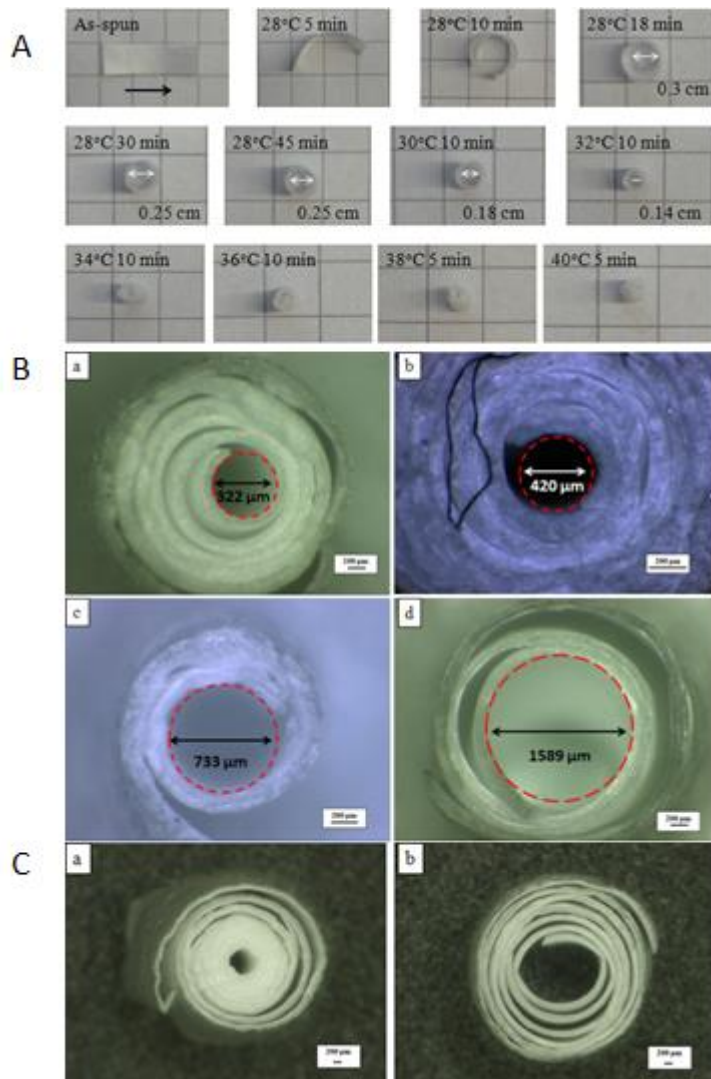


Figure 59: Photos of PLA-bi-PCL bilayer tube. (A) Temperature dependent rolling of (PLA: PCL 2:1 thickness ratio, PLA= 25 μm; PCL = 50 μm: length = 0.5 cm) PLA-bi-PCL bilayer fiber mats. (fibers are aligned along arrow direction, scale of grid is 0.5 cm) (B) PLA-bi-PCL bilayer tubes with different thickness ratios of PLA and PCL. (a) PLA: PCL= 3:1(scale bar 100 μm); (b) PLA: PCL= 2:1 (scale bar 200 μm); (c) PLA: PCL= 1:1 (scale bar 200 μm) and (d) PLA: PCL= 1:3 (scale bar 200 μm). (C) Cross-section images of PLA-bi-PCL bilayer tubes with different thickness ratios of PLA and PCL and sample sizes. (a) PLA: PCL= 2:1 (1x5 cm) and (b) PLA: PCL= 1:1(1x5 cm).

the inner diameter of PLA-bi-PCL tube only depends on the thickness ratio of PLA and PCL layers. By controlling the length of PLA-PCL fiber mat, the number of layers in the wall of PLA-PCL tube (number of coils) can also be controlled (Figure 60).

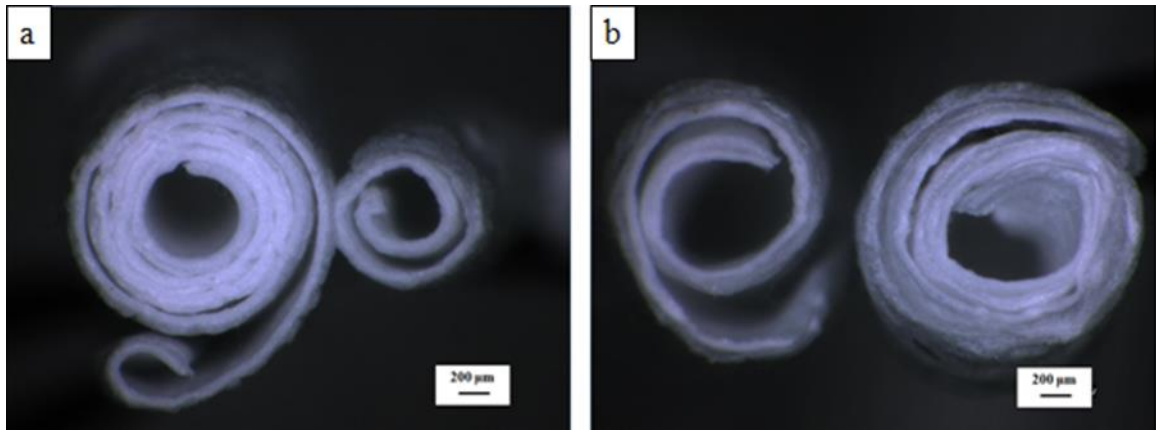


Figure 60: Cross-section images of PLA-PCL bilayer tubes with different layer thickness ratios and different sample sizes. (a) PLA: PCL= 2:1 and (b) PLA: PCL= 1:1.

PLA-PCL fiber mats with different thickness ratio were cut into 1x5 cm size (5 cm length in direction of fibers). Both samples were immersed in 40 °C water for 1 hour. With higher PLA thickness ratio, the number of layers in wall is also higher. (Figure 46C) PLA-PCL=2:1 tube had 9 layers, PLA-PCL=1:3 had 6 layers.

As we know the length of fiber mat, the number of layers in wall can be calculated with an equation (1):

$$\pi [n \times d + 2t \times (1 + \dots + n)] \leq L \quad (1)$$

n: number of layer $n \geq 2$; d: inner diameter of tube; t: thickness of layer; L: length of

fiber mat in direction of fiber).

As show in figure 61, the spiral cross-section of PLA-PCL tube is approximated to a concentric circle. The PCL layer has no shrinking behavior in 40 °C water, so the total outside circumference of PCL layer should be same to the length of as-spun fiber mat. The diameter of PCL layer is the inner diameter of tube plus 2 times thickness of layer.

For PLA: PCL = 2:1 tube, $d = 420\mu\text{m}$, $t = 125\mu\text{m}$, $L = 5\text{cm}$. So $n = 9$.

For PLA: PCL = 1:3 tube, $d = 1590\mu\text{m}$, $t = 120\mu\text{m}$, $L = 5\text{cm}$. So $n = 6$.

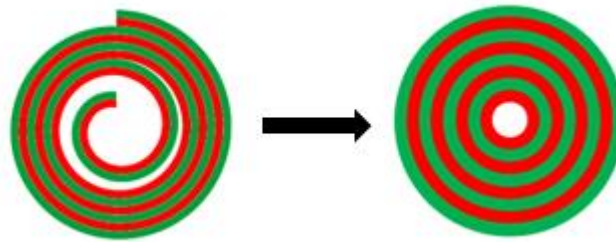


Figure 61: Simulation of cross-section of PLA-PCL tube with multi-layers. Red layer is PLA layer, green layer is PCL layer.

The calculated results are same as the experimental results.

The inner diameter of PLA-PCL tube only depends on the thickness ratio of PLA and PCL layers. By controlling the size of PLA-PCL fiber mat (in direction of fibers), the number of layers in the wall of PLA-PCL tube can be also controlled.

Both PLA layer and PCL layer of as-spun PLA-PCL (2:1) aligned fiber mat are hydrophobic. Contact angle of PCL layer was $142 \pm 5^\circ$; contact angle of PLA layer was $132 \pm 1^\circ$. (Figure 62)

The PCL-PLA aligned fiber mat was treated in water at 40 °C for 1 hour, and dried in oven for 3 days. The PCL layer became hydrophilic: the water drop diffused into the PCL layer of fiber mat after 11 min, contact angle was 0 °. (Figure 63)

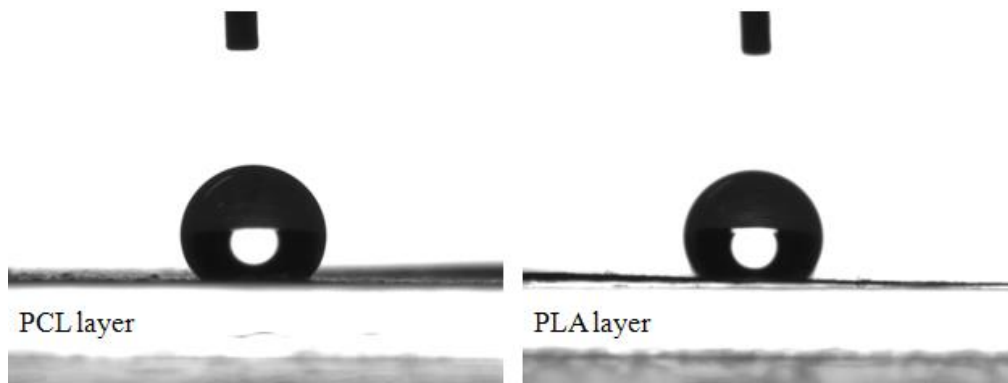


Figure 62: Contact angle images of Polycaprolactone layer and Polylactide layer of as-spun Poly lactide-Polycaprolactone aligned fiber mat.

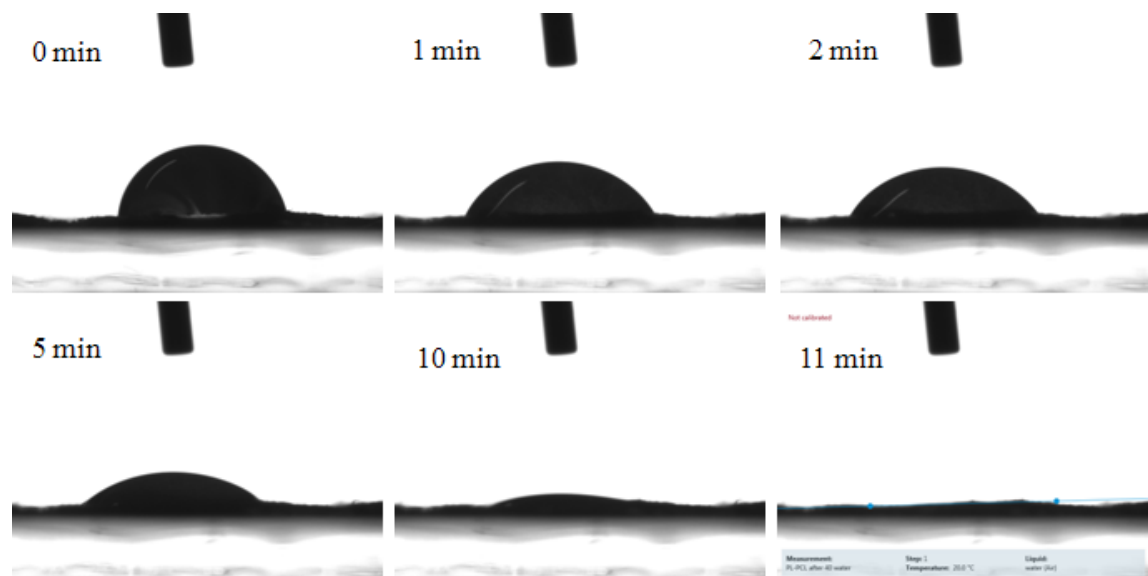


Figure 63: Contact angle images of Polycaprolactone layer of treated Poly lactide-Polycaprolactone aligned fiber mat at different times.

After treating at 40 °C in water, contact angle of PLA layer was also decreased. After 15 min, the contact angle was 117 °.(Figure 64) The PLA layer became also more hydrophilic as before.

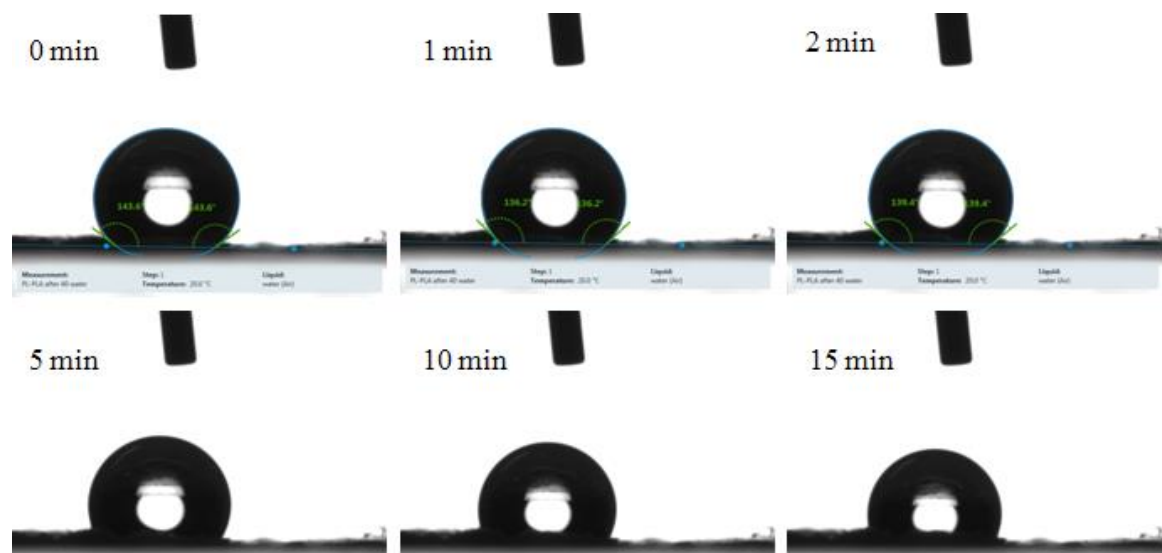


Figure 64: Contact angle images of Poly lactide layer of treated Polylactide-Polycaprolactone aligned fiber mat at different times.

As show in figure 65, after treating at 40 °C in water, the aligned morphology of PCL layer became distorted. At 40 °C in water, the PLA layer started to shrink. The stress generated at the interface pulled the PCL layer to form a tube. Therefore, the orientation of PCL layer was destroyed. Some bigger pores between fibers of PCL layer were occurred. Due to this morphology change, the wettability changed.

Stability performance of polymer tube was tested in different pH environment. 4 pieces of tube (PLA: PCL =2:1) were immersed in buffer solutions with different pH values. All of the samples were kept at 37 ° C for different time intervals. (Figure 66)

Even after 6 days, the tubes kept the form in the buffer solutions.

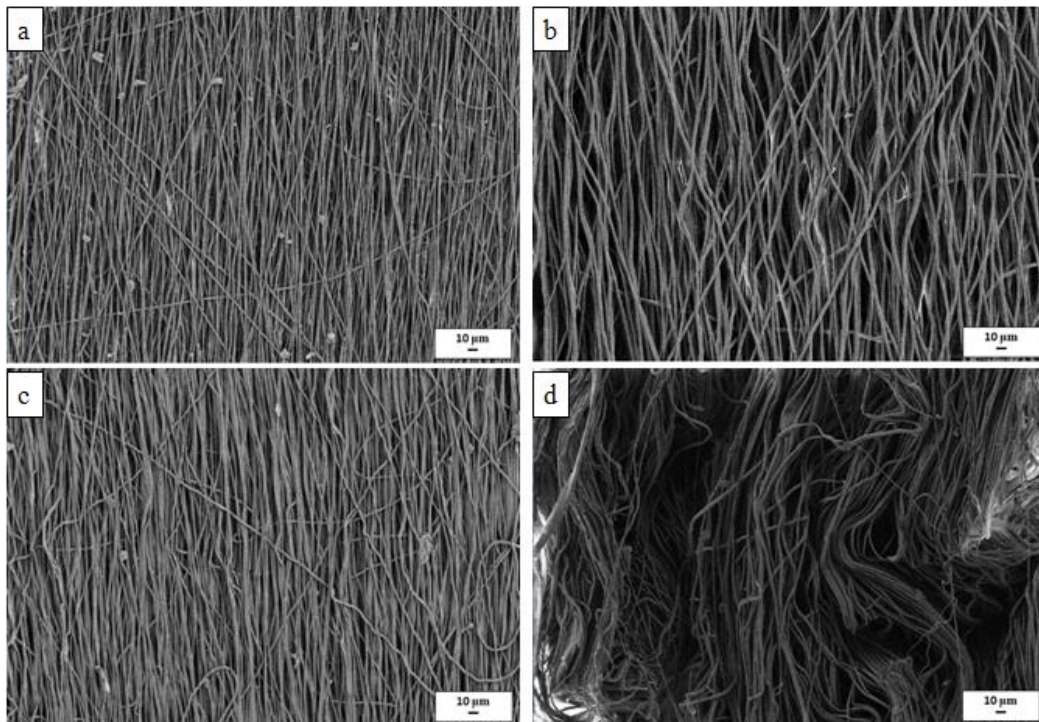


Figure 65: SEM images of PLA and PCL layer of PLA-PCL (2:1) fiber mat. (a) as-spun PLA layer; (b) as-spun PCL layer; (c) PLA layer after treating in 40 °C water and (d) PCL layer after treating in 40 °C water.

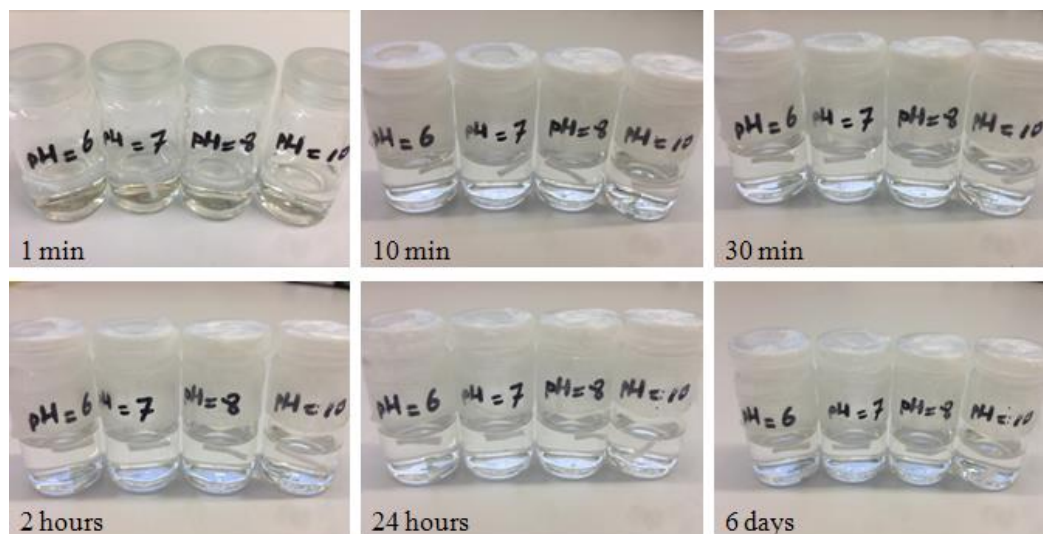


Figure 66: Stability test of PLA: PCL=2: 1 bilayer tube in different buffer solutions.

The mechanical properties of fibrous mats after water treatment at 40 °C in water for 1 h are shown in Table 14. Mechanical properties were dependent upon the direction of fiber alignment. ^[26] Tensile strength and modulus were 11 ± 1 and 146 ± 22 MPa, respectively, in the direction perpendicular to the fiber alignment with $\approx 280\%$ elongation at break for PLA-bi-PCL with thickness ratio PLA:PCL 3:1, whereas the fiber mats showed significantly higher tensile strength and modulus (11.1 ± 0.8 and 146 ± 22 MPa, respectively) in the direction parallel to the fiber alignment. The mechanical properties of PLA-bi-PCL bilayer fiber mats were also dependent upon the thickness ratio of PLA and PCL in the bilayers (Table 14, Figure 67). In all cases, PLA-bi-PCL bilayer scaffolds are able to maintain the range of elasticity of typical vascular structures.^[209, 236] Notably, the mechanical properties reported in the present work are determined using a flat bilayer PLA-bi-PCL sheet obtained after mechanically opening the rolled tubes. The tubes as such in reality should have enhanced mechanical properties due to the multilayered walls formed by rolling. The bilayer fibrous membranes were very porous (60%–70% porosity, Table 10) and retained their porosity even after contact with water at 40 °C, as quantified by calculations based on the density of the bulk films and fibrous mats. In another experiment, the porosity of the self-rolled tube was proved by fixing the mat obtained after mechanically opening the self-rolled tubes at one end of a plastic water pipe, as shown in Figure 68a. The end of the water pipe was closed with the bilayer membrane immersed in a flask containing limewater with phenolphthalein indicator, while the open end was put in another flask containing solid carbon dioxide. The passage of

carbon dioxide through the bilayer mat tied at one end of a plastic tube discolors the phenolphthalein/limewater solution in several seconds, proving the porous nature (Figure 68a).

Table 14: Mechanical properties of electrospun fiber mat (40 °C water treated).

Direction of force was perpendicular to the direction of fiber alignment.

Samples	Young's modulus	Ultimate Stress	Elongation at break
	[MPa]	[MPa]	[%]
PLA treated	46 ± 5.4	3 ± 0.2	446 ± 53
PCL treated	2 ± 0.3	1 ± 0.2	1087 ± 110
PLA:PCL=1: 3 treated	4 ± 0.5	1 ± 0.2	473 ± 20
PLA:PCL=3: 1 treated	31 ± 4.4	3 ± 0.1	287 ± 23

Direction of force was parallel to the direction of fiber alignment.

Samples	Young's modulus	Ultimate Stress	Elongation at break
	[MPa]	[MPa]	[%]
PLA treated	214 ± 32	17 ± 1	329 ± 20
PCL treated	53 ± 4	15 ± 2	657 ± 34
PLA:PCL=1: 3 treated	143 ± 38	11 ± 3	718 ± 40
PLA:PCL=3: 1 treated	136 ± 22	11 ± 1	287 ± 40

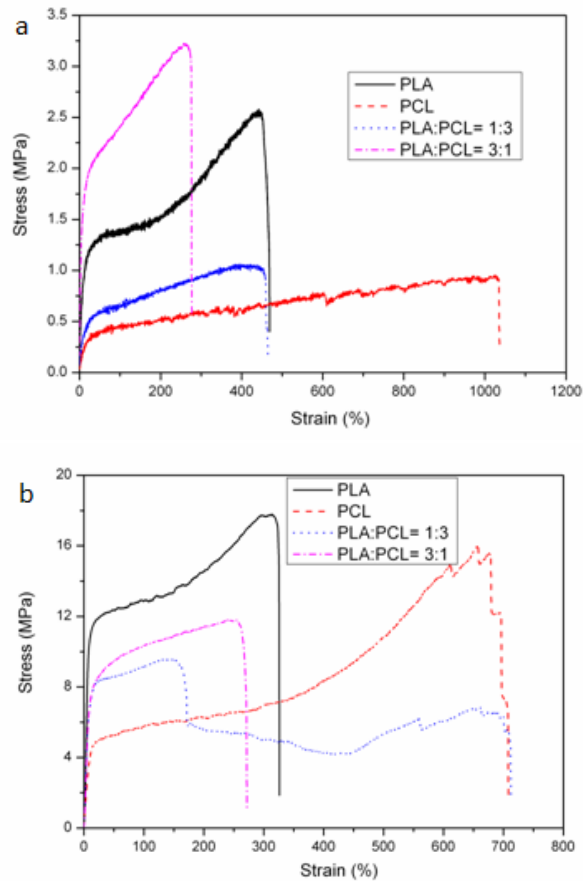


Figure 67: Stress-Strain curves of electrospun PLA, PCL and PLA-bi-PCL fiber mat (treated in 40 °C water for 1 hour): (a) Force in the direction perpendicular to the fiber alignment; (b) Force in the direction parallel to the fiber alignment.

On the other hand, the hollow tubes allowed flow of water without leakage. A water flow test was carried out with PLA-bi-PCL (3:1) bilayer tube (inner diameter around 320 μm). The two separate pieces of a plastic water pipe were connected through a self-rolled PLA-bi-PCL tube. Water with a velocity of 10 cm s^{-1} was pumped through one end of the tube and collected at the other end passing through the connecting self-rolled PLA-bi-PCL tube without leakage. Even multitubular structures can also be made at the same time in a simple way by cutting the 2D bilayer PLA: PCL

membrane in appropriate shapes and putting them in water at 40 °C. One of such structures is shown in Figure 68b.

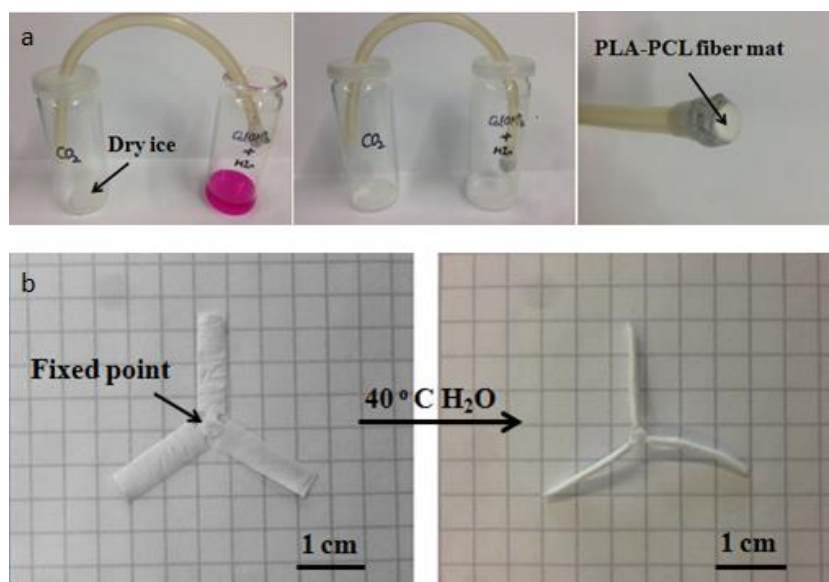


Figure 68: (a) Permeability test of PLA-bi-PCL (3:1) bilayer tube. (b) 3D-tube scaffold of PLA-bi-PCL (2:1) bilayer fiber mat.

3.3.2 Conclusions

In this work, self-folding behavior of multilayer fiber mat without responsive polymers was studied. Firstly, a simple method of making tubular scaffolds in few minutes by self-folding of 2D sheets is shown. This was possible using conventional biodegradable polymers without need of any thermo-/pH-responsive polymers. The inherent tendency of PLA fiber mats made by electrospinning to shrink in water at 40°C was used to generate stress at the bilayer interface required for rolling of a PLA-PCL bilayer system. The folding of bilayer, inner diameter of the tube, and the number of layers in the wall were dependent upon the temperature, thickness ratio of

the two layers, that is, PLA and PCL, and the length of the mat. The combination of good mechanical properties and porosity make such tubes a promising candidate for further studies as scaffolds for blood vessels. The real application requires in-depth experimental and theoretical studies in the future regarding the effect of liquid pressure, number of rolls (i.e., wall thickness), type of liquids, and liquid contact time on stability of tubes.

4. Experimental part

4.1 Chemicals

Azobis(isobutyronitrile)	Fluka, recrystallized from ethanol.
Buffer solution (pH = 6)	Apollo Scientific Limited, used as received.
Buffer solutions (pH = 7, 8, and 10)	VWR Chemicals, used as received.
Fluorescein isothiocyanate isomer I	Aldrich, used as received.
Fluorescein sodium salt	Sigma-Aldrich, used as received.
<i>N</i> -Isopropylacrylamide	Aldrich, recrystallized from cyclohexane.
<i>N,N'</i> -dimethylformamide	Aldrich, $\cong 99.8\%$, used as received.
Polycaprolactone	Perstorp Group, Capa 6800, used as received.
Poly(methyl methacrylate)	Aldrich, $M_w \sim 120000$ g/mol, used as received.
Poly lactide	Natureworks 4043D, used as received.
Poly(<i>L</i> -lactide)	Boehringer Ingelheim, Germany. Resomer L210, i.v. 3.3-4.3 dl/g, used as received.
Rhodamine B	Sigma-Aldrich, used as received.
Thermoplastic polyurethane	Bayer Materials Science, Desmopan DP 2590, used as received.
Toluene	VWR Chemicals, $\cong 99.8\%$, used as received.
1,1,1,3,3,3-hexafluoro-2-propanol	Apollo Scientific Limited, $> 99.9\%$, used as received.

4.2 Characterization methods

4.2.1 Tensile testing of single fiber

The method of preparation of single fiber and tensile tests process were according to the previous reports [237, 238]. First of all, a stainless steel frame with an inner rectangular size 17.5 x 3.0 cm was used as the collector to collect the side-by-side single fibers. The fibers were picked by tweezers. Then a paper frame with an inner rectangular size 8 x 5 mm was used to hold the single fiber. Two pieces of double-side electrically conductive tape were used to fix the single fiber. After that, two pieces of paper were used to cover the ends of the paper frame to make sure that the fiber was tightly adhered to the conductive tape. (Figure 69) After the tensile testing the broken fiber segments were measured by SEM to obtain the accurate diameter of single fiber. Annealing of single fibers was done in MeOH atmosphere for 24 h and by heating at 80 °C for 10h.

To calculate the mechanical properties of single fiber, a diameter displacement method was applied in this experiment. [237] An equation which is based on the relationship between the tensile strength (σ), cross-section area (A) or diameter (D) and applied load (F) is shown as follows:

$$\sigma = F / A = 4F / (\pi D^2) \quad (2)$$

During the tensile testing, the diameter of single fibers was assumed as 1 μm (D_1). The accurate fiber diameter (D_2) was measured by SEM after tensile test. The real tensile strength (σ_2) could be calculated by the following equations:

$$\sigma_1 = F / A = 4F / (\pi D_1^2) \quad (3)$$

$$\sigma_2 = F / A = 4F / (\pi D_2^2) \quad (4)$$

$$\sigma_2 = \sigma_1 (D_1^2 / D_2^2) \quad (5)$$

where the tensile strength (σ_1) were directly obtained from the software of the tensile test machine.

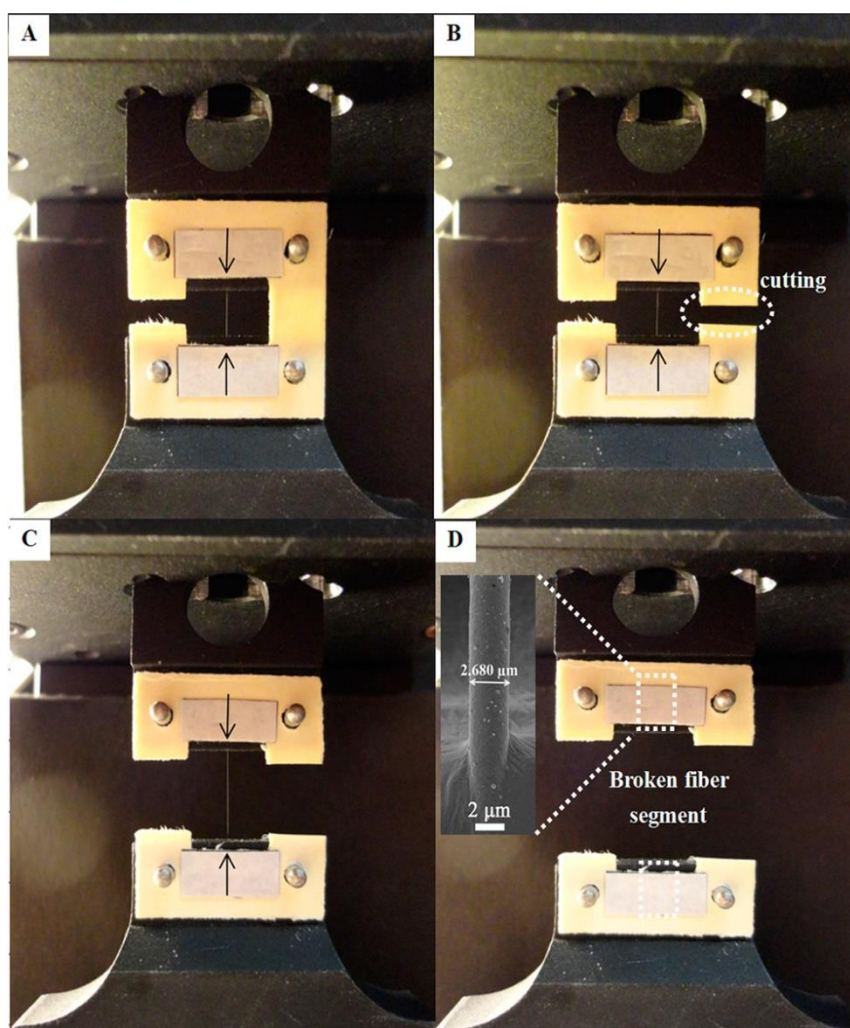


Figure 69: Digital photographs of electrospun single fiber for tensile test: (A) mounting the paper frame with single electrospun fiber (indicated by arrows) on the machine, (B) cutting the paper frame and (C) stretching the single electrospun fiber, and (D) collecting the broken fiber segments for SEM measurements. (Reprinted with permission from Ref 237, Copyright 2014 American Chemical Society)

4.2.2 Tensile testing of fiber mat

The fiber mats were cut into dog-bone shaped samples of dimensions shown in Figure 70 for the tensile tests using Zwick / Roell, BT1-FR0.5TN-D14, Germany tensile tester. TextXpert II software was used to control the tensile test. The test speed was 5 mm/min. For each fiber mat, 5 replicated tests were run for the calculation. Annealing of fiber mats was done in MeOH atmosphere for 24 h and by heating at 80 °C for 10h.

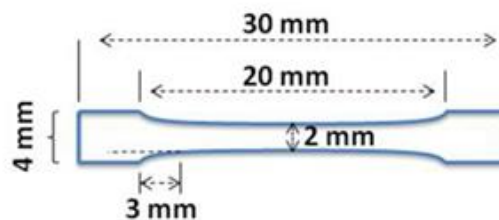


Figure 70: Sketch for tensile-test specimen dimensions.

4.2.3 Scanning electronic microscopy (SEM)

The morphology of electrospun fibers and fiber mats were observed by SEM. The samples were sputter-coated with platinum (3.0 nm). A Zeiss LEO 1530 equipment was used for the study. The diameters of electrospun fibers were measured by ImageJ (Version 1.50b).

Cross sections of fiber mats were observed with desktop SEM (Phenom Pro, Phenom-World B.V.).

4.2.4 Conductivity measurements

The conductivities of polymer solutions were measured with inoLab Cond Level 3 instrument (WTW GmbH, Germany). Ultra-pure water was used to calibrate this equipment.

4.2.5 Fourier transform infrared spectroscopy (FTIR)

FTIR spectroscopy measurements were performed on a DIGILAB FT5 3000 spectrometer, equipped with a ZnSe crystal with attenuated total reflection technique. Analysis was carried out by using Win-IR Pro 3.3 software. The molecular orientation of polymer chains in fibers was characterized by a polarized Fourier transform infrared spectroscopy (FTIR, PerkinElmer Spectrum 100, USA).

4.2.6 Differential scanning calorimetry (DSC)

The thermal behavior and crystallization of polymers was studied by a DSC instrument from Mettler Toledo (Type DSC 821^e), which was calibrated with indium and zinc. The DSC measurements were carried out with ~ 10 mg samples in aluminum pans under N₂ atmosphere from 25 to 250 °C with a heating rate of 10 K/min. The glass transition temperature (T_g) was obtained from the first heating curve using a Mettler Toledo STAR^e software. The degree of crystallinity of PLLA nanofibers was calculated with the method which reported by C. Ribeiro *et al* [169]. The degree of crystallinity (ΔX_c) of the electrospun mats was calculated using the following equation (6):

$$\Delta X_c = \frac{\Delta H}{\Delta H_m^0} 100\% \quad (6)$$

ΔH is the area under the thermogram after T_g and ΔH_m^0 is the enthalpy of melting for a fully crystallized PLLA sample, which the value is 93.1 J/g.

4.2.7 Confocal laser scanning microscopy (CLSM)

Confocal laser scanning microscopy (CLSM, Zeiss LSM 710) was performed with Rhodamine B labeled PLLA and Fluorescein sodium labelled SF nanofibers. Fluorescein sodium was excited with an Argon LASER at 458 nm and fluorescence was detected in the range between 480 and 530 nm. For Rhodamine B a Helium-Neon LASER at 543 nm was used while detecting Fluorescence between 555 and 620 nm. Visualization and analysis of the morphology was done using the ZEN 2008 software.

4.2.8 Fourier self-deconvolution (FSD)

Fourier self-deconvolution (FSD) of the infrared spectra was performed by Opus 6.5 software. The baseline was corrected firstly. Then the original spectra were smoothed with a five-point Savitzky-Golay smoothing filter. Lorentzian line shape with bandwidth 23 cm^{-1} and a noise reduction factor of 0.3 was used to perform deconvolution. After that the baseline was corrected again. 11 peaks (centered around on 1611, 1619, 1624, 1630, 1640, 1650, 1659, 1666, 1680, 1691 and 1698 cm^{-1})^[31] were used to fit the FSD amide I region ($1595\text{-}1705 \text{ cm}^{-1}$). For each sample, 3

measurements were made, and for each measurement, calculations were made twice to get the average value.

4.2.9 Transmission electron microscopy (TEM)

Cross sections of fibers were observed with TEM (Zeiss CEM902). The fibers were cut in epoxy. Samples were prepared onto copper grids.

4.2.10 Digital Microscopy

The images of stained single fibers were observed using fluorescence microscope (Leica DMRX, Type 020-525.706, Germany) with a camera (Leica DC 200). IrfanView software was applied to obtain the images. Cross-sectional images of fibrous hollow tubes were obtained using digital microscope (VHX-100K, KEYENCE Co., Japan).

4.2.11 Gel-Permeation Chromatography (GPC)

The molecular weight of polymer was determined by GPC (solvent DMF, polystyrene-standard, SDV-linear-column 10 μ 8x600 mm from PSS, refractive index detector from Agilent and UV detector from Knauer) using software Win GPC Unity.

4.2.12 Porosity

The porosity was calculated according to the method described by Vaz et al. ^[210] Fiber mats were cut into rectangular samples (1 cm \times 6 cm). Thickness of samples was measured with a micrometer (Mitutoyo, Japan). Dry weight was measured with a

microbalance (Cubis MSA 6.6S, Sartorius, Germany) accurate to 10^{-3} mg. The porosity (ε) was calculated with the measured average density (ρ) of the samples and the standard density (ρ') of polymers ($\rho(\text{PLA}) = 1.2 \text{ g cm}^{-3}$; $\rho(\text{PCL}) = 1.145 \text{ g cm}^{-3}$). (Equation (7))

$$\varepsilon (\%) = \left(1 - \frac{\rho}{\rho'}\right) \times 100\% \quad (7)$$

4.3 General procedures for preparation of polymer solutions

4.3.1 Preparation of silk fibroin solution

10 g *Bombyx mori* silk was first degummed twice, in each case with 2 L 0.5 % (g/L) NaHCO_3 solution at 100 °C for 1.5 hour. Then the sericin-free silk fibers were thoroughly washed with deionized water. After complete drying, the extracted silk fibers were dissolved in HFIP. Before electrospinning the insoluble flocculents were removed by centrifugation. The final concentration of silk fibroin (SF) was about 100 mg/mL. In 1 mL SF solution, 0.4 mg fluorescein sodium was added.

4.3.2 Preparation of PLLA solution

PLLA was dissolved in HFIP at 40 mg/mL. In 1 mL PLLA solution, 0.2 mg Rhodamine B was added.

4.3.3 Preparation of TPU solution

TPU was dissolved in DMF at 18 wt.%.

4.3.4 Preparation of PNIPAM solution

The photo-cross-linker 4-acryloyl-benzophenone (ABP) (figure 71) was made in lab by Dr. Yinfeng Shi according to the literature ^[239].

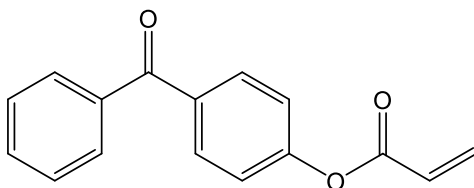


Figure 71: Chemical structure of ABP.

The synthesis of photo cross-linkable PNIPAM with number average molar mass (M_n) 104000 Da and molar mass dispersity ($MWD = 1.92$) was also conducted according to the literature ^[239]. NIPAM (11g), ABP (0.5g) and AIBN (33 mg) were transferred into a 250 Schlenk Flask and dissolved in 80 ml 1, 4- Dioxane. The solution was degassed by the method of bubble for 1.5 h. Then the mixture was placed into a preheated oil bath at 70 °C. Polymerization was carried out for 24 h. After 24 hours, polymerization was quenched by cooling in liquid nitrogen for several seconds and subsequent air contact. The polymer was precipitated in 800 mL diethyl ether giving white solid. The dispersion was transferred in Bucher funnel for suction filtration. Finally the solid was dried at room temperature in a vacuum oven for 24 h.

The photo cross-linkable PNIPAM was dissolved in DMF at 32 wt.%. In 1 mL PNIPAM solution 0.2 mg Fluorescein isothiocyanate isomer I was added.

4.3.5 Preparation of PLA, PCL and PMMA solutions

PLA and PCL were dissolved in HFIP and 8 wt.% solution of each was used for spinning. PMMA was dissolved in HFIP at 15 wt.%.

5. Summary

The work is focused on novel meso-structured bicomponent porous nanofiber mats made by electrospinning with special fiber morphologies, such as side-by-side (Janus), off-centered fiber and layer-by-layer structures, arrangement of two different polymers. The mutual interaction between the two components, both capable of having their own supramolecular structures, could lead to novel meso-structured porous materials with special properties. Bombyx mori silk and synthetic polymers (semi crystalline poly(L-lactide), polycaprolactone, thermoplastic polyurethane and thermoresponsive poly(N-isopropylacrylamide), showing a LCST-type phase transition) were used for making bicomponent fibrous membrane and studies the synergetic effect.

The arrangement of polymers in different morphologies provided special effects, like increasing of the mechanical properties for side-by-side (Janus) arrangement of bombyx mori silk and poly(L-lactide). The two sides of two-in-one fiber retained their individual secondary structure before and after annealing without affecting each-other in a significant way. A size-effect of single nanofibers was observed on the mechanical properties, there is an abrupt increase below 400 nm fiber diameter.

Applying different polymers for making special fiber morphologies provided interesting set of novel properties. The use of a responsive polymer as one of the

components, such as thermoresponsive poly(N-isopropylacrylamide), led to a compressive stress at the interface due to swelling/deswelling at different temperature in bicomponent fibers, which leading to a reversible coling/decoling behavior. Detailed studies were carried out to understand this behavior.

Further, it was discovered that layer-by-layer arrangement of bicomponents with differential elasticities could also lead to actuation by temperature getting compressive stress at the interface. This was proved by making bilayer fiber mat of poly(L-lactide) and polycaprolactone. The bilayer rolled to tubular scaffolds in very short time (few minute, at 40 °C in wet and dry condition). The phenomenon was studied in details by changing the layer thickness ratio and size of fiber mat.

6. Zusammenfassung

Die Arbeit fokussiert auf neuartige meso-strukturierte Bikomponenten-poröse Nanofaser-Matten, die durch Elektrosponnen mit speziellen Fasermorphologien der Anordnung von zwei verschiedenen Polymeren: wie z. B. nebeneinanderliegende (Janus), abzentrierte Faserstruktur und Schicht-für-Schicht, hergestellt werden. Die gegenseitige Wechselwirkung zwischen den beiden Komponenten, die beide ihre eigenen supermolekularen Strukturen haben können, könnte zu neuartigen meso-strukturierten porösen Materialien mit besonderen Eigenschaften führen. Bombyx mori Seide und synthetische Polymere (halbkristallines Poly (L-lactid), Polycaprolacton, thermoplastisches Polyurethan und thermoresponsives Poly (N-isopropylacrylamid), eine LCST-Phasenübergang gezeigt wird) wurden zur Herstellung von Bikomponenten-Fasermembran und Untersuchung der synergetischen Wirkung verwendet.

Die Anordnung von Polymeren in verschiedenen Morphologien lieferte Spezialeffekte, beispielsweise synergistische Zunahme der mechanischen Eigenschaften für die nebeneinanderliegende (Janus) Anordnung von Bombyx mori Seide und Poly(L-lactid). Die beiden Seiten der Zwei-in-Eins-Faser behalten ihre individuelle Sekundärstruktur vor und nach dem Glühen, ohne sich in einer signifikanten Weise zu beeinträchtigen. Bei den mechanischen Eigenschaften wurde ein Größeneffekt einzelner Nanofasern beobachtet: ein plötzlicher Anstieg der mechanischen Eigenschaften unterhalb von

400 nm Faserdurchmesser.

Die Veränderung des Polymertyps zur Herstellung spezieller Fasermorphologien lieferte interessante neuartige Eigenschaften. Die Verwendung eines ansprechenden Polymers als einer der Komponenten, wie z. B. thermoresponsives Poly (N-Isopropylacrylamid), führte zu einer Druckspannung an der Grenzfläche aufgrund von Schwellung /Abschwellung bei unterschiedlicher Temperatur in Bikomponentenfasern, was zu einem reversiblen Windend- / Entfaltungverhalten führte. Detaillierte Untersuchungen wurden um dieses Verhalten zu verstehen durchgeführt.

Weiterhin wurde entdeckt, dass eine Schicht-zu-Schicht-Anordnung von Bikomponenten mit differentiellen Elastizitäten, die durch Temperatur eine Druckspannung an der Grenzfläche erhält können, auch zu einer Betätigung führen könnte. Dies wurde durch die bilayer Fasermatte aus Poly(L-lactid) und Polycaprolacton bewiesen. Die Doppelschicht wurde in sehr kurzer Zeit zu röhrenförmigen Gerüsten gerollt (wenige Minuten, bei 40 ° C nass / trocken Bedingungen). Das Phänomen wurde in Einzelheiten durch Ändern des Schichtdickenverhältnisses der beiden Schichten, der Größe der Fasermatte, untersucht.

7. Outlook

This work was done particularly in regard to bicomponent fibers and fiber mats with novel morphologies and behaviors through bicomponent electrospinning technique. Basic work for future projects has been carried out. Possible research directions with these fibers and fiber mats for potential applications in future have been designed.

As SF-PLLA fiber has better mechanical properties than pure SF fiber, the SF-PLLA fiber may expand the application area of SF fiber. Diameter of fibers and orientation of fibers in fiber mats influence the mechanical properties. It is possible to make single fibers and fiber mats which with the aimed mechanical properties through combination of different materials and control of diameter of fibers and orientation of fibers in fiber mats. The SF-PLLA fiber has a side-by-side morphology, both SF and PLLA sides can be modified. It would be interesting to use such fibers for biodegradation studies, cell culture, scaffold and drug-release applications in nano-scale to exploit the utility of side-by-side morphology, and surface chemistry of two sides.

With the bicomponent PNIPAM-TPU single fiber with off-centered morphology, a self-crimping ability was observed. The single side-by-side spun fiber can reversibly self-coil/decoil in water with the changing of temperature. The sizes of the coils were dependent upon the ratio of the two polymers. With the reversible self-crimping ability, this fiber can be used as a micro actuator or micro spring in aqueous environment.

The PLA-PCL bilayer fiber mat shows a simple method of making tubular scaffolds in few minutes by self-folding of 2D sheets. The folding of bilayer, inner diameter of the tube, and the number of layers in the wall were dependent upon the temperature, thickness ratio of the two layers, that is, PLA and PCL, and the length of the mat. The combination of good mechanical properties and porosity make such tubes a promising candidate for further studies as scaffolds for blood vessels. The real application requires in-depth experimental and theoretical studies in the future regarding the effect of liquid pressure, number of rolls (i.e., wall thickness), type of liquids, and liquid contact time on stability of tubes. The make such fiber mats a promising candidate for further studies as drug release without many limits conditions like temperature, pH etc.

8. Acknowledgments

First and foremost, I would like to express my sincere gratitude to my direct supervisor Prof. Dr. Seema Agarwal for the intensive care and support during my doctor study and giving me interesting topic. Under her constant encouragement and guidance, I can finish my work smoothly.

I would also like to thank Prof. Dr. Andreas Greiner for his enlightening lectures and giving so much good advice on my work.

I thank all members of the work groups Agarwal and Greiner for the pleasant working environment, nice conversations and effective teamwork.

I thank Dr. Shaohua Jiang for the introduction of electrospinning technique and tensile test machine, also many useful discussions and suggestions about my PhD thesis.

I thank Dr. Yinfeng Shi for his advice regarding synthetic problems and GPC measurements.

I am very grateful for secretary of our group Mrs Rösner-Oliver for helping a lot on documents.

Very thankful for Annette Kröckel for her kindly ordering and searching chemicals for me, also introduction of NMR instrument and safety rules in lab.

Thank Li Liu for interesting discussions, from which I got many useful ideas.

Thanks to my laboratory colleague Dr. Ziyin Fan for great working atmosphere.

I want to acknowledge Dr. Holger Schmalz, Dr. Roland Dersch, Dr. Ilka Paulus, Dr. Holger Pletsch, Dr. Fangyao Liu, Dr. Peter Ohlendorf, Dr. Hui Wang, Dr. Melissa

Köhn, Dr. Paul Pineda, Dr. Oliver Hauenstein, Dr. Amanda Pineda, Dr. Gaigai Duan, Matthias Burgard, Florian Käfer, Lu Chen, Pin Hu, Markus Langner, Steffen Reich, Judith Schöbel and Julia Kronawitt for helping with small and big problems in my work, also introduction and measurements with so many good instruments for my work.

I thank Carmen Kunert, Dr. Reiner Giesa, Minde Jin, Prof. Dr.-Ing. Gregor Lang and Ute Kuhn for helping with various measurements of my work.

My sincere thanks are also given to the members of mechanical workshop and electronic workshop for processing so many nice equipments for my work.

Last but not the least, my special gratitude extends to my parents and my young sister who have been continuously and unconditionally assisting, supporting, caring and encouraging for me for so many years.

9. References

- [1] H. Yoshimoto, Y. M. Shin, H. Terai, and J. P. Vacanti, *Biomaterials* 2003, 24, 2077–2082.
- [2] X. Xu, X. Chen, A. Liu, Z. Hong, and X. Jing, *European Polymer Journal* 2007, 43, 3187–3196.
- [3] C. Y. Xu, R. Inai, M. Kotaki, and S. Ramakrishna, *Biomaterials* 2004, 25, 877–886.
- [4] F. Yang, R. Murugan, S. Wang, and S. Ramakrishna, *Biomaterials* 2005, 26, 2603-2610.
- [5] Z. Ma, M. Kotaki, T. Yong, W. He and S. Ramakrishna, *Biomaterials* 2005, 26, 2527-2536.
- [6] Y. Lu, J. Huang, G. Yu, R. Cardenas, S. Wei, E. K. Wujcik and Z. Guo, *WIREs Nanomed. Nanobiotechnol.* 2016, 8, 654-677.
- [7] Y. F. Goh, I. Shakir abd R. Hussain, *J. Mater. Sci.* 2013, 48, 3027-3054.
- [8] Z. Xie, G. Buschle-Diller, *J. Appl. Poly. Sci.* 2010, 115, 1-8.
- [9] D. Liang, Y. K. Luu, K. Kim, B. S. Hsiao, M. Hadjiargyrou and B. Chu, *Nucleic Acids Research* 2005, 33, article e170.
- [10] B. Chu, D. Liang, M. Hadjiargyrou and B. S. Hsiao, *J. Phys.: Condens. Matter* 2006, 18, 2513-2525.
- [11] S. Lee, G. Jin and J.-H. Jang, *Journal of Biological Engineering* 2014, 8:30.

- [12] M. S. Khil, D. I. Cha, H. Y. Kim, I. S. Kim and N. Bhattarai, *Journal of Biomedical Materials Research B* 2003, *67*, 675–679.
- [13] M. Abrigo, S. L. McArthur and P. Kingshott, *Macromol. Biosci.* 2014, *14*, 772-792.
- [14] A. R. Unnithan, N. A.M. Barakat, P.B. T. Pichiah, G. Gnanasekaran, R. Nirmala, Y.-S. Cha, C.-H. Jung, M. El-Newehy and H. Y. Kim, *Carbohydrate Polymers* 2012, *90*, 1786-1793.
- [15] Y. Zhao, Y. Qiu, H. Wang, Y. Chen, S. Jin and S. Chen, *International Journal of Polymer Science* 2016, *2016*, Article ID 4672839.
- [16] Y. Lv, Y. Zhang, Y. Du, J. Xu and J. Wang, *Sensors* 2013, *13*, 15758-15769.
- [17] B. Ding, M. Wang, J. Yu and G. Sun, *Sensors* 2009, *9*, 1609-1624.
- [18] B. Ding, M. Wang, X. Wang, J. Yu and G. Sun, *Mater. Today* 2010, *13*, 16–27.
- [19] M. Zhu, J. Han, F. Wang, W. Shao, R. Xiong, Q. Zhang, H. Pan, Y. Yang, S. K. Samal, F. Zhang and C. Huang, *Macromol. Mater. Eng.* 2017, *302*, 1600353.
- [20] M. Faccini, G. Borja, M. Boerrigter, D. M. Martin, S. M. Crespiera, S. Vazquez-Campos, L. Aubouy and D. Amantia, *Journal of Nanomaterials* 2015, *2015*, Article ID 247471.
- [21] R. Balamurugan, S. Sundarrajan and S. Ramakrishna, *Membranes* 2011, *1*, 232-248.
- [22] M. J. laudenslager, R. H. Scheffler and W. M. Sigmund, *Pure Appl. Chem.* 2010, *82*, 2137-2156.

- [23] J. Miao, M. Miyauchi, T. J. Simmons, J. S. Dordick and R. J. Linhardt, *J. Nanosci. Nanotechnol.* 2010, *10*, 5507-5519.
- [24] Z. Dong, S. J. Kennedy and Y. Wu, *J. Power Sources* 2011, *196*, 4886-4904.
- [25] I. G. Loscertales, A. Barrero, I. Guerrero, R. Cortijo, M. Marquez and A. M. Ganan-Calvo, *Science* 2002, *295*, 1695-1698.
- [26] L. Peng, S. Jiang, M. Seuß, A. Fery, G. Lang, T. Scheibel and S. Agarwal, *Macromol. Mater. Eng.* 2016, *301*, 48-55.
- [27] P. Gupta and G. L. Wilkes, *Polymer* 2003, *44*, 6353-6359.
- [28] S. Chen, H. Hou, P. Hu, J. H. Wendorff, A. Greiner and S. Agarwal, *Macromol. Mater. Eng.* 2009, *294*, 781-786.
- [29] Y. Z. Zhang, J. Venugopal, Z.-M. Huang, C. T. Lim and S. Ramakrishna, *Biomacromolecules* 2005, *6*, 2583-2589.
- [30] F. J. O'Brien, *Materialstoday* 2011, *14*, 88-95.
- [31] A. Tathe, M. Ghodke and A. P. Nikalje, *Int. J. Pharm. Pharm. Sci.* 2010, *2*, 19-23.
- [32] G. H. Altman, F. Diaz, C. Jakuba, T. Calabro, R. L. Horan, J. Chen, H. Lu, J. Richmond and D. L. Kaplan, *Biomaterials* 2003, *24*, 401-416.
- [33] C. Vepari, D. L. Kaplan, *Prog. Polym. Sci.* 2007, *32*, 991-1007.
- [34] D. Kaplan, W. W. Adams, B. Farmer and C. Viney, *ACS Symp. Ser.* 1994, *544*, 2-16.
- [35] Y. Qi, H. Wang, K. Wei, Y. Yang, R.-Y. Zhang, I. S. Kim and K.-Q. Zhang, *Int. J. Mol. Sci.* 2017, *18*, 237-258.

- [36] D. N Rockwood, R. C Preda, T. Yücel, X. Wang, M. L Lovett and D. L. Kaplan, *Nat. Protoc.* 2011, *6*, 1612-1631.
- [37] A. R. Murphy and D. L. Kaplan, *J. Mater. Chem.* 2009, *19*, 6443-6450.
- [38] V. Volkov, A. V. Ferreira and A. Cavaco-Paulo, *Macromol. Mater. Eng.* 2015, *12*, 1199-1216.
- [39] T. Dyakonov, C. H. Yang, D. Bush, S. Gosangari, S. Majuru and A. Fatmi, *Journal of Drug Delivery* 2012, Article ID 490514.
- [40] O. Hakimi, D. P. Knight, F. Vollrath and P. Vadgama, *Composites: Part B* 2007, *38*, 324-337.
- [41] C.-Z. Zhou, F. Confalonieri, M. Jacquet, R. Perasso, Z.-G. Li and J. Janin, *PROTEINS: Structure, Function and Genetics*, 2001, *44*, 119-122.
- [42] L.-D. Koh, Y. Cheng, C.-P. Teng, Y.-W. Khin, X.-J. Loh, S.-Y. Tee, M. Low, E. Ye, H.-D. Yu, Y.-W. Zhang and M.-Y. Han, *Progress in Polymer Science* 2015, *46*, 86-110.
- [43] J. Lunt, *Polymer Degradation and Stability* 1998, *59*, 145-152.
- [44] K. Hamad, M. Kaseem, H. W. Yang, F. Deri and Y. G. Ko, *eXPRESS Polymer Letters* 2015, *9*, 435-455.
- [45] M. Jamshidian, E. A. Tehrani, M. Imran, M. Jacquot and S. Desobry, *Comprehensive Reviews in Food Science and Food Safety* 2010, *9*, 552-571.
- [46] R. Datta and M. Henry, *J. Chem. Technol. Biotechnol* 2006, *81*, 1119-1129.
- [47] J. R. Dorgan, H. Lehermeier and M. Mang, *Journal of Polymers and the Environment* 2000, *8*, 1-9.

- [48] C. A. Mills, M. Navarro, E. Engel, E. Martinez, M. P. Ginebra, J. Planell, A. Errachid and J. Samitier, *J. Biomed. Mater. Res.* 2006, 76, 781–787.
- [49] J. Y. Lim, S. H. Kim, S. Lim and Y. H. Kim, *Macromol. Mater. Eng.* 2003, 288, 50-57.
- [50] M. A. Woodruff and D. W. Hutmacher, *Progress in Polymer Science* 2010, 35, 1217-1256.
- [51] M. Labet and W. Thielemans, *Chem. Soc. Rev.* 2009, 38, 3484-3504.
- [52] C. Braud, R. Devarieux, A. Atlan, C. Ducos and M. Vert, *J. Chromatogr. B* 1998, 706, 73-82.
- [53] H. Dong, H.-d. Wang, S.-g. Cao and J.-c. Shen, *Biotechnology Letters* 1998, 20, 905-908.
- [54] A. Mahapatro, A. Kumar and R. A. Gross, *Biomacromolecules* 2004, 5, 62-68.
- [55] M. Okada, *Progress in Polymer Science* 2002, 27, 87-133.
- [56] M. S. Kim, K. S. Seo, G. Khang and H. B. Lee, *Macromol. Rapid. Commun.* 2005, 26, 643-648.
- [57] R. M. Mohamed and K. Yusoh, *Advanced Materials Research* 2015, 1134, 249-255.
- [58] J. L. Hedrick, T. Magbitang, E. F. Connor, T. Glauser, W. Volksen, C. J. Hawker, V. Y. Lee and R. D. Miller, *Chem. Eur. J.* 2002, 8, 3309-3319.
- [59] J. L. Murphy, L. Vollenweider, F. Xu and B. P. Lee, *Biomacromolecules* 2010, 11, 2976–2984.
- [60] Y. Ikada and H. Tsuji, *Macromol. Rapid Commun.* 2000, 21, 117–132.

- [61] R. Ghizal, G. R. Gatima and S. Srivastava, *International Journal of Engineering Technology, Management and Applied Sciences* 2014, 2, 104-115.
- [62] M. A. Ward and T. K. Georgiou, *Polymers* 2011, 3, 1215-1242.
- [63] R. Pelton, *Journal of Colloid and Interface Science* 2010, 348, 673-674.
- [64] M. Heskins and J. E. Guillet, *J. Macrimol. Sci.: Part A –Chem.* 1968, 2, 1441-1455.
- [65] F. Liu and M. W. Urban, *Progress in Polymer Science* 2010, 35, 3-23.
- [66] R. R Kokardekar, V. K Shah and H. R Mody, *Internet Journal of Medical Update* 2012, 7, 60-63.
- [67] Y. Guan and Y. Zhang, *Soft Matter* 2011, 7, 6375-6384.
- [68] D. Subhash, H. Mody, R. Banerjee, D. Bahadur and R. Srivastava, *11th IEEE International Conference on Nanotechnology* 2011.
- [69] M. Nakayama, T. Okano and M. Winnik, *Material Matters* 2010, 5, 56-58.
- [70] L.-W. Xia, R. Xie, X.-J. Ju, W. Wang, Q. Chen and L.-Y. Chu, *Nature Communications* DOI: 10.1038/ncomms3226.
- [71] Y. Shi, C. Ma, L. Peng and G. Yu, *Adv. Funct. Mater.* 2015, 25, 1219-1225.
- [72] I. Yildiz and B. S. Yildiz, *Journal of Nanomaterials* 2015, Article ID 35059.
- [73] M. Krag, I. Pastoriza-Santos, J. Perez-Juste, T. Hellweg and L. M. Liz-Marzan, *Small* 2007, 3, 1222-1229.
- [74] A. Greiner and J. H. Wendorff, *Angew. Chem. Int. Ed.* 2007, 46, 5670-5703.
- [75] T. Subbiah, G. S. Bhat, R. W. Tock, S. Parameswaran and S. S. Ramkumar, *Journal of Applied Polymer Science* 2005, 96, 557-569.

- [76] S. Agarwal, A. Greiner and J. H. Wendorff, *Progress in Polymer Science* 2013, 38, 963-991.
- [77] S. Agarwal, J. H. Wendorff and A. Greiner, *Polymer* 2008, 49, 5603-5621.
- [78] Z.-M. Huang, Y.-Z. Zhang, M. Kotaki and S. Ramakrishna, *Composites Science and Technology* 2003, 63, 2223-2253.
- [79] F. Ko, Y. Gogotsi, A. Ali, N. Naguib, H. Ye, G. Yang, C. Li and P. Wills, *Adv. Mater.* 2003, 15, 1161-1165.
- [80] J. H. Sung, H. S. Kim, H.-J. Jin, H. J. Choi and I.-J. Chin, *Macromolecules* 2004, 37, 9899-9902.
- [81] J. J. Ge, H. Hou, Q. Li, M. J. Graham, A. Greiner, D. H. Reneker, F. W. Harris and S. Z. D. Cheng, *J. AM. CHEM. SOC.* 2004, 126, 15754-15761.
- [82] M. Naebe, T. Lin, M. P. Staiger, L. Dai and X. Wang, *Nanotechnology* 2008, 19, 305702.
- [83] L. Y. Yeo and J. R. Friend, *Journal of Experimental Nanoscience* 2006, 1, 177-209.
- [84] B. Sun, Y.-Z. Long, Z.-J. Chen, S.-L. Liu, H.-D. Zhang, J.-C. Zhang and W.-P. Han, *J. Mater. Chem. C.* 2014, 2, 1209-1219.
- [85] C. L. Casper, N. Yamaguchi, K. L. Kiick and J. F. Rabolt, *Biomacromolecules* 2005, 6, 1998-2007.
- [86] B. Dong, M. E. Smith and G. E. Wnek, *Small* 2009, 5, 1508-1512.
- [87] C. Huang, S. J. Soenen, J. Rejman, J. Trekker, C. Liu, L. Lagae, W. Ceelen, C. Wilhelm, J. Demeester and S. C. De Smedt, *Adv. Funct. Mater.* 2012, 22, 2479-2486.

- [88] H. Hu, W. Jiang, F. Lan, X. Zeng, S. Ma, Y. Wu and Z. Gu, *RSC Adv.* 2013, 3, 879-886.
- [89] A. Urrutia, P. J. Rivero, J. Goicoechea, F. J. Arregui, I. R. Matias, *Fifth International Conference on Sensing Technology* 2011, 380-383.
- [90] A. Urrutia, P. J. Rivero, J. Goicoechea, Y. Rodriguez, F. J. Arregui, I. R. Matias, *The 14th International Meeting on Chemical Sensors* 2012, 1550-1553.
- [91] W. Salalha, J. Kuhn, Y. Dror and E. Zussman, *Nanotechnology* 2006, 17, 4675–4681.
- [92] M. Gensheimer, M. Becker, A. Brandis-Heep, J. H. Wendorff, R. K. Thauer, A. Greiner, *Adv. Mater.* 2007, 19, 2480-2482.
- [93] Y. Liu, M. H. Rafailovich, R. Malal, D. Cohn and D. Childambaram, *PNAS* 2009, 106, 14201-14206.
- [94] S. W. Lee, A. M. Belcher, *Nano Letters* 2004, 4, 387-390.
- [95] E. Zussman, *Polym. Adv. Technol.* 2011, 22, 366–371.
- [96] C. J River, K. Zhou, R. J Gilbert, D. I Finkelstein and J. S Forsythe, *Biomatter* 2015, 5, e1005527.
- [97] J. Wu and Y. Hong, *Bioactive Materials* 2016, 1, 56-64.
- [98] J. Nam, Y. Huang, S. Agarwal and J. Lannutti, *Tissue Eng.* 2007, 13, 2249–2257.
- [99] J. H. Yu, S. V. Fridrikh and G. C. Rutledge, *Adv. Mater.* 2004, 17, 1562-1566.
- [100] R. W. Tuttle, A. Chowdury, E. T. Bender, R. D. Ramsier, J. L. Rapp and M. P. Espe, *Applied Surface Science* 2008, 254, 4925–4929.
- [101] D. Li, Y. Wang and Y. Xia, *Nano Letters* 2003, 3, 1167-1171.

- [102] H. Wu, W. Pan, D. Lin and H. Li, *Journal of Advanced Ceramics* 2012, *1*, 2-23.
- [103] M. Bognitzki, M. Becker, M. Graeser, W. Massa, J. H. Wendorff, A. Schaper, D. Weber, A. Beyer, A. Götzhäuser and A. Greiner, *Adv. Mater.* 2006, *18*, 2384-2386.
- [104] H. Wu, L. Hu, M. W. Rowell, D. Kong, J. J. Cha, J. R. McDonough, J. Zhu, Y. Yang, M. D. McGehee and Y. Cui, *Nano Letters* 2010, *10*, 4242-4248.
- [105] K. Mondal and A. Sharma, *RSC Adv.* 2016, *6*, 94595–94616.
- [106] D. Li and Y. Xia, *Nano Letters* 2003, *3*, 555-560.
- [107] F. H. Anka and K. J. Balkus, Jr., *Ind. Eng. Chem. Res.* 2013, *52*, 3473–3480.
- [108] C. Wang, K.-W. Yan, Y.-D. Lin and P. C. H. Hsieh, *Macromolecules* 2010, *43*, 6389–6397.
- [109] J. W. Rajala, H. U. Shin, D. Lolla and G. G. Chase, *Fibers* 2015, *3*, 450-462.
- [110] D. Li and Y. Xia, *Nano Letters* 2004, *4*, 933-938.
- [111] F. Ochanda and W. E. Jones, Jr., *Langmuir* 2005, *21*, 10791-10796.
- [112] Q. Gao, J. Luo, X. Wang, C. Gao and M. Ge, *Nanoscale Research Letters* 2015, *10*:176.
- [113] R. Khajavi and M. Abbasipour, *Scientia Iranica, Transactions F: Nanotechnology* 2012, *19*, 2029–2034.
- [114] S.-Y. Gu, Q.-L. Wu, J. Ren and G. J. Vancso, *Macromol. Rapid Commun.* 2005, *26*, 716–720.
- [115] L. S. Carnell, E. J. Siochi, N. M. Holloway, R. M. Stephens, C. Rhim, L. E. Niklason and R. L. Clark, *Macromolecules* 2008, *41*, 5345-5349.

- [116] L. Chen, S. Jiang, J. Chen, F. Chen, Y. He, Y. Zhu and H. Hou, *New J. Chem.* 2015, 39, 8956—8963.
- [117] I. Savva, E. Evaggelou, G. Papaparaskeva, T. Leontiou, T. Stylianopoulos, F. Mpekris, K. Stylianou and T. Krasia-Christoforou, *RSC Adv.* 2015, 5, 104400–104407.
- [118] Lord Rayleigh, *Philos. Mag.* 1882, 14, 184–186.
- [119] J. Zeleny, *Physical Review* 1914, 3, 69-91.
- [120] J. Zeleny, *Physical Review* 1914, 3, 1-6.
- [121] P. K. Baumgarten, *Journal of Colloid and Interface Science* 1971, 36, 71-79.
- [122] I. Hayati, A. I. Bailey and TH. F. Tadros, *Journal of Colloid and Interface Science* 1987, 117, 205-221.
- [123] D. H Reneker and I. Chun, *Nanotechnology* 1996, 7, 216-223.
- [124] Y. M. Shin, M. M. Hohman, M. P. Brenner and G. C. Rutledge, *Appl. Phys. Lett.* 2001, 78, 1149-1151.
- [125] A. Koski, K. Yim and S. Shivkumar, *Materials Letters* 2004, 58, 493–497.
- [126] J. M. Deitzel, J. Kleinmeyer, D. Harris and N. C. Beck Tan, *Polymer* 2001, 42, 261-272.
- [127] S.-Q. Wang, J.-H. He and L. Xu, *Polym. Int.* 2008, 57, 1079-1082.
- [128] W. K. Son, J. H. Youk, T. S. Lee and W. H. Park, *Polymer* 2004, 45, 2959-2966.
- [129] M. M. Demir, I. Yilgor, E. Yilgor and B. Erman, *Polymer* 2001, 43, 3303-3309.
- [130] C. J. Buchko, L. C. Chen, Y. Shen and D. C. Martin, *Polymer* 1999, 40, 7397-7407.

- [131] C. Wang, H.-S. Chien, C.-H. Hsu, Y.-C. Wang, C.-T. Wang and H.-A. Lu, *Macromolecules* 2007, 40, 7973-7983.
- [132] S. Zhao, X. Wu, L. Wang and Y. Huang, *Journal of Applied Polymer Science* 2004, 91, 242-246.
- [133] S. Tripatanasuwan, Z. Zhong and D. H. Reneker, *Polymer* 2007, 48, 5742-5746.
- [134] S. Chen, H. Hou, P. Hu, J. H. Wendorff, A. Greiner and S. Agarwal, *Macromol. Mater. Eng.* 2009, 294, 781-786.
- [135] T. Lin, H. Wang and X. Wang, *Adv. Mater.* 2005, 17, 2699-2703.
- [136] Z. Liu, D. D. Sun, P. Guo and J. O. Leckie, *Nano Lett.* 2007, 7, 1081-1085.
- [137] C. Wang, K.-W. Yan, Y.-D. Lin and P. C. H. Hsieh, *Macromolecules* 2010, 43, 6389-6397.
- [138] R. Liu, N. Cai, W. Yang, W. Chen and H. Liu, *Journal of Applied Polymer Science* 2010, 116, 1313-1321.
- [139] C.-C. Hu, S.-S. Chang and N.-Y. Liang, *Journal of Industrial Textiles* 2016, 0, 1-18.
- [140] K.-H. Roh, D. C. Martin and J. Lahann, *Nature Materials* 2005, 4, 759-763.
- [141] P. Gupta and G. L. Wilkes, *Polymer* 2003, 44, 6353-6359.
- [142] E. Zussman, A. L. Yarin, A. V. Bazilevsky, R. Avrahami and M. Feldman, *Adv. Mater.* 2006, 18, 348-353.
- [143] S. N. Reznik, A. L. Yarin, E. Zussman and L. Bercovici, *Phys. Fluids* 2006, 18, 062101.

- [144] A. L. Yarin, E. Zussman, J. H. Wendorff and A. Greiner, *J. Mater. Chem.* 2007, *17*, 2585-2599.
- [145] Y. Dror, W. Salalha, R. Avrahami, E. Zussman, A. L. Yarin, R. Dersch, A. Greiner and J. H. Wendorff, *Small* 2007, *3*, 1064-1073.
- [146] I. G. Loscertales, A. Barrero, I. Guerrero, R. Cortijo, M. Marquez, A. M. Ganan-Calvo, *Science* 2002, *295*, 1695–1698.
- [147] M. Mondal, K. Trivedy and S. N. Kumar, *Caspian J. Env. Sci.*, 2007, *5*, 63-67.
- [148] R. M. Reddy, *Acad. J. Entomol.*, 2009, *2*, 71-75.
- [149] F. Zhang, B. Q. Zuo and L. Bai, *J. Mater. Sci.*, 2009, *44*, 5682-5687.
- [150] Y. Kawahara, A. Nakayama, N. Matsumura, T. Yoshioka and M. Tsuji, *J. Appl. Polym. Sci.*, 2008, *107*, 3681-3684.
- [151] K. Ohgo, C. Zhao, M. Kobayashi and T. Asakura, *Polymer* 2003, *44*, 841-846.
- [152] S. Sukigara, M. Gandhi, J. Ayutsede, M. Micklus and F. Ko, *Polymer* 2003, *44*, 5721-5727.
- [153] X. Zhang, M. R. Reagan and D. L. Kaplan, *Adv. Drug Deliver. Rev.*, 2009, *61*, 988-1006.
- [154] B.-M. Min, G. Lee, S. H. Kim, Y. S. Nam, T. S. Lee and W. H. Park, *Biomaterials*, 2004, *25*, 1289-1297.
- [155] J. Ayutsede, S. Gandhi, S. Sukigara, M. Micklus, H.-E. Chen and F. Ko, *Polymer* 2005, *46*, 1625-1634.
- [156] W. H. Park, L. Jeong, D. I. Yoo and S. Hudson, *Polymer* 2004, *45*, 7151-7157.

- [157] H.-J. Jin, S. V. Fridrikh, G. C. Rutledge and D. L. Kaplan, *Biomacromolecules*, 2002, 3, 1233-1239.
- [158] W. Zhou, J. He, S.; Du, S. Cui and W. Gao, *Iran. Polym. J.* 2011, 20, 389-397.
- [159] G. Yin, Y. Zhang, W. Bao, J. Wu, D. Shi, Z. Dong and W. Fu, *J. Appl. Polym. Sci.*, 2009, 111, 1471-1477.
- [160] M. J. McClure, S. A. Sell, C. E. Ayres, D. G. Simpson and G. L. Bowlin, *Biomed. Mater.*, 2009, 4, 055010.
- [161] L. Li, H. Li, Y. Qian, X. Li, G. K. Singh, L. Zhong, W. Liu, Y. Lv, K. Cai, and L. Yang, *Int. J. Biol. Macromol.*, 2011, 49, 223-232.
- [162] J. He, Y. Qin, S. Cui, Y. Gao and S. Wang, *J. Mater. Sci.*, 2011, 46, 2938-2946.
- [163] S. Wang, Y. Zhang, H. Wang, G. Yin and Z. Dong, *Biomacromolecules*, 2009, 10, 2240-2244.
- [164] S. Chen, H. Hou, P. Hu, J. H. Wendorff, A. Greiner and S. Agarwal, *Macromol. Mater., Eng.* 2009, 294, 265-271.
- [165] S. Koombhongse, W. Xu and D. H. Reneker, *Journal of Polymer Science: PartB: PolymerPhysics*, 2001, 39, 2598–2606.
- [166] N. Amiraliyan, M. Nouri and M. H. Kish, *Journal of Applied Polymer Science*, 2009, 113, 226–234.
- [167] Y. Ner, J. A. Stuart, G. Whited and G. A. Sotzing, *Polymer*, 2009, 50, 5828–5836.
- [168] D. Papkov, Y. Zou, M. N. Andlib, A. Goponenko, S. Z. D. Cheng and Y. A. Dzenis, *ACS Nano* 2013, 7, 3324-3331.

- [169] C. Ribeiro, V. Sencadas, C. M. Costa, J. L. G. Ribelles and S. Lanceros-Méndez, *Sci. Technol. Adv. Mater.*, 2011, 12, 015001.
- [170] K.-H. Lee, K.-W. Kim, A. Pesapane, H.-Y. Kim and J. F. Rabolt, *Macromolecules*, 2008, 41, 1494-1498.
- [171] X. Hu, D. Kaplan and P. Cebe, *Macromolecules*, 2006, 39, 6161-6170.
- [172] L. Jeong, K. Y. Lee and W. H. Park, *Key Engineering Materials*, 2007, 342-343, 813-816.
- [173] S. H. Kim, Y. S. Nam, T. S. Lee and W. H. Park, *Polym. J.*, 2003, 35, 185-190.
- [174] X. Zhang, R. Nakagawa, K. H. K. Chan and M. Kotaki, *Macromolecules* 2012, 45, 5494.-5500
- [175] G. Mathew, J. P. Hong, J. M. Rhee, D. J. Leo and C. Nah, *J. Appl. Polym. Sci.*, 2006, 101, 2017-2021.
- [176] M. Ma, L. Guo, DG Anderson and R. Langer, *Science*, 2013, 339, 186-189.
- [177] A. Sidoreko, T. Krupenkin, A. Taylor, P. Fratzl and J. Aizenberg, *Science* 2007, 315, 487-490.
- [178] R. M. Erb, J. S. Sander, R. Grisch and A. R. Studart, *Nat. Commun.* 2013, 4, 1712-1719.
- [179] Z. Hu, X. Zhang, Y. Li, *Science* 1995, 269, 525-527.
- [180] S. Jiang, F. Liu, A. Lerch, L. Ionov, S. Agarwal, *Adv. Mater.* 2015, 27, 4865-4870.
- [181] S. Agarwal, A. Yarin, *Polymer* 2016, 97, 604-613.
- [182] G. Stoychev, S. Zakharchenko, S. Turcaud, J. W.C. Dunlop and L. Ionov, *ACS*

- Nano* 2012, 6, 3925-3934.
- [183] G. Stoychev, S. Turcaud, J. W. C. Dunlop, L. Ionov, *Adv. Funct. Mater.* 2013, 23, 2295-2300.
- [184] K. J. Lee, J. Yoon, S. Rahmani, S. Hwang, S. Bhaskar, S. Mitragotri and J. Lahann, *PNAS* 2012, 109, 16057-16062.
- [185] J. Yoon, T. W. Eyster, A. C. Misra and J. Lahann, *Adv. Mater.* 2015, 27, 4509-4515.
- [186] G. Jalani, C. W. Jung, J. S. Lee and D. W. Lim, *Int. J. Nanomed* 2014, 9, 33-49.
- [187] X. Wang, B. Ding, J. Yu and M. Wang, *Nano Today* 2011, 6, 510-530.
- [188] S. Madhugiri, A. Dalton, J. Gutierrez, J. P. Ferraris and K. J. Balkus Jr., *JACS* 2003, 125, 14531-14538.
- [189] J. Luo, F. Wang and B. Xu, *Text. Res. J.* 2011, 81, 538-544.
- [190] S.P. Rwei, Y.T. Lin and Y.Y. Su, *Polym. Eng. Sci.* 2005, 45, 838-845.
- [191] F. Wang, F. Gu and B. Xu, *J. Eng. Fiber. Fabr.* 2013, 8, 50-55.
- [192] M. Horio and T. Kondo, *Text. Res. J.* 1953, 23, 373-386.
- [193] H. J. Woods, *J. Textile Inst.* 1935, 26, T93-T102.
- [194] Z. Hu, X. Zhang, Y. Li, *Science* 1995, 269, 525-527.
- [195] Soft Actuators (Eds: K. Asaka, H. Okuzaki), Springer, Tokyo, Japan 2014.
- [196] S. Jiang, F. Liu, A. Lerch, L. Ionov, S. Agarwal, *Adv. Mater.* 2015, 27, 4865-4870.
- [197] S. Agarwal, A. Yarin, *Polymer* 2016, 97, 604-613.
- [198] W. T. S. Huck, *Materialstoday*, 2008, 11, 24-32.

- [199] J. Y. Park, H. J. Oh, D. J. Kim, J. Y. Baek and S. H. Lee, *J. Micromech. Microeng.*, 2006, *16*, 656-663.
- [200] L. Ionov, *e-Polymers* 2014, *14*, 109.
- [201] M. Ma, L. Guo, DG Anderson and R. Langer, *Science*, 2013, *339*, 186-189.
- [202] L. Liu, S. Jiang, Y. Sun and S. Agarwal, *Adv. Funct. Mater.*, 2016, *26*, 1021-1027.
- [203] Z. L. Wu, M. Moshe, J. Greener, H. Therien-Aubin, Z. Nie, E. Sharon and E. Kumacheva, *Nat. Commun.* 2013, *4*, 1586-1593.
- [204] G. Stoychev, L. Guiducci, S. Turcaud, J. W. C. Dunlop and L. Ionov, *Adv. Funct. Mater.* 2016, *26*, 7733-7739.
- [205] H. Ma, J. Hu and P. X. Ma, *Adv. Funct. Mater.*, 2010, *20*, 2833-2841.
- [206] J. Yang, D. Motlagh, A. R. Webb and G. A. Ameer, *Tissue Eng.*, 2005, *11*, 1876-1886.
- [207] Q. Xu, Y. Lv, C. Dong, T. S. Sreeprasad, A. Tian, H. Zhang, Y. Tang, Z. Yu and N. Li, *Nanoscale*, 2015, *7*, 10883-10895.
- [208] B. Zhang, J. He, X. Li, F. Xu and D. Li, *Nanoscale*, 2016, *8*, 15376-15388.
- [209] S. Wang, Y. Zhang, H. Wang, G. Yin and Z. Dong, *Biomacromolecules*, 2009, *10*, 2240-2244.
- [210] C. M. Vaz, S. van Tuijl, C. V. C. Bouten, F. P. T. Baaijens, *Acta Biomater.*, 2005, *1*, 575-582.
- [211] H. Therien-Aubin, M. Moshe, E. Sharonb and E. Kumacheva, *Soft Matter* 2015, *11*, 4600-4605.

- [212] T. G. Leong, A. M. Zarafshar, D. H. Gracias, *Small* 2010, 6, 792-806.
- [213] L. Yao, D. D. Swartz, S. F. Gugino, J. A. Russell and S. T. Andreadis, *Tissue Eng.* 2005, 11, 991-1003.
- [214] T. Shinoka , C. K. Breuer , R. E. Tanel , G. Zund , T. Miura , P. X. Ma , R. Langer , J. P. Vacanti , J. E. Mayer , Jr. , *Ann. Thorac. Surg.* 1995, 60, 513-516.
- [215] L. E. Niklason , J. Gao , W. M. Abbott , K. K. Hirschi , S. Houser , R. Marini and R. Langer , *Science* 1999, 284, 489-493.
- [216] W. J. Zhang, W. Liu, L. Cui and Y. Cao, *J. Cell. Mol. Med.* 2007, 11, 945-957.
- [217] H. He and T. Matsuda, *Tissue Eng.* 2002, 8, 213-224.
- [218] C. E. Sarraf, A. B. Harris, A. D. McCulloch and M. Eastwood, *Cell Proliferation* 2003, 36, 241-254.
- [219] V. Mironov, V. Kasyanov, X. Z. Shu, C. Eisenberg, L. Eisenberg, S. Gonda, T. Trusk, R. R. Markwald and G. D. Prestwich , *Biomaterials* 2005 , 26 , 7628-7635.
- [220] C. B. Weinberg and E. Bell, *Science*, 1986, 231, 397-400.
- [221] J. D. Berglund, M. M. Mohseni, R. M. Nerem and A. Sambanis, *Biomaterials*, 2003 , 24 , 1241-1254.
- [222] J. D. Berglund, R. M. Nerem and A. Sambanis, *Tissue Eng.* 2004, 10, 1526-1535.
- [223] E. D. Grassl, T. R. Oegema and R. T. Tranquillo, *J. Biomed. Mater. Res.* 2002, 60, 607-612.
- [224] B. C. Isenberg, C. Williams and R. T. Tranquillo, *Ann Biomed Eng.* 2006, 34, 971-985.

- [225] D. D. Swartz, S. F. Gugino, J. A. Russell and S. T. Andreadis, *Am. J. Physiol Heart Circ Physiol.* 2005, *288*, 1451-1460.
- [226] S. Zakharchenko, E. Sperling and L. Ionov, *Biomacromolecules*, 2011, *12*, 2211-2215.
- [227] V. Stroganov, S. Zakharchenko, E. Sperling, A. K. Meyer, O. G. Schmidt and L. Ionov, *Adv. Funct. Mater.* 2014, *24*, 4357-4363.
- [228] L. Liu, A. Ghaemi, S. Gekle, S. Agarwal, *Adv. Mater.* 2016, *28*, 9792-9796.
- [229] Y. Mei, D. J. Thurmer, C. Deneke, S. Kiravittaya, Y. F. Chen, A. Dadgar, F. Bertram, B. Bastek, A. Krost, J. Christen, T. Reindl, M. Stoffel, E. Coric and O. G. Schmidt, *ACS Nano* 2009, *3*, 1663-1668.
- [230] T. G. Leong, C. L. Randall, B. R. Benson, A. M. Zarafshar and D. H. Gracias, *Lab Chip* 2008, *8*, 1621-1624.
- [231] N. Bassik, G. M. Stern, M. Jamal and D. H. Gracias, *Adv. Mater.* 2008, *20*, 4760-4764.
- [232] O. G. Schmidt and K. Eberl, *Nature* 2001, *410*, 168.
- [233] R. Dersch, T. Liu, A. K. Schaper, A. Greiner and J. H. Wendorff, *J. Polym. Sci., Part A: Polym. Chem.* 2003, *41*, 545-553.
- [234] V. Stroganov, M. Al-Hussein, J. U. Sommer, A. Janke, S. Zakharchenko and L. Ionov, *Nano Lett.* 2015, *15*, 1786-1790.
- [235] C. Azra, D. Alhazov and E. Zussman, *Polymer*, 2015, *58*, 162-169.
- [236] A. Mol and S. P. Hoerstrup, *Int. J. Cardiol.*, 2004, *95*, 57-58.
- [237] S. Jiang, G. Duan, E. Zussman, A. Greiner and S. Agarwal, *ACS Appl. Mater.*

Interfaces 2014, 6, 5918-5923.

[238] F. Chen, X. Peng, T. Li, S. Chen, X-F. Wu, D. Reneker and H. Hou, *J. Phy. D: Appl. Phys.* 2008, 41, 025308.

[239] S. Zakharchenko, N. Puretskiy, G. Stoychev, M. Stamm and L. Ionov, *Soft Matter* 2010, 6, 2633-2636.

[240] M. Gernhardt, L. Peng, M. Burgard, S. Jiang, B. Förster, H. Schmalz and S. Agarwal, *Macromol. Mater. Eng.* 2017, 1700248.

Publications in peer-reviewed scientific journals

From PhD work:

1. **L. Peng**, S. Jiang, M. Seuß, A. Fery, G. Lang, T. Scheibel and S. Agarwal, *Macromol. Mater. Eng.* 2016, *301*, 48-55.
2. **L. Peng**, J. Zhu and S. Agarwal, *Macromol. Rapid. Commun.* 2017, DOI: [10.1002/marc.201700034](https://doi.org/10.1002/marc.201700034)
3. M. Gernhardt, **L. Peng**, M. Burgard, S. Jiang, B. Förster, H. Schmalz and S. Agarwal, *Macromol. Mater. Eng.* 2017, 1700248.

From collaboration:

1. H. Pletsch, **L. Peng**, F. Mitschang, A. Schaper, M. Hellwig, D. Nette, A. Seubert, A. Greiner and S. Agarwal, *Small* 2014, *10*, 201-208.

Versicherungen und Erklärungen

(§ 9 Satz 2 Nr. 3 PromO BayNAT)

Hiermit versichere ich eidesstattlich, dass ich die Arbeit selbständig verfasst und keine anderen als die von mir angegebenen Quellen und Hilfsmittel benutzt habe (vgl. Art. 64 Abs. 1 Satz 6 BayHSchG).

(§ 9 Satz 2 Nr. 3 PromO BayNAT)

Hiermit erkläre ich, dass ich die Dissertation nicht bereits zur Erlangung eines akademischen Grades eingereicht habe und dass ich nicht bereits diese oder eine gleichartige Doktorprüfung endgültig nicht bestanden habe.

(§ 9 Satz 2 Nr. 4 PromO BayNAT)

Hiermit erkläre ich, dass ich Hilfe von gewerblichen Promotionsberatern bzw. -vermittlern oder ähnlichen Dienstleistern weder bisher in Anspruch genommen habe noch künftig in Anspruch nehmen werde.

(§ 9 Satz 2 Nr. 7 PromO BayNAT)

Hiermit erkläre ich mein Einverständnis, dass die elektronische Fassung meiner Dissertation unter Wahrung meiner Urheberrechte und des Datenschutzes einer gesonderten Überprüfung unterzogen werden kann.

(§ 9 Satz 2 Nr. 8 PromO BayNAT)

Hiermit erkläre ich mein Einverständnis, dass bei Verdacht wissenschaftlichen Fehlverhaltens Ermittlungen durch universitätsinterne Organe der wissenschaftlichen Selbstkontrolle stattfinden können.

.....
Ort, Datum, Unterschrift